UNIVERSITY OF GHANA

COLLEGE OF BASIC AND APPLIED SCIENCES

EXTRACTION AND CHARACTERIZATION OF CELLULOSE NANOCRYSTALS FROM TWO LOCAL PLANT MATERIALS

BY

FAITH ZANU

(10286341)

A THESIS SUBMITTED TO THE SCHOOL OF GRADUATE STUDIES IN PARTIAL FULFILLMENT OF THE AWARD OF DEGREE OF MASTER OF PHILOSOPHY IN CHEMISTRY

DEPARTMENT OF CHEMISTRY

JULY 2019

UNIVERSITY OF GHANA

COLLEGE OF BASIC AND APPLIED SCIENCES

EXTRACTION AND CHARACTERIZATION OF CELLULOSE NANOCRYSTALS FROM TWO LOCAL PLANT MATERIALS

BY

FAITH ZANU

(10286341)

A THESIS SUBMITTED TO THE SCHOOL OF GRADUATE STUDIES IN PARTIAL FULFILLMENT OF THE AWARD OF DEGREE OF MASTER OF PHILOSOPHY IN CHEMISTRY

DEPARTMENT OF CHEMISTRY

JULY 2019

DECLARATION

I, FAITH ZANU, declare that I have personally, under supervision, undertaken this research herein submitted.

Signed: 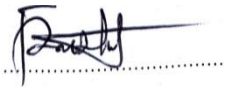 Date: 25/08/2020

MPhil Candidate: **Faith Zanu (10286341)**

I declare that I have supervised the student in undertaking this project submitted herein and confirm that the student has my permission for presentation and assessment.

Signed:  Date: 25/08/2020

Principal Supervisor: Dr. Enock Dankyi

Department of Chemistry, University of Ghana

Signed:  Date: 25/08/2020

Co – Supervisor: Dr. Vitus Apalangya

Department of Food Processing Engineering, University of Ghana

DEDICATION

This work is dedicated to God Jehovah Almighty and my dear family.

ABSTRACT

Cellulose is a linear homopolysaccharide of repeating D-glucopyranose units which form about 15 – 20 % of the dry weight of plant biomass. It is the world's most abundant renewable natural polymer with unique properties such as high strength, biocompatibility, low density and excellent mechanical properties. These excellent characteristics of the isolated cellulose nanocrystals coupled with their wide availability enable their potential application in areas of packaging materials to replace fossil-fuel based materials, in optical sensors, paints, and as reinforcements in composite materials. In this work, cellulose nanocrystals were isolated from two local plant biomass, *Acasia sp*. (sawie), and *Palmae sp*. (keteku), through a series of acid and alkaline hydrolysis to get rid of lignin, hemicellulose and other impurities, leaving crystalline cellulose nanocrystals. Cellulose nanocrystals were characterized by Fourier Transform Infra-Red (FT-IR) Spectroscopy, Optical Microscopy, Scanning Electron Microscopy (SEM), X-Ray Diffraction (XRD) and Thermogravimetric Analysis (TGA). SEM morphological analysis showed slender nanosize particles of CNCs of approximately less than 10 µm. FTIR analysis confirmed a removal of lignin and hemicellulose due to the disappearance of peaks at 1230 cm^{-1} (C – O bending) and 1765 – 1715 cm^{-1} (C = O stretching of aldehyde) respectively. Peak at 1160 cm^{-1} showed the presence of sulphonated groups which was evidenced by the uniform dispersibility of CNCs in solution due to the repulsive forces. The crystallinity index at 2Θ (18^o – 25^o) was approximately -163.04 % for *acacia sp.* and -5460 % for *palmae sp.* Thermogravimetric analysis of both *acacia sp.* and *palmae sp.* showed high thermal stability of approximately 363.8 ^oC and 336.3 ^oC respectively. The characterized CNCs generally exhibited outstanding properties of high crystallinity, thermal stability and tunable surfaces enabling even dispersion in aqueous solution.

ACKNOWLEGEMENT

My profound gratitude goes to Dr. Enock Dankyi and Dr. Vitus Apalangya for their guidance, corrections and patience in making this work successful.

I am grateful to the lecturers, staff and colleagues of Department of Chemistry especially Mr. Bob Essien and Mr. Samuel Owusu.

Many thanks to my colleagues, Peter Osei, Richard Owusu and Pascal Tofah for their support.

I also appreciate WACCBIP, Banga and Dr. Salifu Ali Azeko of Worcester Polytechnic Institute for their immense help in bringing this work to a completion.

A very big thank you to the Youth Outreach family of the Global Evangelical Church, my best friend Enoch Akoto and Mr. Jeffery Brown for their tremendous help.

TABLE OF CONTENTS

TABLE OF FIGURES

LIST OF TABLES

LIST OF ABBREVIATIONS

CNC	Cellulose Nanocrystals
CNC-A	Cellulose nanocrystals from Acacia sp.
SAB	*Acacia sp.* after base hydrolysis
SABL 1	*Acacia sp.* after first bleaching
SABL 2	*Acacia sp.* after second bleaching
SAA	*Acacia sp.* after acid hydrolysis
CNC-P	Cellulose nanocrystals from Palmae sp.
KAB	*Palmae sp.* after base hydrolysis
KABL 1	*Palmae sp.* after first bleaching
KABL 2	*Palmae sp.* after second bleaching
KAA	*Palmae sp.* after acid hydrolysis
CNF	Cellulose Nanofibers
CNW	Cellulose Nanowhiskers

CHAPTER ONE

1.0 INTRODUCTION

1.1 Background

During the past few years, the use of renewable resources to meet the increasing human demands of the world has received much attention. One of such environmentally friendly renewable resources is cellulose which is considered as the most abundant polymer with a broad range of industrial applications. It is estimated that about $7.5x10^{10}$ tons of cellulose is manufactured per annum on a global scale (Beltramino *et al.*, 2015).

Cellulose is a polyglucose with beta 1:4 glycosidic linkages (Figure 1.1) which make the polymer linear and does not coil into a helical structure. It contains about 3000 monomers and has a molecular weight of about 500 atomic mass unit (Lu & Hsieh, 2010). Individual strands of cellulose tend to align with one another and are connected by strong hydrogen bonds which make cellulose insoluble in water, rigid and a fibrous polymer. Cellulose materials constitute the major component of plant fiber; 40 – 50 %. The rest is composed of hemicellulose; about 20 – 30 % and lignin; 10 – 20 % (Kargarzadeh *et al.*, 2012; Taflick *et al.*, 2017). Additionally, cellulose possesses several hydroxyl groups that could be functionalized for varied products and purposes. Cellulose may be obtained in the form of nanomaterials which are considered more suitable for easy fabrication into other products and application.

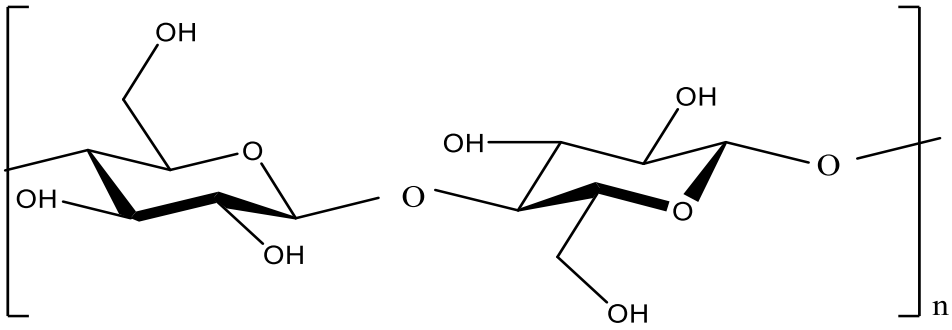

Figure 1.1. Chemical composition of cellulose showing repeating units of glucose linked through 1,4-β-glycosidic linkage.

Two major cellulosic nanomaterials that can be derived from cellulose are cellulose nanofibrils (CNFs) and CNCs (Postek *et al.*, 1997), which are isolated from plant sources; cotton, biomass, wood, bacteria and some sea living organisms, e.g. tunicates (Cherian *et al.*, 2008). CNFs are relatively longer than CNCs and are usually derived from strong mechanical fibrillation of lignocellulosic fibers. On the other hand, CNCs are cellulose-based materials or particles that can be isolated *via* acid treatment from a wide range of natural biodegradable materials (Grishkewich *et al.*, 2017; Postek *et al*., 1997).

In recent years, there has been much research on the isolation of CNCs via acid hydrolysis and the investigation of their unique physicochemical properties and possible industrial applications in aviation, plastic, automobiles, packaging and sensors (E. Csiszar & Nagy, 2017). The acid hydrolysis breaks down the inter- and intra-molecular hydrogen bonds to create hydrophilic facile surfaces which can be modified for several industrial applications. In most cases, sulfuric acid and hydrochloric acid are employed. However, the use of hydrochloric acid produces unstable colloidal particles, and hence its application is limited (H. Yu *et al.*, 2013). On the other hand, sulfuric acid used in the hydrolysis has relatively higher water consumption. Sulfuric acid treatment is used for the degradation and displacement of the amorphous or non-crystalline

components of cellulose through a hydrolytic breakdown. Both hydrochloric and sulfuric acid affect the type of nanocellulose particles in structure and morphology. Different sources of CNCs also have different dimensions of length and width sizes which eventually result in varied aspect ratios (ratio of length to width size). The rod-like CNCs particles have an approximate width of 3 – 20 nm and length 50 – 2000 nm (Nguyen *et al.* 2016). For example, Cotton rod-like CNCs have dimensions of 100 – 390 nm length and 7 – 15 nm diameter whereas flax CNC is estimated at 100 – 500 nm length and 10 – 30 nm diameter (Postek *et al.*, n.d.). Cellulose nanoparticles from wood produces a lateral size of 3 – 5 nm and length 100 – 300 nm whereas CNCs from tunicates are 15 – 30 nm lateral and 1000 – 1500 nm length (E. Csiszar & Nagy, 2017).

The CNCs, popularly referred to as nanowhiskers show some specific unique characteristics such as high thermal steadiness up to ~300 ^{o}C, stiffness (~150 GPa), tensile stress (approximately 7.5 GPa), aspect ratio (~10 – 100), low coefficient of thermal expansion (~1ppm/K), density (~1.4 g/cm^3), liquid crystalline action in suspension (Postek *et al.*, 1997). Other chemical and physical characteristics are large surface area (~250 m^2/g), surface modification of hydroxyl group and excellent colloidal stability (A. Csiszar *et al.*, 2000; Tang *et al.*, 2015). These unique properties are characterized by employing varied instrumentations such as laser diffraction (LD), TEM, zeta potential analyzer, UV-visible spectroscopy, SEM, XRD, tensile tester and TGA.

Due to the existence of several hydroxyl groups on the CNCs surface, many modifications are feasible because of the high reactivity of the hydroxyl group. These modifications are done using compounds such as silver nanoparticles, porphyrin, polymers, rosins, lectin, and functional groups that bind with the matrixes (Hajlane *et al.*, 2017). These unique features enable their use in a wide variety of applications such as, wastewater treatment, biomedical, electronics, energy and sensors. For example, recent works on the alteration of the CNC surfaces have seen their

applications in the biomedical sector as antibacterial and anti-viral agent, biocatalyst scaffolds, biomarkers or sensors, tissue engineering scaffolds, gene vectors and drug delivery vectors (Barud *et al.*, 2015). CNCs also have low or no toxicity effect when used in humans and hence their usage in inhalers (Muthulakshmi *et al.*, 2017).

Morphological and mechanical properties of CNCs also make them good substrates for fabrication into matrixes to improve their mechanical properties such as high Young modulus of 78 MPa for a 5 %wt of nanocellulose fillers. In some instances, CNCs have been considered as good replacement materials for synthetic petroleum-based materials due to the quest for bio-based and eco-friendly nanocomposites that have arisen in the world for the past two decades. CNCs have great potentials in their application as reinforcement agents due to their excellent mechanical and barrier properties. Additionally, the transparent nature of CNC makes them suitable for use in paper products and packaging material to reduce the humidity effect on paper (F. Huang *et al.*, 2017). Furthermore, CNCs are good potential particles to be applied as nanocomposite fillers, reinforcements, in molecular biology and regenerative medicine (Tan *et al.*, 2015). Biomedically, in a study by Moreno et al. (2016), CNCs composites of protein binding serve as good substitutes for biosensors and cell supports (Moreno *et al.*, 2016). CNCs as a green and cheap material are also applied in many areas including, particular enzyme immobilization, medical materials, emulsion stabilizers, biosensors and drug delivery. In this study, two locally grown plants, namely *acacia sp.* and *palmae sp.* were investigated as sources of cellulose nanocrystals for potential applications in industries.

The *acacia sp.* is a local plant popularly grown in the Eastern region of Ghana. It is called Akutsa in Ewe and Sapo or Sawie in Asante Twi. They are usually beaten from hard woods. The *acacia sp.* has length of about 100 cm and diameter 2 cm. Its natural colour is yellow or pink and

may have high level of lignin which impart on the colour of plant. Some decades ago, *acacia sp.* was very useful when used as a sponge in bathing and washing plates. However, modernity has made it to be of less importance in Ghana due to the introduction of synthetic sponges. Most Ghanaians don't patronize it anymore as sponge. Some people also use it as chewing stick but now have less function due to the use of toothpaste and toothbrush. Currently, there has not been any known research work on *acacia sp.* The *acacia sp.* was selected due to its physical strength, low cost and availability. It also has the ability to be bent into different shape without breaking.

The second plant used is the *palmae sp.* It is popularly called Keteku in Ewe, one of the Ghanaian south-eastern local tribes. It is also known as Afie in Asante Twi, because of its use as a cane for punishing students. The *palmae sp.* is usually pinkish in colour with lots of colour pigment called lignin. Palmae sp. varies in sizes from few millimeters in diameter and about 300 - 400 centimeters in length. It is usually grown around central part of Ghana and it's a non-fruit producing plant which is not grown for food. Keteku is widely used in Accra in weaving basket, hats and mats and strong for rope. The *palmae sp.* was also selected for its physical strength, bendability, low cost, and availability. Research has shown that there has not been any known study on both the *acacia sp.* and *palmae sp.* plants in Ghana and hence the need for this studies.

1.2 Problem Statement

About 40 – 50 % of plant biomass is constituted by cellulose from which cellulose nanocrystals are extracted. These extractions of CNCs are affected by the type of plants, environment and various methods of isolation. As a result, the aspect ratio of CNCs varies from one geographical location to the other. In Ghana, there are many plant and biomass materials that have these potentials of providing a good source of cellulose for the production of CNCs through base and

acid hydrolysis. However, little or no work has been done on the local plant biomass in Ghana as far as the isolation of CNCs is concerned. In this study, two novel local plant materials namely *acacia sp.* and *palmae sp.* have been selected as the major source of the extraction of CNCs in Ghana.

1.3 Justification

Even though there exist many biomass in Ghana, not much has be done in using them as potential starting materials for the isolation of cellulose nanocrystals. This work therefore seeks to extract CNCs from two local plant materials, namely *acacia sp.* and *palmae sp.* that have not been worked before. Additionally, since the environment, type of plants and mode of extraction affect the aspect ratio and for that matter the physicochemical properties of the isolated CNCs, this work would serve as a good ground to compare these isolated CNCs with other standards.

1.4 Aim

The main purpose of this project is to isolate cellulose nanocrystal from two local plant materials and compare their physicochemical properties which can be used as a reinforcement material in biodegradable films comparable to petrochemical-based packaging films.

1.4.1 Objectives

The specific objectives are:

- to extract CNCs from two local plant materials, *acacia sp.* and *palmae sp.*
- to characterize cellulose nanocrystals using SEM, XRD, FTIR and TGA
- to compare the physicochemical properties of the extracted CNCs

CHAPTER TWO

2.0 LITERATURE REVIEW

2.1 Introduction

Cellulose is one of the most important components of plant cell wall. It is a hard, fibrous and water-insoluble polymer which plays a vital role in preserving the structure of plant cell walls (J. George *et al.*, 2014; J. George *et al.*, 2011). It forms about 15 – 20% of the dry weight of plant cell wall and is present in greater amount in secondary cell wall than primary cell wall. Cellulose fibers in the cell wall of plants are surrounded by two main components namely lignin and hemicellulose coupled with other materials such as ash and with an amorphous and crystalline domain. It is a homopolysaccaharide of repeated D-glucopyranose units made up of carbon, hydrogen, oxygen with a general formula of $(C_6H_{10}O_5)n$ (Razalli *et al.*, 2017), where 'n' refers to degree of polymerization, DP. Depending on the DP, there are three main type of cellulose, namely alpha (α), beta (β) and gamma (γ). Alpha, beta and gamma type of cellulose have degree of polymerization of more than 200, between 10 and 200 and below 10 respectively. Alpha cellulose dissolves faster in about 16.5% NaOH at 20 ^{o}C followed by beta and gamma (Ritter, 1929).

The alpha cellulose is usually used to express the highest form of purity of cellulose. Different plant species have different types and level of cellulose in their cell wall. Plant sources of cellulose include cotton, bamboo, wood, agricultural waste, maize and biomass. Bacteria and other sea living organisms like tunicate are also great sources of cellulose. Among all these sources, cotton has been discovered as the purest source of cellulose. Studies have also shown that depending on the climatic conditions and soil types for plant growth, the percentage of cellulose may differ. Thus the cellulose content of plants in tropical areas may be different from

those in temperate regions. Cellulosic materials are of substantial demands and importance due to the distinctive properties of the nanocellulose crystals with their varied green and sustainable application in industries. Because of these special characteristics, many scientists have developed key interest in working on cellulose.

2.2 Cellulose

2.2.1 Chemistry of cellulose

The component of cellulose is found to be homopolysaccharide of anhydroglucose units joined by glycosidic linkage bonds with repeated cellobiose as the coupling units. Figure 2.1 shows the chemical component of cellulose made of repeated unit of cellobiose joined covalently by β-1,4 glycosidic bonds (Johnsy George, 2012; J. George *et al.*, 2014; Johnsy George *et al.*, 2011; Johnsy George *et al.*, 2012). The cellobiose units are composed of two β-D-anhydroglucopyranose units bonded by the 1-4 glycosidic bond. This is shown in Figure 2.1. Cellulose has three hydroxyl groups for intra and inter hydrogen bonding which gives the rigid and tough property of cellulose in plant cell walls. This interaction of the three hydroxyl groups of the glucose units form microfibril or elementary fibril of dimensions, 3- 4nm in diameter and 1-2 um in length. Microfibrils of diameter 10 -15 nm entwine into a network to form fibril and this makes them stronger than steel of same length. (Du *et al.*, 2017; Y. Wang *et al.*, 2006). The microfibrils combine to form macrofibrils of diameter 15 to 16 nm and length, few micrometers which are later packed into cellulose fibres of diameter 20 to 50 um and length 1 to 4 mm (Lavoine & Bergström, 2017). Each microfibril of cellulose contains nanocrystalline rod-like fragments which is referred to us cellulose nanocrystals or cellulose nanowhiskers which have regular arrangement of anhydrous glucose. This regular arrangement known as micelle also makes cellulose crystalline, rough and rigid. (Du *et al.*, 2017) The crystalline part of cellulose is

a major part of cellulose made up of regular arrangement of beta-anhydroglucose units joined together by 1-4 glycosidic linkage. This regular arrangement makes cellulose exhibit crystalline nature with unique physical properties.

The amorphous part of cellulose is the non-crystalline part of cellulose with irregular structured arrangement of anhydrous glucose via glycosidic bonds. This irregular arrangement enables them to be removed by acid hydrolysis (Cherian *et al.*, 2011; Cherian *et al.*, 2010).

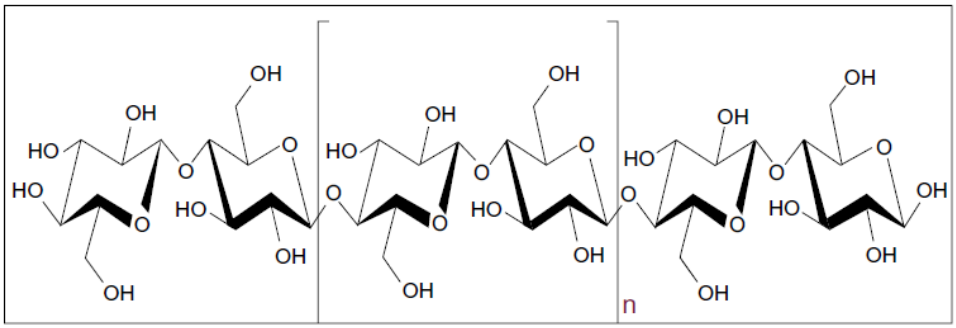

Figure 2. 2 The chemical structure of cellulose, made of cellobiose covalently linked with β (1–4) glycosidic bonds.

2.2.2 Sources of cellulose

The main source of cellulose is plants. Others include algae, bacteria, and some sea living organism known as tunicate. Many cellulosic materials have been used to produce nanocellulose crystal over the past few years. The source of cellulose is one of the vital factors that affect the shape and structure of nanocellulose crystals. Each cellulosic material produces its own unique form of nanocellulose crystals in length, diameter, and morphology. Different materials have different level of cellulose which eventually affect the yield of CNC produced. Example of materials used are cotton (E. Csiszar & Nagy, 2017; de Morais Teixeira *et al.*, 2010; Yang *et al.*, 2018), pineapple (Cherian *et al.*, 2011; R. B. Santos *et al.*, 2013; R. M. d. Santos *et al.*, 2013),

rice straw (Ahmadi *et al.*, 2015; Lu & Hsieh, 2010, 2012), corn (S. Huang *et al.*, 2017; Yu *et al.*, 2014), sugarcane bagasse (de Oliveira *et al.*, 2016), coconut husk (M. F. Rosa *et al.*, 2010) soy (Neto *et al.*, 2016; Neto *et al.*, 2013), potato (D. Chen *et al.*, 2012), garlic (Kallel *et al.*, 2016) and tomato (Jiang & Hsieh, 2015). The following are some of the major sources of cellulose.

2.2.2.1 Plant/Agricultural residue source of cellulose

Plant sources of cellulose are cheap and readily available. Different parts of plants including stem, leaf and fruit serve as the major source of cellulose. Some of the plants include jute, ramie, sisal, flax, hemp, cotton and wood (E. Csiszar & Nagy, 2017; de Morais Teixeira *et al.*, 2010; Yang *et al.*, 2018). Wood is a major source of cellulose, (B. Li *et al.*, 2015; Moriana *et al.*, 2016; M. F. Rosa et al., 2010) but Cotton contains the highest form of pure cellulose, 95 – 97% with a diameter fibril of 500 nm and longitudinal length of few microns with a high crystallinity. (E. Csiszar & Nagy, 2017; de Morais Teixeira *et al.*, 2010; Morais *et al.*, 2013). This is ascribed to the low noncellulosic parts of cotton cellulose when contrasted to wood. Studies have shown that most agricultural biomass such as wheat, sawdust, oil palm, corn straw, rice straw, sugarcane bagasse, sugar beet, jute, pineapple, bamboo, mengkuang leaves and cotton stables produce an appreciable level of cellulose (Cherian *et al.*, 2011; Khoshkava & Kamal, 2014; Z. Li *et al.*, 2016). However, wood is a fetching source of cellulose because of its relative abundance on earth. Plant materials are usually strong, stiff, tough and low in density with high proportion of cellulose.

2.2.2.2 Bacterial source of cellulose

Bacteria cellulose is made by microbial actions of certain bacteria species. Some examples of these species include *Komagataeibacter xylinus and K. xylinus* during vinegar fermentation.(J. George *et al.*, 2014; J. George *et al.*, 2011; Johnsy George *et al.*, 2012). The most common bacteria species used is the Gluconacetobacter xylinus. These bacteria species produce thick gel usually with high volume of water, 97 – 99 mL in a well culturing environment. Bacteria cellulose are also considered as one of the purest form of alpha cellulose devoid of hemicellulose and lignin. (Chi & Catchmark, 2017; Mohammadkazemi *et al.*, 2015; Nogi & Yano, 2008; Shankar *et al.*, 2018). The degree of polymerization is relatively high in bacterial cellulose, between 2000 and 6000. Even though different sources of cellulose produce different characteristic nanocellulose crystals, research shows that both bacterial and wood sources have similar properties. However, these pure form may cause contamination in the alimentary carnal of humans. (M. George *et al.*, 2017)

2.2.2.3 Algae source of cellulose

The cell wall of many algae is composed of highly crystalline cellulose. Red, green and yellow algae are the main types of algae that produce cellulose in moderately high quantity. Of these three types, green algae are considered to be the most favorable *(Mihranyan, 2011).*

2.2.2.4 Tunicate

The cellulose is found in their thick skeletal mantle which covers the epidermis of tunicate.(J. George *et al.*, 2014). It is produced by enzyme action in the membrane of the epidermis and may vary from one species to another. The cellulose produced in the outer skin of tunicates are called

tunic. These tunics are used to form the pure form of cellulose referred to us tunicin. Different species of tunicate have been used to produce CNC. These include sea squirts Ascidiacea, Halocynthia roretzi, Halocynthia papillosa. and Metandroxarpa (Cherian *et al.*, 2010)

2.2.3 Forms of cellulose

Cellulose occurs in varying forms. Below are the forms of cellulose.

2.2.3.1 Cellulose nanofibrils

Generally cellulose nanofibrils, CNFs have dimensions of 3 to 50 nm in diameter and few micrometers in length (Lavoine & Bergström, 2017) which is usually produced via caboxymethylation, carboxylation, quaternation, pre-enzyme treatment or pre mechanical treatment. The cellulose nanofibrils contain both crystalline and amorphous parts which are further broken down into nanocellulose crystals via acid hydrolysis.

2.2.3.2 Nanocellulose crystals

Nanocellulose is a nanomaterial with distinct chemical and physical properties of low density, renewability, biocompatibility, tunable surface chemistry of the hydroxyl groups and high strength. In 1950 Ranby and Ribi produced the first colloidal sulphonated CNC using sulfuric acid hydrolysis from wood and cotton (R. M. d. Santos *et al.*, 2013). Researchers have used several acids such as hydrochloric, phosphoric, hydrochromic and phosphotungstic acid to extract CNCs (Tang *et al.*, 2015).

Nanocellulose may exist as aerogel which are mesoporous material with approximate porosity of 90% (2 to 50 nm pore size). This flexible and strong aerogels can be used in sound absorption and insulation due to their low thermal conductivity and dielectric property. In addition the ultra-

low density, tunable surface chemistry and unique mechanical characteristics of CNC make them favorable in constructing biomedical scaffolds, insulators, and devices for storage. (Lavoine & Bergström, 2017).

2.2.4 Properties of CNCs

2.2.4.1 Mechanical properties

CNCs are unique in mechanical properties. They are very stiff, strong and elastic. This is as a result of the regular arrangement of the crystalline glucose domain of cellulose. Presence of both crystalline and amorphous domain of cellulose, make nanocrystals have different modulus. The theoretical estimated axial modulus of CNC is approximately 50 – 170 GPa, giving a value close to Kevlar (60 – 125 GPa) which is tougher than steel (200 – 220 GPa) (Kaushik, 2016).

The theoretical predictions of the tensile strength are approximately 0.3 – 22 GPa. High tensile strength of nanocellulose emanate from the increased chain structure of crystalline cellulose domain, large number of inter and intra hydrogen bonding. In addition, there is high density of covalent bonds in CNCs which make them exhibit high tensile strength.

2.2.4.2 Physical properties

The 4-anhydro-D-glucopyranose in glucose possesses a chair conformation sequentially and is able to rotate through 180^{o}. The three OHs on each constituent can form high hydrogen bonds to form slender fibre structures and semicrystalline packing which account for the high cohesiveness of cellulose. Each nanocrystalline particle is an elongated needle-like or rod-like structure of diameter, 5 – 30 nm and length, 100 – 500 nm. CNCs are very stiff and strong with young modulus of approximately 139.5 ± 3.5 (Wu *et al.*, 2010).

2.2.4.3 Rheological properties

The deformation and flow of particles is yet another unique property of CNCs. This is influenced by the liquid crystalline nature of CNCs. Other factors influencing such properties are the spatial ordering and gelation of the particles. Dilute suspension of CNCs also show shear thinning at low concentration (Bercea & Navard, 2000). However, CNCs at high concentration deviate from the original shear property. And this is due to the rod-like structure of CNCs which make them orient at critical shear rate that destroys the chirality of the crystals. The aspect ratio also affects the rheology of the crystals. At higher aspect ratio, the particles in CNCs tend to have high relaxation time which favors the alignment after shear (Majoinen *et al.*, 2012). Different acid exhibit varying shear thinning. CNCs produced via sulfuric acid tend to have low shear thinning where as those of hydrochloric acid have very high shear thinning. This is because, the CNC produced via hydrochloric acid do not have chiral centers (Hasani *et al.*, 2008).

2.2.4.4 Chemical properties

CNCs have many hydroxyl groups which enable them to be subjected to several surface modifications with different chemical substances. The ability to undergo surface modification or functionalization makes them have positive or negative charges for further applications. Some of the surface functionalization includes esterification, etherification, amidation, oxidation, carbamation, polymer grafting, silylation and nucleophilic substitution. Sulfation and phosphorylation are the basic esterification processes which lead to formation of chiral centers for further application. The surface modification of cellulose also enhances the production of nanocomposites for applications in the industries such as plastics, water, biomedical engineering.

2.2.4.5 Liquid crystalline properties

Under suitable conditions, CNCs exhibit liquid crystallinity due to the regular ordered arrangement of the particles called a nematic phase. The rod-like structure of the CNCs particles forms chiral centers when dispersed in water to exhibit crystallinity. Their liquid crystallinity emanates from their hardness, aspect ratio and the capacity to orient in solution. The CNCs have cholesteric phase or chiral nematic phase due to helical twist structure like a screw. The liquid crystallinity property is affected by shape, electrolyte, size, charge and external stimuli factors. Due to the liquid crystallinity property, CNCs exhibit unique bi-refrigerant property which produces interesting optical phenomena.

2.3 Hemicellulose

Hemicellulose contributes about 20 - 30% of dry weight of soft and hardwood. It is the alkali soluble component of plant cell wall after the removal of pectic substances. Like cellulose, hemicellulose has degree of polymerization in the range of 50 – 300 and heteropolysacharides constituents with their monomeric components as anhydrohexoses, anhydropentoses and anhydrouronic acids (Table 2.1). Hemicellulose is vital in plant cell wall in crosslinking with cellulose fibrils and lignin matrix to increase the mechanical strength of cell wall. Hemicellulose, like lignin has low decomposition, which is made of acetyl and uronic ester groups. In the determination of the presence of hemicellulose in a plant material using the FTIR, an eminent peak at 1200 to 1300 cm^{-1} is characteristic of C-O bending vibration in the uronic ester group. (Deepa *et al.*, 2011; Maiti *et al.*, 2013).

Table 2. 3: Relative amount (%) and degree of polymerization of major hemicelluloses in different softwood and hardwood species

Material	Hemicellulose content	Degree of polymerization
Softwood		
Loblolly pine	15.3	……
Black Spruce	17.4	……
Galactogucomannan	~20	40-100
Gluconoxylan	5-10	50-185
Hardwood		
Birch	33	……
Gluconoxylan	15-30	~200
Gluconomannan	2-5	~70

2.3.1 Chemical Structure of Hemicellulose

Structurally, there are four main types of hemicellulose, namely; xyloglycans (xylans), mannoglycans (mannans), β-glucans, and xyloglucans.

2.3.1.1 Xylans

Xylans, constitute the main component of hemicellulose of about 20 - 15 % in softwood (juniper, pine, redwood and yew), 10 - 35% in hardwood (mahogany, oak, walnut and balsa) and 35 - 40%

of the total biomass residue of some annual plants. Xylan, also called xyloglycans has two forms, homoxylans and heteroxylans. The homo unbranched xylan comprises of β (1-4)-D-xylopyranose joined together by (1-3, 1-4) or (1-3) glycosidic linkages which are commonly found in seaweeds. Heteroxylans, have more complex substituted structures made of glucuronoxylans and arabinoxylans.

2.6.1.2 Mannans

Mannans refer to the linear polymer polysaccharides of sugar mannose monomers. It is usually found in plant yeast. Galactoglucomannan is the main hemicellulose in soft wood of about 20%.

2.6.1.3 Beta – glucans

Beta-glucans are sugars linked by β-glycosidic bonds which are usually found in cell walls of bacteria, yeast, fungi, lichens and algae. Glycosidic linkage in beta glucan exist between carbon 1 and 3 or 1 and 6. Research shows that beta-glucans have some health benefits in treating diabetes, HIV/AIDs, cancer, high cholesterol level, cold, skin diseases and hepatitis.

2.6.1.4 Xyloglucans

Xyloglucans are the most inexhaustible hemicellulose in the cell wall of vascular plants. Xyloglucan often binds cellulose fibrils together and has a β1→4-linked glucose, most of which are replaced with 1-6 linked xylose side chains. Xylose remnants are usually capped with a galactose remnants, sometimes followed by a fructose residue. Below is the structure unit of xyloglucans.

2.4 Lignin

In 1813, the Swiss botanist A. P. de Candolle defined lignin as a fibrous, insipid material which does not dissolve in water and alcohol but dissolves in weak base and can be precipitated by an acid (de Candolle, 1813). Lignin is a complex polymer of cross-linked phenols which plays a very important role in plants particularly, wood and bark for their rigidity because it does not rot easily. It constituent about 20 - 35% (J. Li *et al.*, 2011) of dry wood, 14 - 25% herbaceous plants (Y. Chen *et al.*, 2009) and about 30% (Boerjan *et al.*, 2003) of non-fossil organic carbon. Physically, lignin is very hard, compact and strong. Lignin has phenylpropanoid as repeating unit held together by ether bond or carbon-carbon bond which enhance the hardness of plant cell wall, as well as the mechanical support of plants via high link network (Song *et al.*, 2013). The phenolic compounds in lignin is the colour pigment which gives colour to each cellulosic material. Thus an indication for the absolute elimination of lignin is the perfect change of color in the plant materials.

2.7.1 Chemical composition and structure of lignin

Lignin is a heterogenous polymer of guaiacyl propane (G), syringyl propane (S) and hydroxylphenyl propane (H) units linked by ether bond, carbon-carbon bond and β-O-4 ether bond. It is a crosslink of the three main lignols which are consolidated into lignin in the structure of phenylpropanoids. Depending on the type of plants lignin varies in the combination of the various constituents. In the dicotyledonous angiosperm plant, G and S are present. Whereas in monocotyledonous lignin, all the three constituent are present in approximately equal proportion. The degree of polymerization, DP of lignin is approximately 4000 and has molecular unit above 10000 u. They are usually of aromatic polymers which are relatively hydrophobic. Lignin is

highly cross-linked and also amorphous like hemicellulose. The ester linkage between the hydroxyl group of lignin and carboxyl of uronic acid of hemicellulose are highly affected by alkali treatment. Thus lignin is partly removed by base hydrolysis but more effectively removed via bleaching using hydrogen peroxide, and sodium chlorite. Lignin however does not dissolve in acid and therefore usually hinder acid hydrolysis. In order to facilitate the acid treatment, delignification via bleaching is paramount for the extraction of pure nanocellulose cyrstals.

2.5 Inorganics

Another component of plant materials is inorganics which basically refers to the ash content. The ash content represents the mineral salts and other inorganic matter like silica. Their percentage in plant is minute but may interfere with chemical processes. Usually they are burnt and removed at relatively high temperatures (Han & Rowell, 1997).

2.6 Proteins

Proteins form approximately 1% of the chemical component of plant materials. They are large polymers of amino acids, enzymes, toxins and occur in three main classes namely, glycine-rich protein, proline-rich protein and hydroproline protein. The proteins are usually connected to the lignin in plant materials that makes them to be removed during the bleaching process.

2.7 Extractives

Extractives are made up of various monomers, dimers and polymers of waxes, resin acid, steroids, terpenes, phenols, fatty alcohols, fatty acid and fats. They are easily removed by one of the many extraction processes and hence the name extractives. These also refer to other non-cellulosic components such as pectin, ash, suberin, cutin, wax and fatty substance which reduce

water losses from cell wall. Pectin substances are easily broken by enzymes and acids to be washed away. The extractives are also usually hydrophobic and plasticized. (Song *et al.*, 2013).

2.8 Nanocellulose extraction

The preparation of cellulose whiskers or CNCs involves two main stages, namely, base and acid treatments. The main aim of these treatments is to extricate lignin, hemicellulose, ashes and other impurities. The following are the stages of extraction of nanocellulose crystals.

2.8.1 Mechanical treatment

Plant materials usually come in big and large surface areas. Many plant substances are chopped into smaller sizes and milled into powder. Simple blender is used for soft wood plant materials. However, in milling hardwoods, robust milling machines are used. The powdered samples are sieved to obtain uniform surface area. This enhances the subsequent chemical treatments.

2.8.2 Base hydrolysis

The first hydrolysis process in the extraction of cellulose nanocrystrals is the alkaline hydrolysis which requires the addition of bases such as sodium hydroxide or potassium hydroxide. This process removes the irregular amorphous hemicellulose domain of the fiber. Usually, dilute base of 4 or 5%wt of NaOH or KOH is enough to break into the hemicellulose structure. The alkaline hydrolysis dissolves the hemicellulose which is washed away to a pH of 7 using a centrifuge. Often, some extractives like terpens, resin, fats, fatty acid, waxes and toxins are removed with the hemicellulose during the alkali treatment. (Ng *et al.*, 2015)

2.8.3 Bleaching process

The bleaching treatment of the cellulosic material is usually done after the base hydrolysis. The aim of this process is to isolate the lignin component of the fiber. The lignin component which is the color pigment of the fiber is bleached using hydrogen peroxide, glacial acetic acid and sodium chlorite. The hydroxyl radical or chlorine radical is able to break into the aromatic phenolic rings of the lignin and washed away.

Bleaching reaction scheme;

$$H_2O_2 \longrightarrow H^+ + HO_2^-$$

$$HO_2^- \longrightarrow OH^- + [O]$$

$$[O] + I \longrightarrow IO$$

Where 'I' refers to the lignin materials and some impurities associated with cellulose (Ng *et al.*, 2015).

2.8.4 Acid hydrolysis

Acid treatment is the last stage of the hydrolysis process in the isolation of nanocellulose crystals. Surface sulfate ester groups are often produced when sulfuric acid is used (Beltramino et al., 2015; Du et al., 2017; J. George et al., 2011; Q. Q. Wang *et al.*, 2012; Y. Wang et al., 2006; H.-Y. Yu *et al.*, 2013). Other acids commonly used are hydrochloric acid (H.-Y. Yu et al., 2013; H. Yu et al., 2013) (Figure 2.3), oxalic acid (Deepa *et al.*, 2011), bromic acid, formic acid and phosphoric acid (Tang *et al.*, 2015) (Table 2.2).

Sulfuric acid is usually preferred to other acids because of the stability of the surface charged nanocellulose crystals which lead to a colloidal suspension of cellulose fibers as a result of the electrostatic negative charges from the O-SO_3H (Figure 2.3). Other acids like HCl are unable to produce surface charges during the hydrolysis process (Figure 2.2).

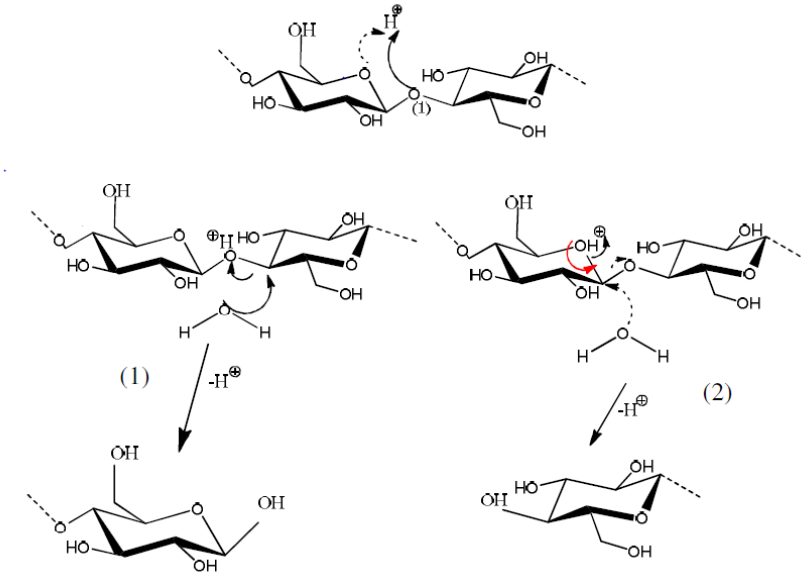

Figure 2. 2: Mechanism of acid hydrolysis of cellulose using hydrochloric acid

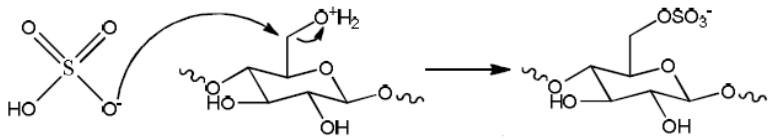

Figure 2. 3: Mechanism of acid-catalyzed hydrolysis of cellulose using sulphuric acid

Table 2. 4: Diverse acid hydrolysis for extraction of CNCs (Tang *et al.*, 2015)

Sources	Chemicals	Conditions
Old corrugated container	Phosphoric acid	25^{o}C, 6 h
Cotton	Sulfuric acid	60^{o}C, 2 h
Kenaf fiber	Sulfuric acid	80^{o}C, 4 h
Corncob	Sulfuric acid	45^{o}C, 45 min
Rice husk	Sulfuric acid	50^{o}C, 40 min
Coconut husk fiber	Nitric acid	70^{o}C, 1 h
H. Sabdariffa fiber	Oxalic acid	20^{o}C, 3 h

2.9 Characterization techniques.

In order to confirm the extracted nanocellulose crystals for further application, the following characterization techniques are employed.

2.9.1 FTIR

The FTIR of a sample is one of the main parameters in characterizing cellulose nanocrystals. In this characterization technique, functional groups of the isolated compound are used to determine the intrinsic physicochemical properties of the nanocellulose crystals. For example a peak at 3400 cm^{-1} corresponds to a hydroxyl group on the cellulose. A close examination of FTIR spectrum is able to determine when all hemicellulose and lignin have been removed due to the disappearance of some important peaks from the original. In a research by Hanieh Kargarzadeh

et al. (2012) where a study on the effects of treatment conditions on the shape, crystallinity and thermal stability of CNCs extracted from Kenaf fibers were conducted, the FTIR spectra of the raw fiber, after base and bleaching, confirm a complete removal of the hemicellulose (Kargarzadeh *et al.*, 2012).

2.9.2 SEM

Morphology, topography, composition and crystallographic information of CNC are major characteristics that distinguish it from other materials. The rod-like (may be curled) or needle-like shape of CNC is determined by the scanning electron microscopy, SEM. (Morais *et al.*, 2013). The SEM is employed because of the nano-size of the cellulose materials. It is also employed due to its high magnification, high resolution, 3-dimensional image and larger depth of analysis (Sheltami *et al.*, 2012).

2.9.3 TEM

TEM is of higher resolution than SEM and gives the geometric dimensions of diameter and length of the isolated crystals in nano-size. The TEM also help calculate the aspect ratio (length/diameter) (Chi & Catchmark, 2017; Deepa *et al.*, 2011; Du *et al.*, 2017; Morais *et al.*, 2013; Moriana *et al.*, 2016; Tummala *et al.*, 2017) which determines the suitability of the crystals as reinforcement (W. Chen *et al.*, 2011).

2.9.4 TGA

Internal stability due to high resistivity to heat is one of the unique inherent physical characteristics of CNC. CNCs are very stable with a high crystal structure which prevents them

from getting decomposed easily. This intrinsic characteristic of CNCs makes it suitable for the production of plastics for packaging. The CNC basically decompose at high temperatures of approximately 300 ^{o}C (Deepa *et al.*, 2011; Fortunati *et al.*, 2014; Jung *et al.*, 2017; Maiti *et al.*, 2013; Y. Wang *et al.*, 2006)

2.9.5 XRD

X-ray diffraction is used to determine the crystallinity of cellulose by calculating the crystallinity index, I_x of the sample. Basically, the crystallinity of cellulose increases through the extraction stages from base hydrolysis, bleaching to acid hydrolysis because of the removal of the irregular non-crystalline components of cellulose. X-ray diffraction is therefore able to identify the crystalline material and the non-crystalline part. It is also used to determine the crystal structure and the d-spacing of the constituent particles. In this process a cathode ray is generated by heating the filament at a particular voltage to release electrons. These electrons are converted into a monochromatic light intensity and irradiated against the samples. The monochromatic light is therefore diffracted at a specific unique angle since each particle interacts with the light differently. The crystallinity index is recorded and plotted against the diffraction angle. The diffraction angular range 2Ɵ is in the range of 5 – 40^{o} and a step time of 2.0 s

$$CrI = (I_{200} - I_{am}) / I_{200}$$

CrI is the crystallinity index

I_{200} is the maximum intensity at the 200 lattice plane

I_{am} is the amorphous intensity at approximately 2Ɵ = 18 ^{o}

2.10 Factors affecting isolation of CNC

2.10.1 Concentration of Acid and Base

The concentration of the base and acid affects the CNC produced in morphology, structure, and geometry. At high concentration, hydrolysis is very effective in breaking the glycosidic bonds of the cellobiose to produce high crystalline nanocellulose (Ahmadi et al., 2015; Beltramino et al., 2015; Bondeson *et al.*, 2006). However, high concentration of the acid, over a long period of treatment may burn the cellulose samples due to the excessive heat produced by the acid (Bondeson *et al.*, 2006). At low concentration, the hydrolysis may not be effective due to the low level of protons produced to penetrate the amorphous region of cellulose. Different concentrations produce varied diameter and length of CNC with different aspect ratio. For example, concentrations of H_2SO_4 from 64, 63 and 59 %w/w produce CNCs with different dimensions in diameter and length (Kargarzadeh *et al.*, 2012).

2.10.2 Temperature

Basically, hemicellulose and lignin which are the main impurities associated with cellulose tend to dissolve at high temperature of 70 to 80^{o}C. (Eronen *et al.*, 2011; Yoshida *et al.*, 2008). In a study by Yang et al. (2018), it was observed that hemicellulose, lignin and cellulose degrade at varying temperatures due to structural changes. In effect, individual components can be isolated depending on the temperature of the process. The base hydrolysis temperature for the removal of hemicellulose is higher than the acid hydrolysis. Acid hydrolysis may occur at room temperature and increase to about 70 ^{o}C depending on the concentration (Beck-Candanedo *et al.*, 2005). At

high concentration of acid, temperature will have to be reduced due to the excessive heat produced via the preparation of acid solution (Kargarzadeh *et al.*, 2012).

2.10.3 Time

Isolation of nanocellulose crystals is time dependent in the base and acid hydrolysis as well as the one-step-ammonium persulphate (APS) process. The minimum time of base hydrolysis is 2 hours (Bondeson *et al.*, 2006). The time of the hydrolysis depends on the concentration of the base used. High concentration of sodium hydroxide, about 4 M requires 2 hours whereas low concentration of about 2 M requires longer time, about six to eight hours (Cherian *et al.*, 2010). During the acid treatment of cellulose to remove the irregular amorphous region, the duration of the process also influences the diameter, length and structure of CNCs. Long time (about 5 hours) of hydrolysis reduces the length of rod-like CNCs as evidenced during the extraction of CNC from cotton (Dong *et al.*, 2016), wood (Beck-Candanedo *et al.*, 2005), pea hull fibers (Y. Chen *et al.*, 2009), microcrystalline cellulose (Bondeson *et al.*, 2006) and coconut husk fibers (M. Rosa *et al.*, 2010). In this research work it was observed that the at high concentration of acid, approximately 64 %w/w, less time of about 30 mins is required whereas low concentration of about 2 %w/w may require a whole day. The one step Ammonium persulfate, APS process requires about 24 hours when concentration is relatively low. However, at very high concentrations, about 6hours is required. Comparatively, the APS method saves time as base and acid hydrolysis process are time consuming.

2.10.4 Type of acid

Different acids produce varying forms of nanocellulose crystals. Some of the acids that have been used include, sulfuric acid (Beltramino et al., 2015; Du et al., 2017; Q. Q. Wang et al., 2012; Y. Wang et al., 2006), formic acid (B. Li *et al.*, 2015), hydrochloric acid , phosphoric acid (Tang *et al.*, 2015) and bromic acid. Among these acid types, sulfuric acid and phosphoric acid have produced more stable cellulose nanocrystals due to their ester formation at the surface of cellulose. Their nematic structure enhances their stability. In addition, the sulfate ions and phosphate ions generate a high electrostatic force of repulsion that enhances the uniform dispersibility of nanocellulose in solution (Beck-Candanedo *et al.*, 2005; de Souza Lima & Borsali, 2004). Those produced via hydrochloric acid tend to lack chiral nematic centers which do not enhance dispersion.

2.10.5 Type of base

Sodium hydroxide has been the most widely used base in the alkaline hydrolysis process for the synthesis of CNC due to its ready availability, cheap cost and easy to handle. Other bases that have been used over the past decade include potassium hydroxide. The concentration of base ranges from 2 M to 4 M which determine the length of the base hydrolysis process. Lower concentration of base requires longer time for the removal of hemicellulose whereas high concentration takes few hours for effective removal of hemicellulose.

2.11 Applications of Nanocellulose

CNCs have great advantage in their application because of their high mechanical strength, surface area, availability, sustainability, renewability, biodegradability, and specific aspect ratio. The hydroxyl groups are modified by the process such as esterification and acetylation to

produce surface carboxylic acid, amine, protein and thiol functional group for several industrial applications such as waste water treatment, biomedical and reinforcements in packaging materials

2.12 Cellulose nanocrystal studies in Ghana

Studies on the extraction of CNCs from Ghanaian local plants have been very minimal. Very few studies have been carried out on the potential application of cellulose nanocrystals in the packaging industries, water treatment and biomedical engineering (Suopajärvi *et al.*, 2013).

CHAPTER THREE

3.0 EXPERIMENTAL

This chapter focuses on the detailed procedures in isolating nanocellulose crystals from two local Ghanaian plants and their characterization.

3.1 Containers and cleaning process

All glassware and Eppendorf tubes used in the isolation of nanocellulose crystals were cleaned in a detergent for 6 h, washed and rinsed with deionized water two times. They were later immersed in 50 % HNO_3 bath at 90 ^oC for a period of 24 h, rinsed several times and dried overnight.

3.2 Reagents

All chemicals used were of analytical reagent grade. Sulfuric acid, H_2SO_4 (98 %) was purchased from Kosdaq Company, 30 % w/w Hydrogen peroxide, H_2O_2 from Qualikems Laboratory, sodium hydroxide, NaOH pellet and sodium chorite, NaClO were obtained from the Department of Chemistry.

Phytochemical reagents used for phytochemical tests were prepared according to the following procedures to carry out the presence of chemical compounds such as saponins, flavonoids, alkaloids and polyphenols which naturally occur in plant extracts.

3.2.1 Preparation of alkaloids testing and screening for alkaloids

a) Wagner's reagent: about 1 g of iodine and 2.0 g of potassium iodide were dissolved in water in a volumetric flask and the solution made up to 100 mL with water. The reagent was dark-brown in colour.

b) Dragendorff's reagent: 4.0 g of hydrated bismuth was dissolved in 20 mL concentrated nitric acid and the resulting solution added to a 13.5 g of potassium iodide in 25 mL of water. Black precipitate formed was filtered off and the filtrate made up to 50 mL with water. Reagent was orange in colour.

c) Meyer's reagent: 1.4 g of mercury iodide in 60 mL of water was added to a 10 mL solution of 5.0 g potassium iodide in water and made up to 100 mL with deionized water. Reagent was pale yellow in colour.

3.2.2 Preparation of 2, 4-Dinitrophenylhydrazine solution.

3.0 g of 2, 4 dinitrophenylhydrazine was placed in a beaker and 20 mL distilled water and 70 mL of 95 % ethanol added. Mixture was stirred, placed in ice bath and 15 mL of concentrated sulphuric acid was added. A clear orange solution was obtained.

3.2.3 Preparation of Iron (II) chloride solution

100 mL of iron (II) chloride solution was prepared by mixing 10 mL aqueous iron (II) chloride and 90 mL of distilled water. A clear pink solution was obtained.

3.2.4 Preparation of Potassium ferrocyanate solution

0.2 g of solid potassium ferrocyanate was dissolved in 10 mL of distilled water to obtain a clear solution.

3.2.5 Sodium hydroxide (4 %w/w) in a 250 mL volumetric flask

10.0 g of sodium hydroxide pellets were weighed and dissolved in a beaker of water. The resulting solution was transferred into a 250 mL volumetric flask and topped up to the mark.

3.2.6 Sulfuric acid (64 %w/w)

64 mL of 98 % w/v H_2SO_4 analytical reagent grade was measured and added to a beaker of 36 mL deionized water. The solution was prepared over an icebath due to the excessive heat produced during the preparation of the highly concentrated solution (Filson & Dawson-Andoh, 2009).

3.3 Sampling of plant materials.

3.3.1 Acacia sp.

Samples used for this research work were purchased from the Madina market in Accra and milled at a commercial mill at Koforidua. Figure 3.1 shows the nature of the raw and milled *acacia sp.*

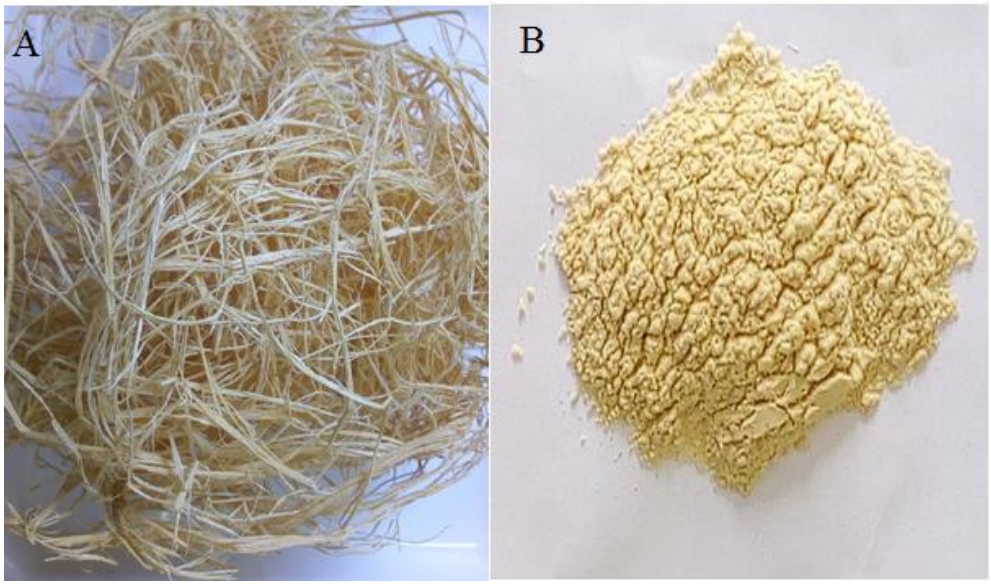

Figure 3. 3: Photographs of (A): raw *acacia sp.* and (B): powdered *acacia sp.*

3.3.2 Palmae sp.

Samples were purchased from the Madina market in Accra, Ghana and milled at Koforidua using the commercial mill. Below is a picture of the raw and milled form of *palmae sp*.; Figure 3.2.

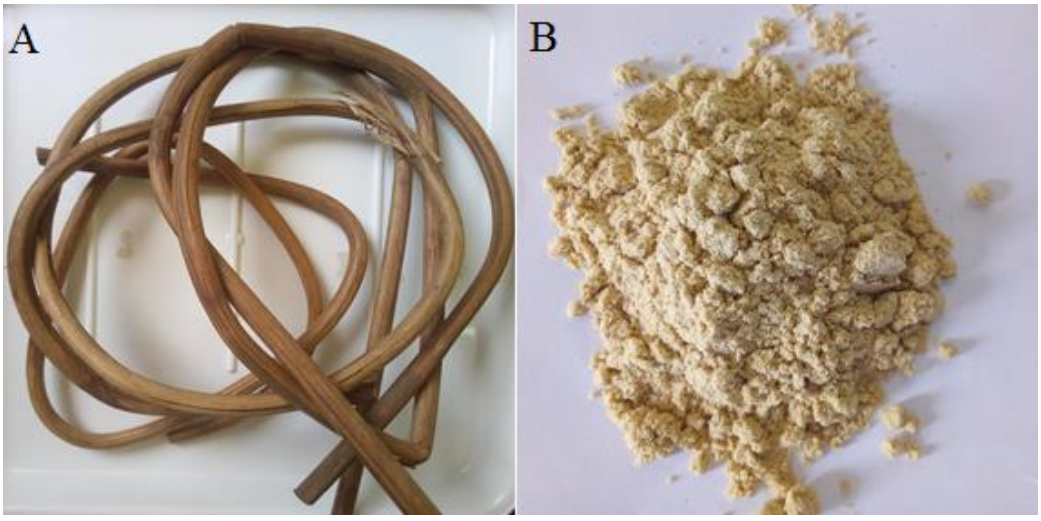

Figure 3.2: Photograhs of (A):raw *palmae sp.* and (B): powdered *palmae sp.*

3.4 Isolation of nanocellulose crystals

Milling, base treatment, bleaching and acid treatment were carried out to extract CNCs from both *acacia sp.* and *palmae sp.*

3.4.1 Milling

Samples were cut into small lengths of about 5 cm and width 2 cm with a pair of secateurs and milled into powder with a commercial milling machine.

3.4.2 Base hydrolysis

150 mL of 4 % w/w of an already prepared sodium hydroxide, NaOH, was used to treat 5.0 g of raw palmae sp. to remove hemicellulose. The solution was heated over a water bath at a temperature of 70 to 80 ^{o}C for 3 h. The process was repeated for *acacia sp*. Pinkish colour of the *palmae sp.* turned into a deep dark-brown solution whereas the yellowish color of the acacia sp. turned into a brown solution. Solution was left to cool and washed with distilled water using a centrifuge at 3500 rcf to a pH of 6 - 7. During washing, the colors faded gradually to light brown.

3.4.3 Bleaching

Repeated bleaching of base hydrolyzed samples was done using 30 % w/w H_2O_2 and NaClO. 150 mL of H_2O_2 was used for the first treatment for 6 h under constant stirring at 70 rpm (Table 3.1). The color of the acacia sp. changed to a pale yellow and centrifuged to decant the supernatant. 150 mL of the NaClO was used for the second bleaching for 24 h to a white color. Solution was centrifuged and supernatant decanted leaving the samples for acid hydrolysis. The same steps were repeated for the *palmae sp*. Here the color change was from light brown to

yellow, pale yellow and white. It was observed that the *palmae sp*. took more time of about 48 h to a white coloration.

3.4.4 Acid hydrolysis

The highly concentrated sulfuric acid of 64 % w/w prepared was used to treat the bleached samples at a temperature of 45 ^{o}C for 30 min (Table 3.1). This was done over an ice bath due to the excessive heat produced by the acid.

3.5.5 Dialysis

In the extraction of cellulose nanocrystals, dialysis plays a vital role. In this process, residual hydrogen ions and other excess ions are removed to present a pure CNCs. This was done for 7 days to ensure a complete removal of ions. A liter of bucket full of deionized water was used each day. During this process, the dispersion is put in a dialysis bag and later placed in the bucket full of water until a constant pH is obtained.

3.4.6 Sonication

Sonication is another vital treatment in the extraction of cellulose nanocrystals. In this process, suspended sulfonated CNCs particles were forced into cloudy colloidal solution by a sonicator. The sonicator was set at thirty second pulse and amplitude at 25 m for 10 min.

3.4.7 Freeze drying

Freeze drying of sonicated samples were done at a very high pressure and very low freezing temperature for three days. Samples however were first frozen and drying was done at high pressure to suck water through sublimation. The resultant products were crystalline.

Table 3. 2: Summary of sequential extraction procedure

Steps	Reagents	Extraction conditions	Name of Process
1	Sodium hydroxide (4% w/w)	70 ^{o}C to 80 ^{o}C for 3 h	Base hydrolysis
2	Hydrogen peroxide (30 % w/w) and Sodium chlorite	Room temperature	Bleaching
3	Sulfuric acid (64 %w/w)	45 ^{o}C for 30 min	Acid hydrolysis

3.5 Sample analyses

3.5.1 Test for Alkaloids:

About 4 mL of the extracted cellulose nanocrystals colloidal solution was treated with 20 mL of 2.0 M HCl solution and the mixture warmed, filtered and divided into three test tubes. To each tube was added a few drops of Meyers, Dragendorff's and Wagner's reagents respectively and observed for appearance of yellowish or reddish-brown precipitate.

3.5.2 Test for steroids:

About 2 mL of acetic anhydride was added to 1 mL of the extracted cellulose nanocrystals colloidal solution. The mixture was boiled, cooled and 2 mL of sulphuric acid was added. A brown ring at the joint of the two layers and the upper layer changing green indicates the existence of steroids.

3.5.3 Test for Flavonoids (NaOH Test)

About 2 mL of the colloidal solution of the extracted cellulose nanocrystals was put in a test tube and added 5 mL of the diluted sodium hydroxide followed by addition of 5 mL of dilute hydrochloric acid. A yellow solution with NaOH turns colorless with dilute HCl which indicates the presence of flavonoids (Table 3.2).

3.5.4 Test for Polyphenolic compounds

About 1 mL of the colloidal solution of the extracted cellulose nanocrystals was put in a test tube and freshly prepared 10 % $FeCl_3$ solution was added and observed for dark green coloration.

3.5.5 Test for saponins

A little amount of the extract was added to 4 mL of water and the resulting solution was shaken strongly and allowed to stand for about 10 minutes. Thick persistent foam indicates the presence of saponins.

3.5.6 Test for tannins

To about 2 mL of colloidal solution of the extracted cellulose nanocrystals in a test tube a freshly prepared iron (III) chloride solution was added. Formation of a dark blue or greenish grey coloration of the solution indicates the presence of Tannins.

3.5.7 Test for Terpenes

About 2 mL of extracted cellulose nanocrystals colloidal solution was put in a test tube and heated to dryness and carbon tetrachloride (CCl_4) was added followed by few drops of acetic anhydride. Concentrated sulfuric acid was added in drops and observed for formation of red solution.

3.5.8 Test for terpenoids

About 2 mL of colloidal solution of the extracted cellulose nanocrystals was put in a test tube with 2 mL of chloroform. 1 mL of concentrated sulphuric acid was gently added along the wall of the tube. The observation of the presence of the reddish brown color at the interface shows the presence of terpenoids.

3.6 Characterization of nanocellulose crystals

FTIR spectroscopy, Optical microscopy, SEM, XRD and TGA were used to characterize the extracted nanocellulose crystals.

3.6.1 Optical microscopy analysis

The raw sample of *palmae sp.* and CNCs were mounted on a microscope slide and viewed with Leica DMLM optical microscope. Bright images were detected and collected on a computer screen. Process was repeated for acacia sp. samples.

3.6.2 SEM

The surface morphology and cross-section of the nanocellulose crystal standard and sample were analysed on scanning electron microscope, SEM (Fei Quanta 250 FEG, USA). The samples were sputter-coated with gold prior to examination. SEM images of pure CNCs were taken at an accelerated voltage of 5.0 kV at three-dimensional plots for individual visualization effect. Statistical experimental designs were constituted and analyzed using Design Expert 7.0 (Stat-Ease, Inc., USA). All experiments were done randomly and independently according to DOE's (Design of Experiment) run order in triplicate and average value of responses were used. (Bilgi *et al.*, 2015)

3.6.3 XRD

The X-ray diffraction analyses were carried out with a Shimadzu diffractometer (XRD-6000, USA) controlled at 40 kV and 30 mA with graphite filtered CuK (λ = 1.5433 Å) radiation. Data were acquired on a 2θ scale from 5 to 40°. The crystalline index of cellulose, CI_r, of the CNCs was determined using Segal's empirical method:

$$CI_r(\%) = [(I_{200} - I_{am})/I_{200}] \times 100 \qquad (1)$$

The I_{200} refers to the peak intensity corresponding to crystalline cellulose I, and I_{am} is the peak intensity of the non-crystalline part. (Segal *et al.*, 1959)

3.6.4 FT-IR

The FTIR of all samples were carried out using Shimadzu, IR Prestige-21, USA over an absorbance range of 4000 – 500 cm^{-1}. The Fourier transform infrared (FTIR) spectroscopy determination was made with KBr pellets in the 500 - 4000 cm^{-1} region with a resolution of 4 cm^{-1} for 30 scans and 0.5 cm^{-1} interval. The mixture of KBr and sample were dried (100 °C, 1 h), and the samples were prepared instantly before measurement. The background spectra were collected, using spectroscopic grade KBr. (Barud *et al.*, 2015; Lustri *et al.*, 2015)

3.6.5 TGA

Thermogravimetric analyses of palmae sp. and acacia sp. nanocrystals were carried out in a Pyris 1 thermal analyzer (Perkin Elmer, USA) at a temperature range of room temperature to 800 °C at a heating rate of 10 °C per minute. The thermogravimetric analysis was done to examine the thermal stability composition, purity, decomposition temperature and absorbed moisture content. It is usually run with a differential scanning calorimeter. In this analysis about 9 mg of the sample was put in an aluminium oxide crucible and subjected to heating in a nitrogen atmosphere. The rate of decomposition was detected as 5 ^{o}C/min. All samples were preserved under an inert atmospheric nitrogen with a flow rate of approximately 20 mL/min. The derivative of each TGA curve was derived using the program Origin 8.1 (OriginLab, USA). (Kiziltas *et al.*, 2015)

3.7 Quality assurance (QA) and quality control (QC)

Experiments were reproduced two or more times to verify the precision of the modified extraction procedure. A certified reference cellulose nanocrystals was analyzed simultaneously with the samples to examine the accuracy of the instrumental analysis.

CHAPTER FOUR

4.0 RESULTS AND DISCUSSION

4.1 Alkali Treatment

Alkali treatment was carried out using 4 % wt of sodium hydroxide. In this process, the main aim was to remove the hemicellulose component of the plant material. Since hemicellulose materials are irregularly arranged, the hydroxyl ion penetrates the structure thereby breaking down the acetyl and pulcoumaric chains or bonds of hemicellulose. The presence of the hemicellulose in the raw *palmae sp.* and *acacia sp.* was established by a peak at 1730 cm^{-1} which is attributed to vibrations of acetyl and uronic ester groups. After the base hydrolysis, the band at 1730 cm^{-1} in the FTIR spectrum disappeared showing the removal of hemicellulose. Similarly, part of lignin is also removed after the base treatment. This is evident in the disappearance of the 1244 cm^{-1} peak in the FTIR spectrum which is attributed to a stretching vibration of C=O bond. In addition, color of the *palmae sp.* and *acacia sp.* changed slightly; the colour of *palmae sp.* treated with 4 % wt NaOH changed from dark brown to yellow after complete washing to a pH range of 6.00 – 7.00 and the *acacia sp.* base treated hydrolysis changed from brown coloration to pale yellow. This color change confirms a partial removal of the lignin since the aromatic groups in the lignin are the color pigment in plant. It was observed that the base treatment swelled, cracked and solubilized the fiber structure which enlarges the surface area of the polymeric components making it easily hydrolysed and washed away resulting in defibrillation. After the base hydrolysis the pH of the resultant solution is highly basic of approximately 13. The solution is washed to a neutral pH of 6.00 – 7.00. The pH changes are a major factor in isolating cellulose nanocrystals. 6.00 – 7.00 pH level indicates a complete removal of the hemicellulose and other extractives (Ng *et al.*, 2015). It is only at this pH that the next process can be carried out.

Figure 4.1 below is the gradual change in color of the supernatant after the first five washing using a centrifuge at 3500 rcf for 3 mins for each spin. It was observed that the first supernatant was the darkest of the five. This could be due to the high concentration of the hemicellulose, lignin and extractives in solution. From the fourth washing the color of the supernatant is constant with varying pH-levels. Thus subsequent washing reduced the pH of solution to neutral to get rid of any residual components of hemicellulose, lignin and extractives.

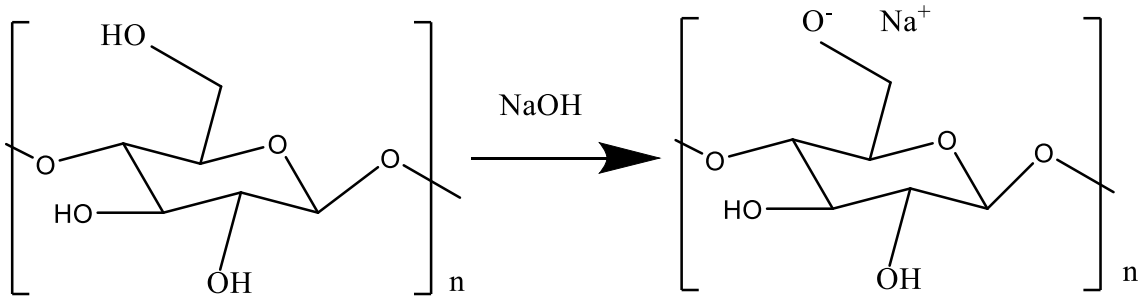

Figure 4. 1: Reaction mechanism of the base hydrolysis using sodium hydroxide

4.2 Bleaching Treatment

The color of the plant material changes gradually throughout the bleaching process. For the *palmae sp.* the color change was from pink to dark-brown, then to yellow, pale yellow and white. The most effective color change occurred during the bleaching process where all lignin which is responsible for the color are removed (Kargarzadeh *et al.*, 2012; Singh *et al.*, 2017). Bleaching for the plant species used was repeated once for effective and complete removal of lignin. The *acacia sp.* which was yellow got converted to pale yellow and finally white. After the first bleaching, the color change was pale yellow and the second bleaching completely removed the lignin leading to a pure white cellulose. It was observed that the color pigment in the *palmae sp.* is more than the acacia. This is because the color transition of both *palmae sp.* and *acacia sp.* was different even though the treatments were the same. After the first bleaching, the color of the

palmae sp. was yellow whereas the *acacia sp.* was pale yellow. Consequently, acacia sp. took less time for the second bleaching to convert to pure white. The bleaching treatment is significant because the presence of lignin interfere with the acid treatment process since the lignin forms a thin layer cover over the cellulose which prevents breakdown of the cellulose into the smaller nano-size particles.

4.3 Acid Treatment

The most effective part of the extraction process is the acid hydrolysis which breaks down the non-crystalline part of pure cellulose leaving nanosized crystalline particles. The acid hydrolysis process is most effective with a highly concentrated sulfuric acid. In this process a highly concentrated sulfuric acid, 64 %wt was used. The hydroxonium ion, H^+ hydrolyses the glycosidic bond between the amorphous and crystalline medium to release the pure cyrstallilne leaving the amorphous domain to be washed away via repeated washing with deionized water. The acid hydrolysis process also further breaks down the cellulose particles into nanocrystals by reducing their length and diameter. It is easier breaking through the amorphous region due to the irregular arrangement of the fibers. However, the crystalline domain is closely and regularly packed which prevents the H^+ ions from hydrolyzing. Eventually, the hydroxyl, OHs on the cellulose are substituted for by the sulfonated ion, O_3SH^-. This interaction makes the surface of the nanocrystals more reactive. This also enhances the uniform dispersion of CNCs in solution due to inter and intra electrostatic force of repulsion in solution. In the reaction, the OH on the carbon 6 is more susceptible to react with the sulfuric acid due to less steric hindrance. Thus, the OHs on carbon 2 and carbon 3 are not affected by the sulfuric acid hydrolysis. Below is a brief scheme of the acid hydrolysis;

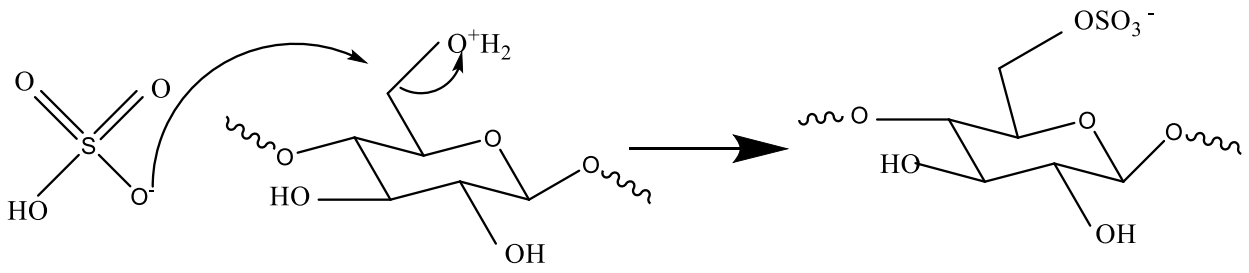

Figure 4. 2: Reaction mechanism of acid treatment using sulfuric acid

The crystallinity of the cellulose increases through the process. This is because, amorphous and non-crystalline part of the plant materials is removed. Accordingly, Battista et al. reported that the defect of the non-crystalline region is responsible for the transverse cleaving of the pure cellulose which enhances the acid hydrolysis.

4.4 Phytochemical screening

Phytochemical screening of the raw *palmae sp.* and *acacia sp.* tested positive whereas the extracted and standard CNCs tested negative indicating an effective base and acid treatments coupled with bleaching.

Table 4.1 represents the results from the phytochemical screening tests for alkanoid, polyphenols, flavonoid and sapponins in the palmae sp. samples and CNC standard sample obtained from cotton. The test confirms the presence of lignin, hemicellulose, residual pectin, nitrogenous compounds and ash in the raw samples. CNCs from *acacia sp.*, *palmae sp.* and standard from cotton tested negatives, suggesting that all the lignin, hemicellulose, the residual pectin, nitrogenous bases and ash were thoroughly removed by base and bleaching treatment.

Table 4. 1: Phytochemical screening of the raw *palmae sp.* and *acacia sp.*, CNCs from *palmae sp.* and *acacia sp.* and Standard CNC.

Sample	Flavonoid	Polyphenols	Saponins	Alkaloids
A-Raw	+	+	+	+
P-Raw	+	+	+	+
CNC-A	-	-	-	-
CNC-P	-	-	-	-
CNC-Standard	-	-	-	-

(+) phytochemical present; (–) phytochemical absent

4.5 Characterization of isolated CNCs

To further corroborate the pure crystals, the following characterization were carried out.

4.5.1 FTIR Analysis

The FTIR technique was used to examine the functional groups in the samples at various stages of the extraction. Figure 4.3 and 4.4 show the FTIR spectra of the untreated, bleached, hydrolysed and cellulose nanoparticles. Dominant spectra band at 3339 cm^{-1} corresponds to the stretching vibration of -OHs of intra and intermolecular hydrogen bond whereas 710 cm^{-1} is assigned to -OH out of plane bending. Changes in strength of the H-bonding during the extraction process affected the intensity and width of the spectra (Meyabadi *et al.*, 2014). The change in intensity of the spectra band of the OH group is also as a result of changes in the number of H-bonding during the hydrolysis process. The presence of the spectra band in the

region 1639 – 1648 cm^{-1} in all the fiber shows the presence of the -OH of the absorbed water. The absorbed moisture at the peak of 1640 cm^{-1} show spectra intensity differences in the untreated, bleached, hydrolysed samples and nanoparticles. Larger surface area of the treated samples contributes to the intense broad peak of the OH band. Also after the base hydrolysis more OHs are produced in solution which contributes to intense broad peak of the OH band. Throughout the process the OH band progressively increases in height/intensity and width as a result of the excess OHs.

Peaks in the regions of 2900 and 2930 cm^{-1} refer to the antisymmetric and symmetric vibrations of – CH_2 aliphatic bonds or groups. Also peaks in the region of 1410 – 1420 cm^{-1} are due to the – CH_2 scissoring motion in the cellulose. Similarly C-H bending vibration in the molecule is shown in the region of 1338 – 1368 cm^{-1}. 1317 cm^{-1} shows – CH_2 wagging. Also the peak at the 1040 cm^{-1} represents the C-O-C ether group of pyranose ring stretching vibration in the cellulose. The peak at the 890 – 896 cm^{-1} corresponds to the beta-glycosidic linkage in cellulose (Soni & Mahmoud, 2015). In addition, a spectra band at 1150 – 1159 cm^{-1} represents C-C stretching vibration. Intense peak at 1750 cm^{-1} designates C=O stretch of aldehyde which is corresponds to the presence of hemicellulose and lignin. The peak at 1230 cm^{-1} also represents aromatic rings of lignin. Similarly, the presence of functional groups such as methoxyl-O-CH_3, C -O-C and aromatic C=C at peaks in the region between 1830 and 1730 cm^{-1} were observed (Reddy & Yang, 2005a, 2005b). 2905cm^{-1} peak represents the HCH and OCH out of plane bending vibrations. It is classified as a crystalline absorption peak. Vibration at 1370 cm^{-1} is designated as CH deformation of the cellulose (Meyabadi *et al.*, 2014). Additionally the band at 1160 is attributed to the asymmetric bridge stretching vibration of the C_1-O-C_4.

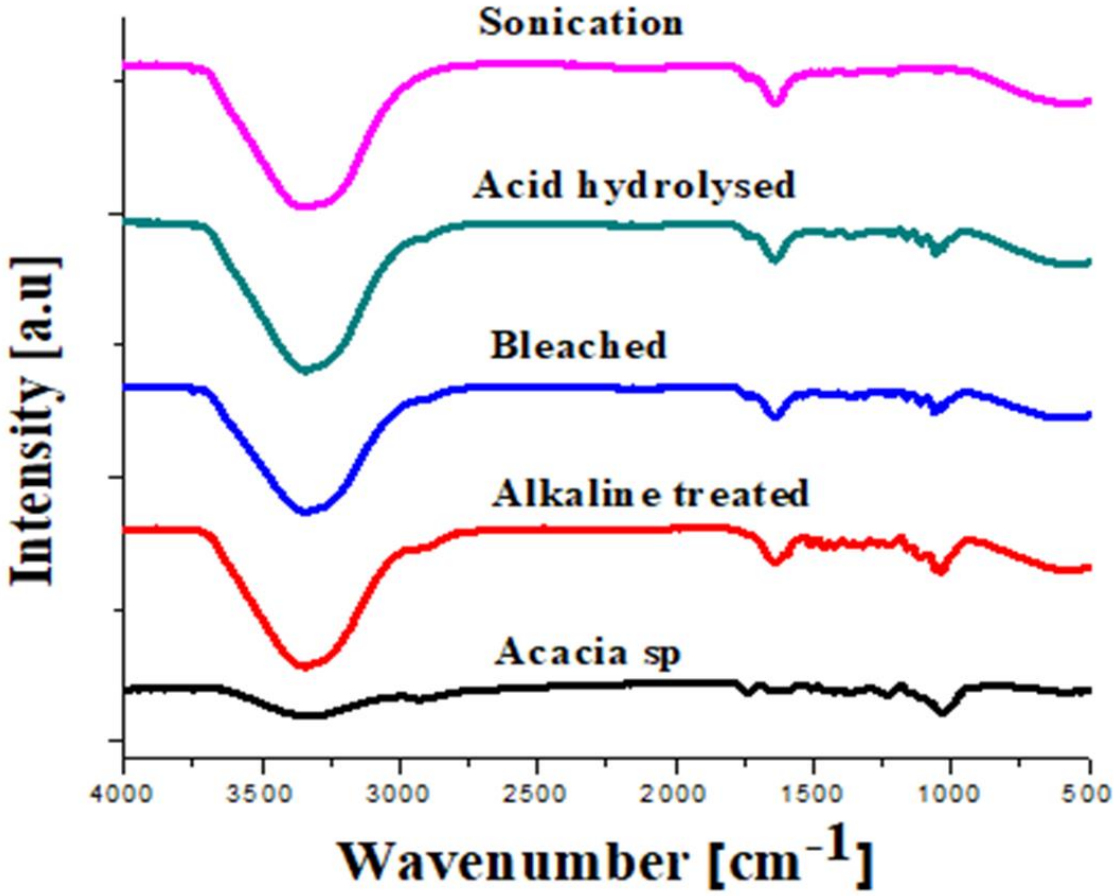

Figure 4. 3: FTIR of *acacia sp.* from various treatment processes

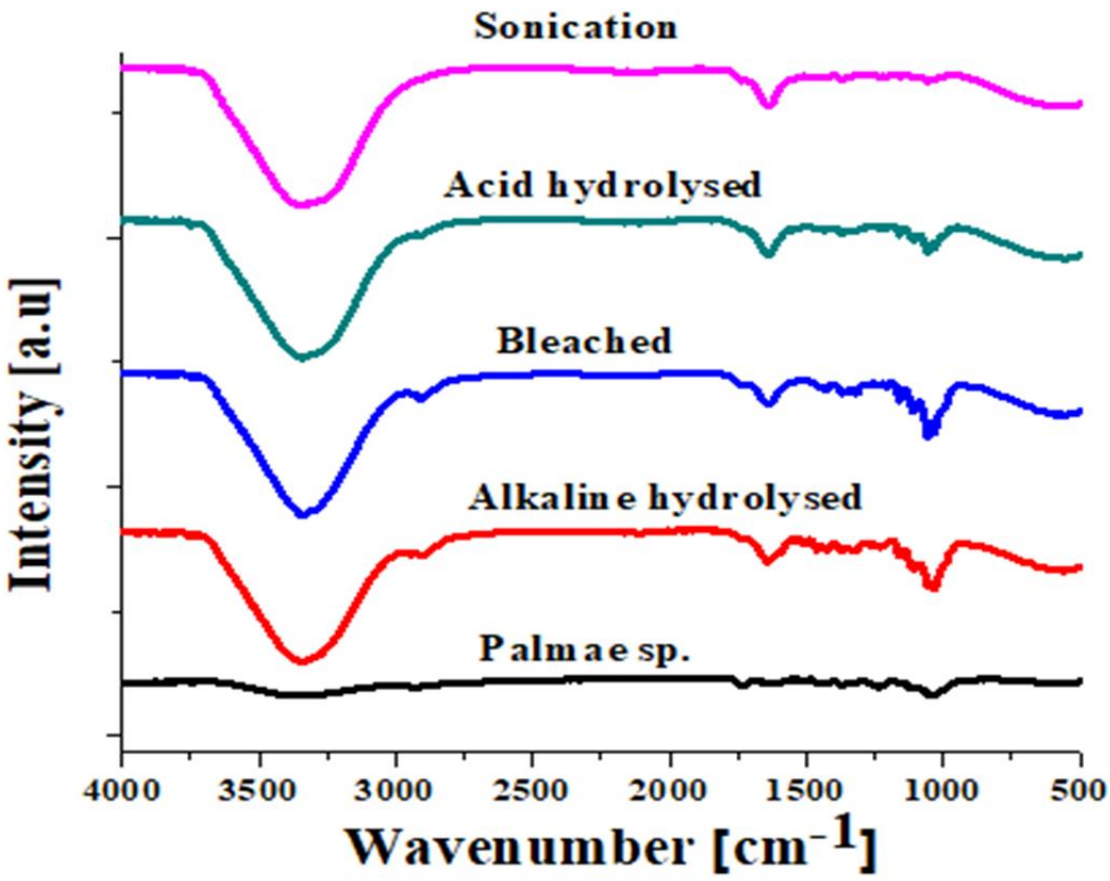

Figure 4. 4: FTIR of *palmae sp.* from various treatment processes

The peak present at 1765–1715 cm^{-1} in the spectrum of the raw fiber is indicative of the presence of C=O linkage and aromatic stretch of C=C which is characteristic of ferulic and p-coumaric acids of lignin and ester acetyl and uronic acid groups of hemicellulose (E Abraham *et al.*, 2011; Eldho Abraham *et al.*, 2013). Peak at 1508 cm^{-1} corresponds to an aromatic stretch of C=C which is responsible for lignin. 1247 cm^{-1} also corresponds to C-O-C of aryl, alkyl and ether group. C=O stretching of the acetyl and uronic ester groups of hemicellulose or the ester linkage of carboxylic groups of ferulic and p-coumaric acids were also designated at 1735 cm^{-1} (Alemdar & Sain, 2008a, 2008b). Also there is non-crystalline absorption peak related to COC, CCO and CCH twist modes as well as stretching vibrations at C_5 and C_6 for the peak at 889 cm^{-1}.

1060 and 895 cm^{-1} corresponds to C-O stretching and C-H rocking respectively of the carbohydrates. Bands at 1053 cm^{-1} and 1030 cm^{-1}correspond to the C-OH stretching vibration of secondary and primary alcohols of cellulose, respectively (Johnsy George *et al.*, 2011). The band at 1623 cm^{-1} is due to the stretching vibration of C=O groups of cellulose rings.

Decreasing intensity of spectra band at 1730 cm^{-1}, 1556 $cm^{-1}$and 1240 cm^{-1} shows the removal of hemicellulose, lignin and extractives associated with cellulose (Costa *et al.*, 2015). Appendix A – D. The absence of absorbed moisture was confirmed by the peak at 1638 cm^{-1}. It was discovered that peak at 1738 cm^{-1} disappeared after base hydrolysis during the extraction process confirming the successful removal of hemicellulose from the plant samples (Soni & Mahmoud, 2015). Lignin was not absolutely extricated after alkali hydrolysis but disappeared completely after bleaching. It was also observed that the C=O stretching vibration of the ether bond in the hemicellulose disappeared after the alkali hydrolysis. This could be due to the effectiveness of the base hydrolysis in scattering of the ester linked substances of the hemicellulose. Accordingly, in a research by Chieng et al., (2017), variation in the peaks of the FTIR spectra at 2916 cm^{-1} (C-H stretching), 1732 cm^{-1} (C=O stretching) and 1234 cm^{-1} (C-O stretching) showed that the base hydrolysis entirely extricated hemicelluloses and lignin from the fiber surface (Chieng *et al.*, 2017). This was also confirmed by Larissa et al. in their research using corn stover. In this research it was indicated that changes in the peak at 1731, 1556 and 1244 cm^{-1} of the FTIR spectrum showed a removal of hemicellulose, and partly lignin (Costa et al., 2015). The results were further confirmed by a second method called the Ammonium persulfate (APS). This was a 24 hour treatment of alkali hydrolysis, bleaching and acid hydrolysis using a concentrated solution of ammonium persulfate. It was evidenced that the peaks in the CNCs from both methods are virtually the same. Table 4.2.

Table 4. 2: FTIR vibrational frequency and peak assignment for palmae sp. and acacia sp.

Sample	Vibrational frequencies (cm^{-1})	Peak assignment
Untreated	3344.94	OH stretch vibration
	2923.14	C-H stretch vibration
	1737.20	C=O stretch of aldehyde
	1595.31	C=C stretch of aromatic
	1421.92	C-H bending of alkanes
	1371.72	C-H bending of alkanes
	1232.10	C-O bending
	1035.27	C-O bending of alcohols
Alkaline treatment	3339.14	OH stretch vibration
	2849.14	C-H stretch vibration
	1637.92	OH bending
	1421.89	C-H bending of alkanes
	1370.14	C-H bending of alkanes

	1109.25	C-O bending of ethers
	1057.15	C-O bending of ethers
	1033.90	C-O bending of ethers
Bleach treatment	3341.21	OH stretch vibration
	2903.04	C-H stretch vibration
	1638.29	OH bending
	1370.38	C-H bending of alkanes
	1160.65	S-O stretch & C-O of esters
	1057.59	C-O bending of ethers
Acid treatment	3339.25	OH stretch vibration
	2903.04	C-H stretch vibration
	1639.12	OH bending
	1316.59	C-O bending of esters
	1160.26	S-O stretch & C-O of esters
	1105.54	C-H bending of alkanes

	1054.88	C-O bending of ethers
	1032.46	C-O bending of ethers
Dialyzed	3339.03	OH stretch vibration
	2904.56	C-H stretch vibration
	1638.65	OH bending
	1316.86	C-O bending of esters
	1160.41	S-O stretch & C-O of esters
	1107.35	C-O bending of ethers
	1056.32	C-O bending of ethers
	1033.43	C-O bending of ethers

Table 4. 3: Vibrational frequency and peak assignment of palmae sp. using Amonium persulfate method of extraction.

Sample	**Vibrational frequencies (cm^{-1})**	**Peak assignment**
Palmae sp. (raw)	3344.94	OH stretch vibration
	2923.14	C-H stretch vibration
	1737.20	C=O stretch of aldehyde

	1595.31	C=C stretch of aromatic
	1421.92	C-H bending of alkanes
	1371.72	C-H bending of alkanes
	1232.10	C-O bending
	1035.27	C-O bending of alcohols
CNC	3339.08	OH stretch vibration
	2902.35	C-H stretch vibration
	1638.08	OH bending
	1316.65	C-O bending esters
	1160.51	S-O stretch & C-O of esters
	1106.61	C-O stretch
	1055.21	C-O stretch & C-H rocking
	1032.89	C-O stretch & C-H rocking

4.5.2 SEM

The effect of the treatments (alkali, bleaching and acid) on the structure of the CNCs was investigated by the use of scanning electron microscopy. Figures 4.5, 4.6, 4.7, 4.8 and 4.9

summarize the micrographs of the CNCs obtained from both samples, CNC - A and CNC - P. SEM images revealed a change in the structure compared to the optical images of the untreated samples. This shows that the treatments may have removed the amorphous compounds of hemicellulose, lignin, pectin, saponins, gums, wax, and polysaccharides.

4.5.2.1 Acacia sp.

The scanning electron microscopy was used to analyse the morphology of the extracted CNCs. Figure 4.5 and 4.6 display the micrograph of the various images obtained at different magnifications. It was observed that the images of the cellulose fibers are large aggregates comprising of slender particles with dimensions of approximately less than 10 µm. Thus nanoparticles have been produced but agglomerated. This agrees with works done by Brinchi et al. when nanocellulose were extracted from lignocellulosic biomass. (Brinchi *et al.*, 2013). The formation of the CNCs also confirms the successful removal of the hemicellulose, lignin, wax, pectin and other impurities on the surface of cellulose. In Fig. 4.6, the particles are well dispersed in solution after filtration followed by dialysis. Filtration removed the larger particles which may have a residual components of homocellulose and lignin leaving a more crystalline particles. Furthermore, the uniform dispersivity of the particles suggested a more sulfonated group of CNC particles which repel each other due to the electrostatic repulsive interaction of the negative charge sulphonated ions in solution.

. .

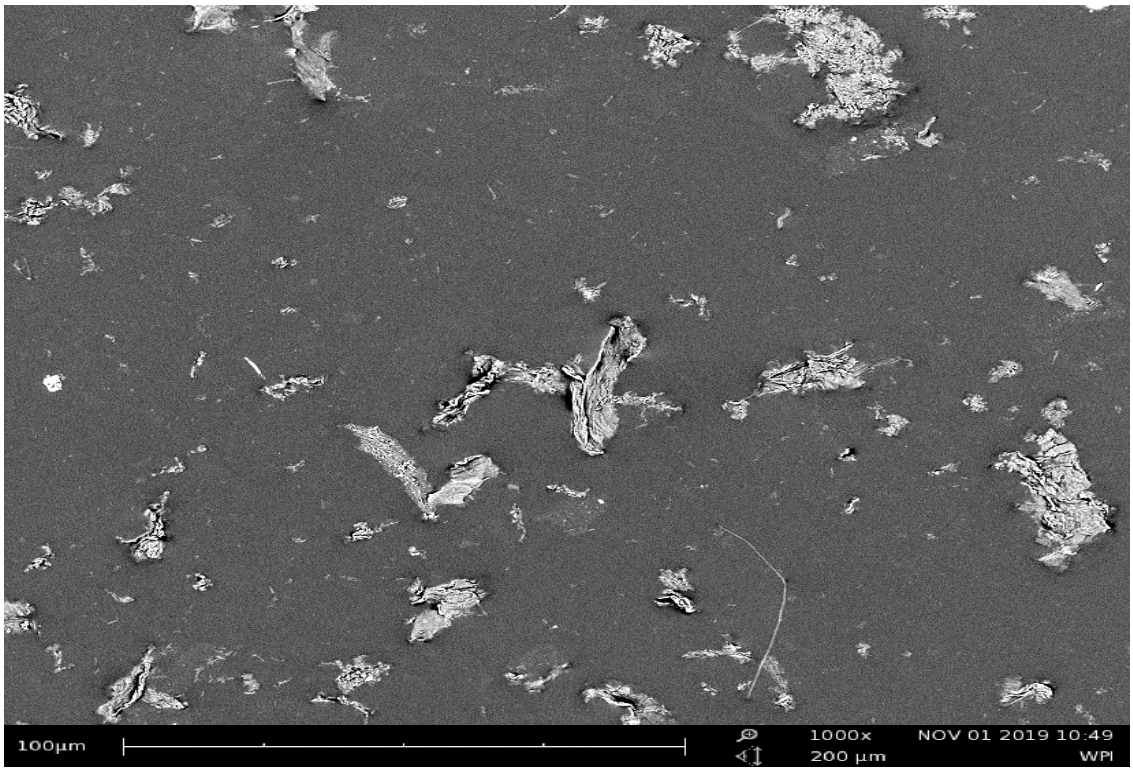

Figure 4. 5: SEM image of the CNCs from *Acacia sp.* (CNC - P, 1000x, scale bar = 100 µm)

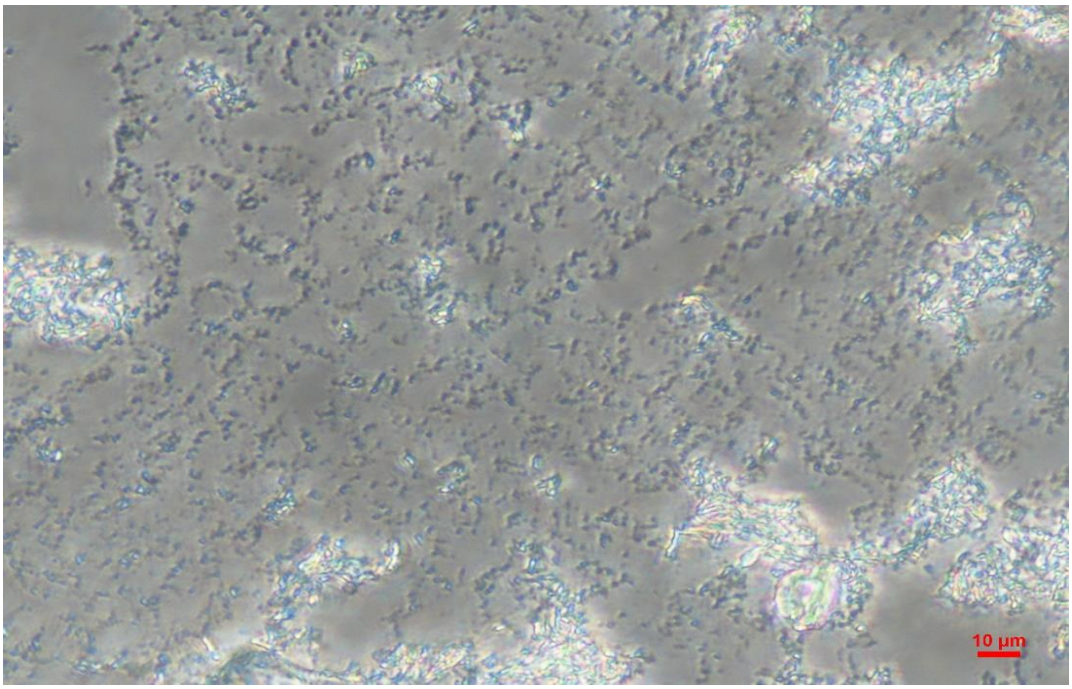

Figure 4. 6: SEM image of the cellulose nanocrystals from *Acacia sp.* after filtration followed, followed by hydrolysis (CNC - P, scale bar = 10 µm)

4.5.2.2 Palmae sp.

The SEM images of the cellulose nanocrystals from the *Palmae sp.* are shown in Figure 4.7 and 4.8. Images of the cellulose nanocrystals in structure or morphology from the *Palmae sp.* appeared to be similar to the *Acacia sp.* with few variations. However, the aspect ratio may differ when the exact dimensions of the nanoparticles are determined with a transmission electron microscope since the aspect ratio is the ratio of the length to width (Favier *et al.*, 1995). Appearance of the white images indicated the effectiveness of the treatment process during the base hydrolysis and bleaching. This is because folded ribbon-like shape in the form of bundles (Abe & Yano, 2009) as seen in the optical image of the raw sample was absent in the CNCs. Like in the *Acacia sp.*, the particles are approximately less than 10 µm with less agglomeration.

This suggests a more effective acid hydrolysis in cleaving the 1,4-β-glycosidic linkage which produced a more highly sulfonated CNCs particles which could disperse more uniformly in solution due to the pronounced counter-ion interaction (Bondeson *et al.*, 2006). In Figure 4.9 image, white protrusion called tyloses which is responsible for the presence of residual starch are absent which is indicative of thethe successful removal of the starch making the CNCs more pure. Additionally, the particles were seen not to be uniform in dimensions. This is also due to the random cleaving of the glycoside bonds during the acid hydrolysis as well as the cracking of the fasciculus which were held by the strong inter and intra molecular hydrogen bonding. The degree of depolymerization may also have been reduced and eventually wide diverse range of CNCs are produced due to the geographical locations and treatments processes (Bendahou *et al.*, 2009).

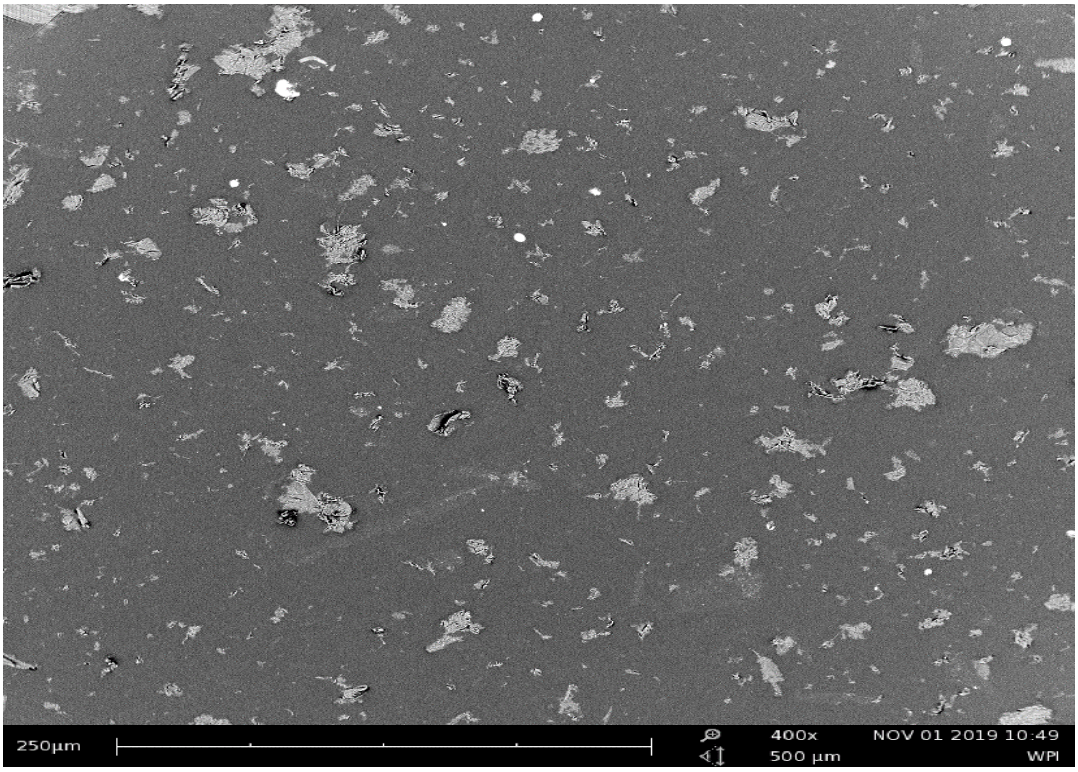

Figure 4. 7: SEM image of the CNCs from *palmae sp.* (CNC - P, 400x, scale bar = 500 µm)

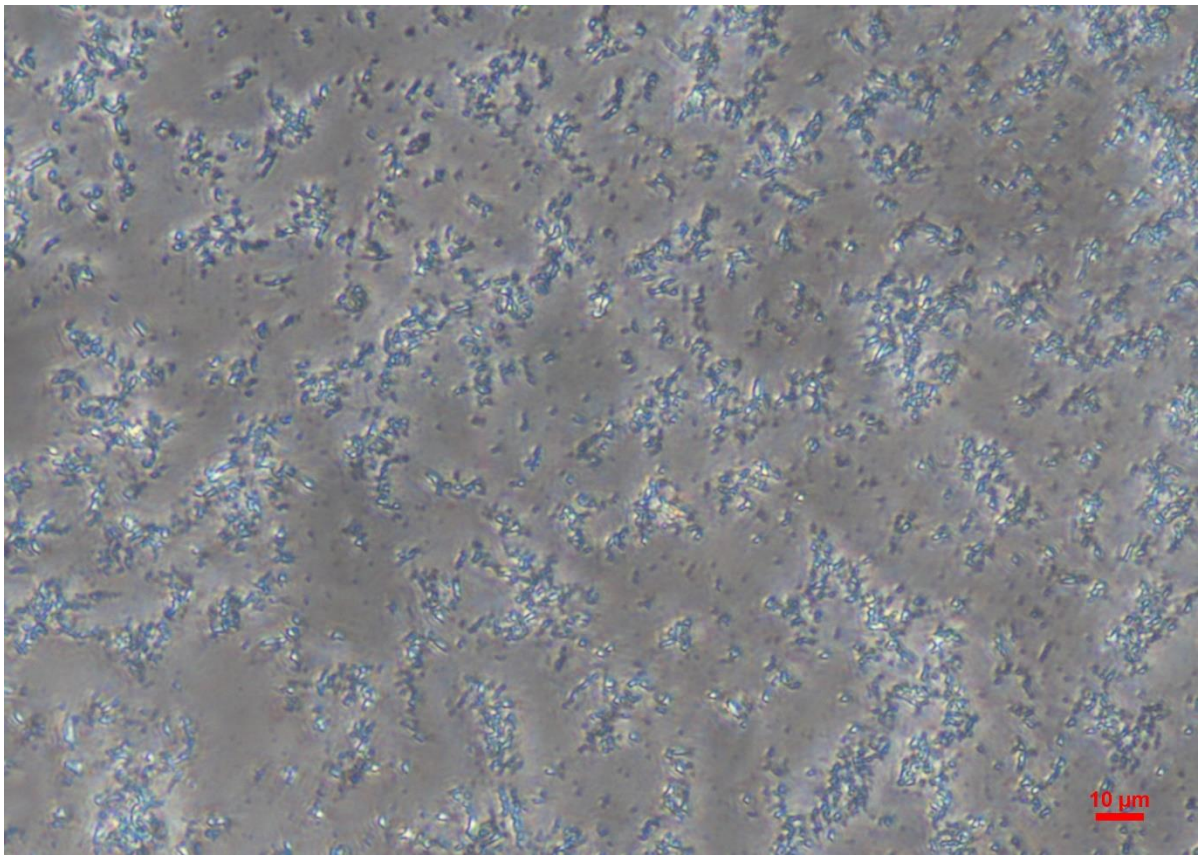

Figure 4. 8: SEM image of the cellulose nanocrystals from *palmae sp.* after filtration, followed by dialysis (CNC - P, scale bar = 10 µm)

4.5.3 XRD

The X-ray diffraction analysis was carried out to examine crystallinity, thermal stability, elasticity, absorptive capacity and other physical properties which may be vital to the industry. Crystalline index which is the ratio of the crystalline to the non-crystalline region of cellulose was used to examine the crystallinity of all samples. An increase in crystallinity index signifies high strength due to high stiffness and rigidity. This is also indicative of high resistance to cracks (Chieng *et al.*, 2017). Peak intensity at 2θ value of 16^{o} to 18^{o} shows crystallinity of the amorphous arrangement whereas 22^{o} to 23^{o} is related to the crystalline form of cellulose. Within the limit of experimental errors peak intensity values at 22-23^{o} are supposed to increase whilst those at 16-18^{o} decrease due to the removal of the non-crystalline part of cellulose. Figure 4.11 shows the X-ray diffractograms of *acacia sp*. (a) untreated (b) bleached (c) acid hydrolyzed and (d) CNC. Table 4.4 presents a summary of the crystallinity index of the various stages.

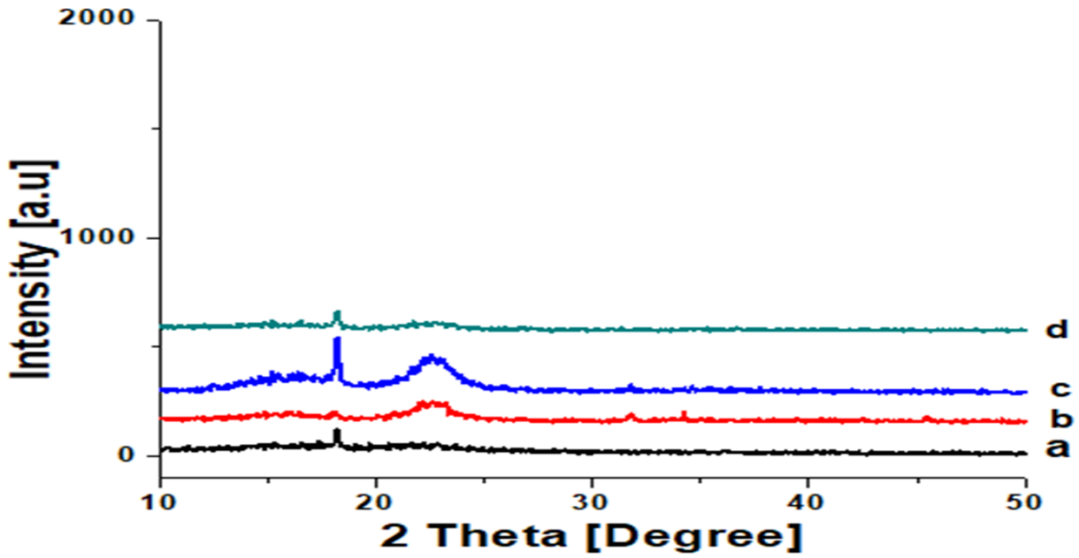

Figure 4. 9: The X-ray diffractograms of *acacia sp.* (a) untreated (b) bleached (c) acid hydrolyzed and (d) CNC.

Table 4. 4: Crystallinity index (%) of untreated, base treated, bleached, acid hydrolyzed and CNC of a*cacia sp.*

Sample	2θ (Amorphous) (◦)		2θ(002)(◦)		CrI (%)
	Degree	Intensity (I_{am})	Degree	Intensity (I_{002})	
Untreated	18.15	121	22.55	46	-163.04
Base hydrolyzed	18.15	136	22.55	52	-161.54
Bleached	18.15	45	2255	101	55.45
Acid hydrolyzed	18.15	270	22.55	193	-39.90
CNC	18.15	86	22.55	28	-207.14

The crystallinity was calculated utilizing the equation

$CI_r(\%) = [(I_{200} - I_{am})/I_{200}] \times 100$

Where l_{200} is the height of the peak at $2\Theta=22.5^o$ referring to the crystalline and amorphous fraction and I_{am} is the height measured at $2\Theta=18^o$ referring to the amorphous fraction (Ahmadi et al., 2015).

4.5.3.1 Untreated Acacia sp.

The untreated *acacia sp.* gave the second lowest crystallinity index of -163.04 %. However, this was expected to be the lowest since it has the greatest amount of amorphous cellulose as well as lignin and hemicellulose. From Figure 4.9, peaks at 18.15 and 22.55^o were approximately absent due to the numerous amorphous components and impurities associated with the cellulose.

4.5.3.2 Base hydrolysis

Crystallinity index of the alkaline treated *acacia sp.* increased to -161.54 %. This was expected but not in the negatives as reported by Chieng et al. in their work using Oil Palm Front. This also shows partial removal of hemicellulose associated with the cellulose (Chieng *et al.*, 2017).

4.5.3.3 Bleaching

From Figure 4.9, the peak intensity at 2θ value of 22.55^{o} appeared after bleaching showing the presence of crystalline component of the cellulose. However, the amorphous peak value at 18.15^{o} didn't appear. This explains the increase in the crystallinity index after bleaching of the *acacia sp.* Thus the bleaching was effective in removing few amorphous component associated with the cellulose.

4.5.3.4 Acid hydrolysis

The acid hydrolyzed curve shown in Figure 4.9 indicates two main peaks at 18.15^{o} and 22.55^{o}. However, the crystallinity index as summarized in Table 4.6 indicated a decrease in the crystallinity. Decrease in the crystallinity index after acid treatment shows that the sulfuric acid hydrolysis was not effective in breaking the amorphous component of cellulose away. Thus the hydrolytic cleavage of the glycosidic bond was not too successful. This could be due to the working environment in terms of temperature, concentration of acid and time of hydrolysis.

4.5.3.5 Cellulose nanocrystals

The crystallinity index computed for the isolated CNCs was -207.4%. This is the lowest of all the crystallinity index values of the acacia sp. Additionally, the diffractogram of the CNC showed

almost no peak at the 18^{o} and 22^{o}. These findings contradict what is reported in the FTIR results and literature. For example in the isolation of CNCs from Menkuage leaves and Pineapple biomass, the crystallinity index values increased gradually from the untreated plant material to the isolated CNCs (Cherian *et al.*, 2011; Sheltami *et al.*, 2012).

4.5.3.6 Palmae sp.

Table 4. 5: Crystallinity index (%) of untreated, bleached, acid hydrolyzed and CNC from Palmae sp.

	2θ(Amorphous)(◦)		2θ(002)(◦)			
Sample	**Degree**	**Intensity (I_{am})**	**Degree**	**Intensity**	**(I_{002})**	**CrI (%)**
Untreated	18.2	84	22.9	68		-23.53
Bleached	18.2	52	22.9	137		62.04
Acid hydrolyzed	18.2	90	22.9	156		42.30
CNC	18.2	1390	22.9	25		-5460

4.5.3.7 Untreated

The untreated *palmae sp.* showed a very low crystallinity index of -23.53%. This is second to that of the CNCs produced. Although from Figure 4.10 there isn't any peak at the 18^{o} and 22^{o} showing crystallinity. This is ascribed to the presence of numerous amorphous component coupled with lignin and hemicellulose covering the crystalline cellulose in the plant material.

4.5.3.8 Bleaching

XRD of the bleached *palmae sp.* exhibited a sharp peak at 22º indicative of the presence of crystalline cellulose structure of 1,4-β-glycosidic linkages. From Table 4.5, the crystallinity of the cellulose increased tremendously to 62º. The increase can be credited to the effective removal of lignin, hemicellulose and other impurities leaving pure cellulose.

4.5.3.9 Acid hydrolysis

Crystallinity index after acid hydrolysis was 42.30%. This percentage suggest a higher crystallinity but a decrease in value from bleaching treatment. The XRD results show that the crystalline cellulose structure was not maintained during acid treatment. With Wang et al. who reported that the crystal structure of cellulose was conserved after acid treatment, it was expected that the crystallinity index increased progressively such that the CNCs gives the highest crystallinity index (X. Wang *et al.*, 2011).

4.5.3.10 Cellulose nanocrystals

The diffraction intensity peak at 2Ɵ=18º which is related to the non-crystalline component of cellulose was very strong for the CNCs produced (Ahmadi *et al.*, 2015). However there was no peak at 2Ɵ=22º which correspond to the crystalline sections of cellulose. This culminated to the CNC having the lowest crystallinity index of -5460% which could be treated as an outlier. The results suggest that the treatment processes, base hydrolysis, bleaching and acid hydrolysis were not too successful extracting and isolating the CNCs. Temperature variation, concentration of base and acid as well time of reactions could also account for the not too good XRD results.

However, from Figure 4.11, it was observed that the *palmae sp.* was more crystalline than the *acacia sp.*

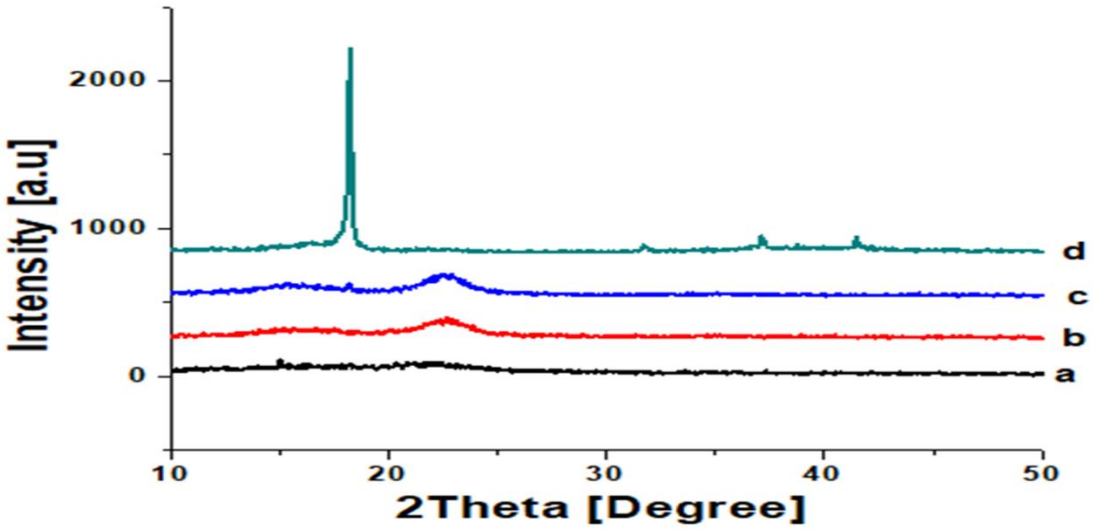

Figure 4.10: The X-ray diffractograms of *palmae sp.* (a) untreated (b) bleached (c) acid hydrolyzed and (d) CNC.

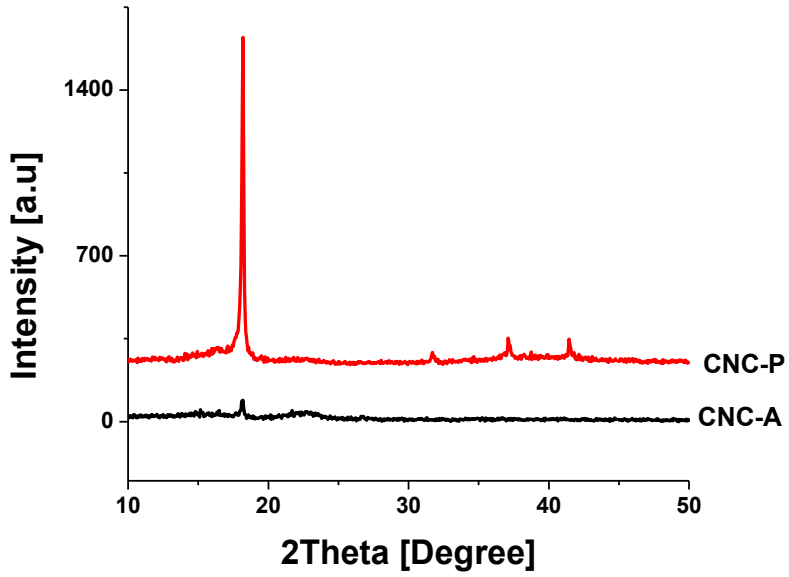

Figure 4. 11: X-ray diffractograms CNC from *palmae sp.* (P) and *acacia sp.* (A).

4.5.4 TGA

Usually, the TGA curve is divided into five major temperature components. First is temperature below 150 ^{o}C which is due to loss of moisture, lower molecular weight solvents and desorption. Next is the temperature between 150 and 250 ^{o}C. This is responsible for the loss of lower molecular weight compounds such as additives, crystallization of water plasticizers. The third temperature range is 250 ^{o}C and 500 ^{o}C which is responsible for decomposition of inert gasses or oxidation of certain organic matter or simultaneous degradation processes such as depolymerization, dehydration, and degradation of the glycosyl rings and later formation of a charred remnants. Temperatures above 500 ^{o}C cause carbonization of hydrocarbonated compounds which pyrolysis has no volatile formation. Beyond 500 ^{o}C is the decomposition of metallic oxides or inorganic salts, ashes and also oxidation and breakdown of the burnt residue into gaseous products with low molecular weight (Meyabadi *et al.*, 2014)

TGA study was done at each stage of the extraction process and material was characterized by measuring the change in mass as a function of temperature. Degradation patterns appeared to be the same for all samples. It was observed that the decomposition peak temperature increased gradually from the base hydrolysis to bleaching, and acid hydrolysis. This was expected because in each stage there was a removal of various components of impurities like hemicellulose, lignin, mucilage, wax, pectin, gums, tannins, proteins and starch. In the analysis, two decomposition temperatures were observed. The first decomposition was loss of moisture whilst the second was organic matter (Chartas *et al.*, 2001). This could be due to the evaporation of surface moisture and inside moisture by chemisorbed of the fiber sample which was confirmed by the moisture detected by the FTIR peak at 1640 cm^{-1}, a bending vibration of water intermolecular hydrogen bonding. Also, Lignin decomposed at 200 ^{o}C and hemicellulose at 220 ^{o}C. Additionally,

degradation at 231 ^{o}C is due to hemicellulose and 317 ^{o}C due to alpha cellulose 1. Here the major characterization parameter of the material is the weight loss, residual weight, decomposition peak, onset and maximum temperatures. The amount of mass loss was computed as

$m\ (\%) = [\ (m_o - m_t) /\ \ m_o\ ] \times 100\ \%$

where m is the mass loss

m_o is the initial mass and

m_t is the final mass after decomposition

The parameters that characterize the samples are mass loss, mass residue, decomposition peak, onset and end temperature.

4.5.4.1 Acacia sp.

The Figure 4.12 below shows the thermogram of the raw Acacia sp. before the treatment processes. Moisture loss at the first decomposition was below 275.9 ^{o}C with a small weight loss of 10%. It is expected that other components such as hemicellulose were included in the 10% since hemicellulose decomposes at 170 ^{o}C (Chieng *et al.*, 2017). The decomposition temperature range was 275.9 ^{o}C to 367.6 ^{o}C. Of the 10.5 mg mass used in the analysis, the mass change was -71.77% with a residual mass of 28.17% at 899.2 ^{o}C. During this temperature change organic matter such as starch, pectin, protein and mucilages are decomposed. The residual temperature which is the temperature at which no more organic matter is lost continued up to 899.2 ^{o}C. Here decomposition of inorganic compounds at a temperature of 650 ^{o}C may occur. An example is a conversion of wedelite to calcium oxide, CaO (Frost & Weier, 2003). Peak decomposition temperature was 323.9 ^{o}C which was relatively low. The weight percentage of the char,

carbonaceous residue beyond the 500 ^{o}C was 28.17%. This was the lowest instead of being the highest which suggest the presence of few or impurities.

4.5.4.2 Base hydrolysis

The onset decomposition temperature after the alkali treatment (T_{on}) increased to 325 ^{o}C with a maximum rate of decomposition, (T_{max}) at 387.7 ^{o}C. This is evidenced in the removal of hemicellulose and some aspect of wax and pectin during the base hydrolysis as seen in the FTIR analysis. Percentage of moisture loss was supposed to be less but was still appreciable of about 10% even though hemicellulose was lost since it decomposes at a 170 ^{o}C and hence the mass. Onset temperature rose from the 275.9 ^{o}C in the raw sample to 325.0 ^{o}C. This result shows that the alkaline hydrolysis could eventually increase the thermal stability of the sample.

4.5.4.3 Bleaching

The onset temperature for the bleached sample decreased to 273.9 ^{o}C with a maximum decomposition temperature of 387.7 ^{o}C. Apparently, the onset temperature was supposed to have increased with the maximum decomposition temperature. This could be due to the presence of some impurities and inorganic mineral salts. It could also mean that the bleaching was not too effective in removing the xylan or lignin component of cellulose (Tang *et al*., 2015). This result almost agrees with the XRD peak obtained after bleaching meaning that the crystallinity didn't really increase. The char weight percent increased from alkaline treated to the bleached which suggests that the treatment process might have introduced some impurities into the cellulose.

4.5.4.4 Acid hydrolysis

After the acid hydrolysis, the onset temperature decreased again to 273.9 ^{o}C with a corresponding decrease in the maximum decomposition temperature at 355.6 ^{o}C. Thus instead of having the thermal stability increased it rather decreased. This could be due to harsh treatment process or condition not too effective. Additionally, the modification of the concentrations of the acid used might have influenced the crystallinity. Howerver, this agrees with work done by Oun et al. which showed that the use of sulfuric acid decreases the crystallinity due to the introduction of the active sulphate group (Y. W. Chen *et al.*, 2016). And one way to curb this occurrence as reported by Oun et al. is to treat the acid hydrolyzed sample with 1M NaOH to diminish the active effect of the sulphate. Similarly, the larger surface area of the nanoparticles which make them more exposed to faster thermal change may also account for these changes. In addition, the larger surface area causes faster heat transfer and hence lowering the thermal stability. It is reported that the activation energy of the acid hydrolysed sample was minimized resulting in low thermal stability.

4.5.4.5 Cellulose nanocrystals

Onset temperature and maximum decomposition temperature increased to 301.5 and 363.8 ^{o}C respectively in the final CNCs. This could be due to the fact that the CNCs became more dense and compact after successive removal of the amorphous component of the plant species (Usha *et al.*, 2016). In addition, the impurities associated with the cellulose which could have accelerated the thermal decomposition may have been removed (Chirayil *et al.*, 2014). In addition, after the dissolution of the amorphous components of the cellulose the crystals structure rearranged and

reorients to give a high composition of crystalline domain. This agrees with work done by Mandal et al. (Mandal & Chakrabarty, 2011).

The residual weight beyond 500 ^{o}C could be carbonaceous residues resulting from carbonization of cellulose under the nitrogen atmosphere. This carbonaceous residues, popularly known as char could result from pyrolysis. This is because more ordered pairs of cellulose fibers require more energy to degrade, resulting in the partial change in the weight percent. The weight percentage of the char was given as 28.62 %.

Table 4. 6: Amount of Weight loss (%) and Charred residue (%) for different samples of Acacia sp.

Sample	Weight Loss	Char yield (%)
Untreated	-71.77	28.17
Base hydrolyzed	-67.27	32.66
Bleached	-64.23	35.75
Acid hydrolyzed	-68.13	31.85
Cellulose nanoparticles	-71.36	28.62

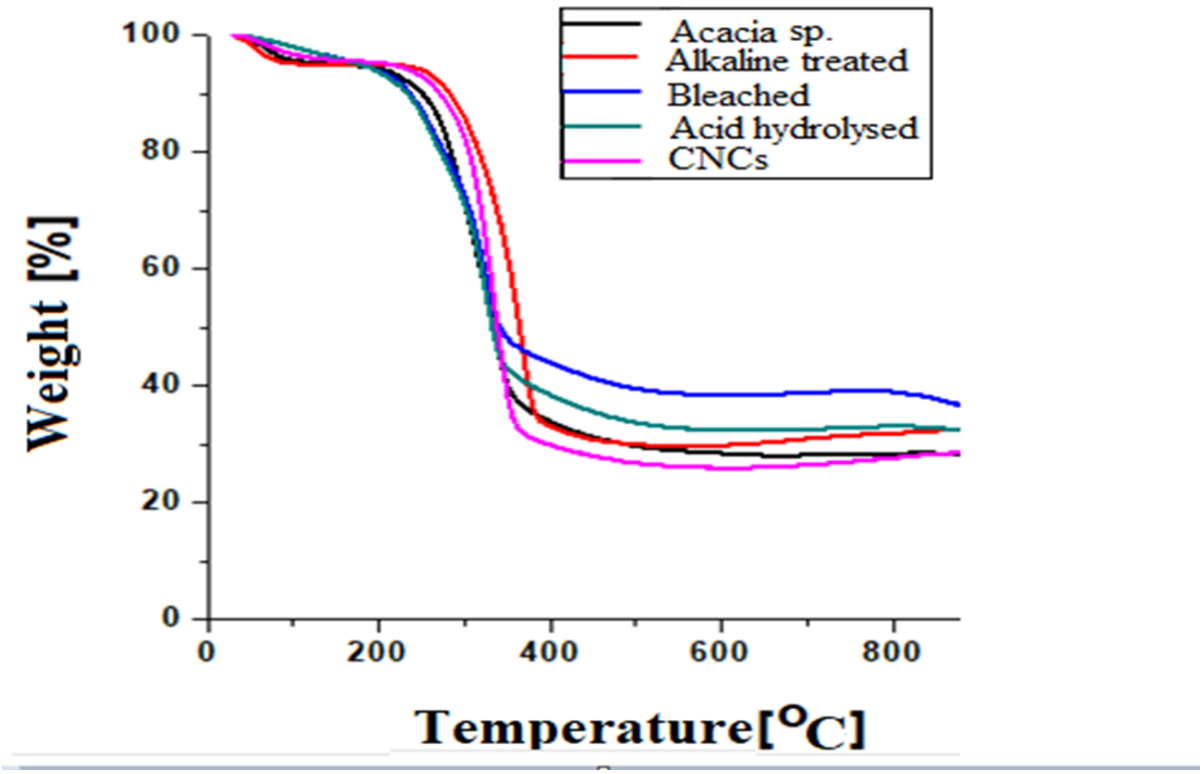

Figure 4. 12: Thermogram of acacia sp., alkaline treated, bleached, acid hydrolysed and CNC

4.5.4.6 Palmae sp.

The onset temperature for the untreated *palmae sp*. was 277.4 ^{o}C with a maximum decomposition temperature at 366.4 ^{o}C. This is shown in Figure 4.15. Below 250 ^{o}C is the decomposition of hemicellulose at about 170 ^{o}C or 220 ^{o}C and the loss absorbed moisture (Chieng *et al.*, 2017). This first decomposition gives a weight loss of approximately 10%. Out of the 11.0 mg sample used, the weight loss at the decomposition temperature was 72.61% leaving a residual mass of 27.24% at the residual temperature of 899.2 ^{o}C. Compared to other treatment stages the untreated *palmae sp.* gave the highest mass change. And this agrees with work done by Moran et al. (Morán *et al.*, 2008). Thus the untreated was evidenced to have contained a lot of impurities as well as non-cellulosic materials associated with the pure cellulose.

4.5.4.7 Bleaching

The onset temperature for the bleached sample increased to 283.9 ^{o}C with a maximum decomposition temperature of 308.2 ^{o}C. Apparently, the onset temperature was supposed to increase with the maximum decomposition temperature. However, the maximum decomposition temperature dropped quite significantly. This could be due to the presence of some impurities and inorganic mineral salts. It could also mean that the bleaching was not too effective in removing the xylan or lignin component of cellulose. The char weight percent which was recorded as residual mass (%) increased greatly from the untreated 27.24 % to 41.21% after bleaching. This is indicative of the fact that more carbon compounds were present together with other inorganic material like CaO.

4.5.4.8 Acid hydrolysis

For the acid hydrolysis, the onset temperature increased to 287.4 ^{o}C with a corresponding increase in the maximum decomposition temperature at 308.8 ^{o}C. This result indicates that the thermal stability of the cellulose nanocrystals increased through the process treatments. Thus the treatments are seen to be effective. However, this is contrary to some works which reported that the use of sulfuric acid decreases the crystallinity due to the introduction of the active sulphate group (Y. W. Chen *et al.*, 2016). It also means that the particles became more orderly arranged and became more compact and hence highly resistant to temperature changes.

4.5.4.9 Cellulose nanocrystals

The onset temperature of the Palmae sp. increased from 308.2 ^{o}C to 363.7 ^{o}C. Residual mass decreased to 27.92 % at residual temperature of 899.3 ^{o}C. The decomposition peak temperature

was also very high to a level of 336.3 ºC. These increase in temperature of the CNCs show high thermal stability and crystallinity. Meaning the cellulose nanocrystals produced has unique physical properties of high resistance to heat. Additionally, the chemical properties of individual atoms in the CNCs are seen to reorient and rearrange orderly making them look dense and more compact. In a related study using the sulfuric acid by Chirayil et al. the thermal stability increased (Chirayil *et al.*, 2014). It also suggests that the impurities like pectin, wax and protein were effectively removed. The non-cellulose amorphous part also was seen to have been removed effectively leaving a more crystalline particle which is resistant to heat (Mandal & Chakrabarty, 2011)

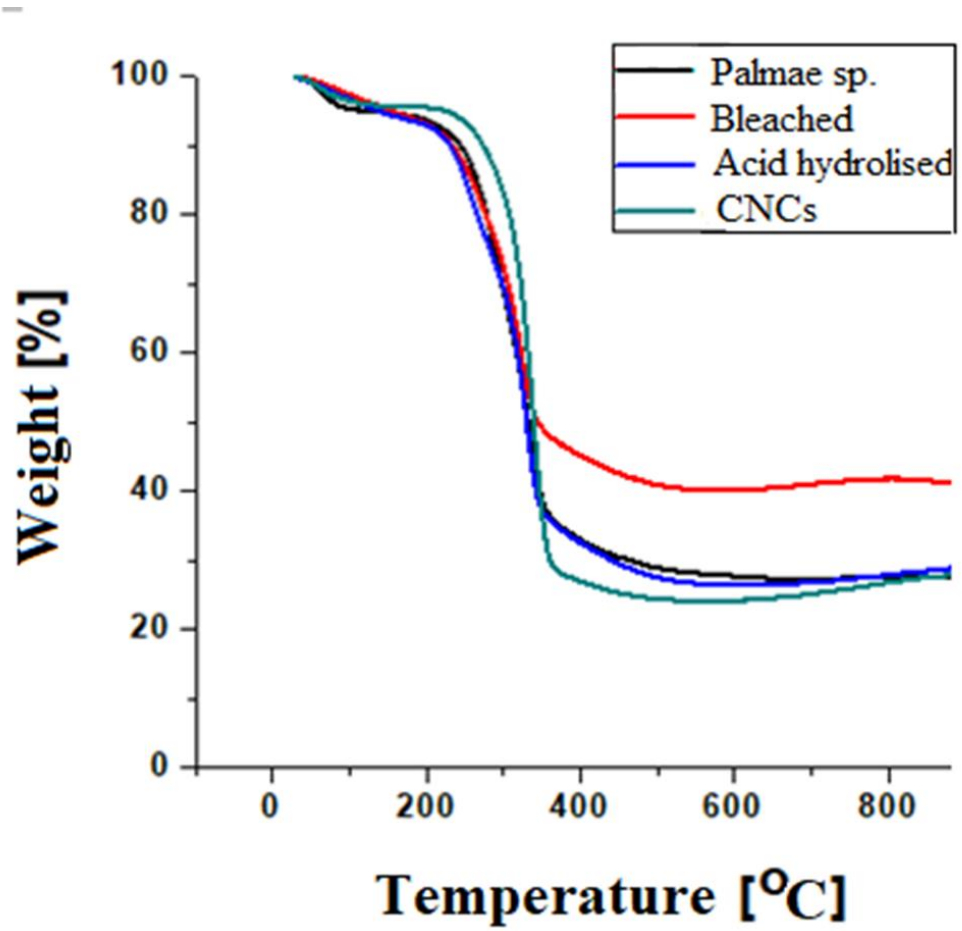

Figure 4. 13: Thermogram of palmae sp., bleached, acid hydrolysed and CNC

Table 4. 7: Amount of Weight loss (%) and Charred residue (%) for different samples of Palmae sp

Sample	Weight Loss (%)	Char yield (%)
Untreated	-72.61	27.24
Base hydrolyzed	-68.27	30.67
Bleached	-58.78	41.21
Acid hydrolyzed	-63.03	28.96
Cellulose nanoparticles	-72.08	27.92

CHAPTER FIVE

5.0 CONCLUSION AND RECOMMENDATION

5.1 CONCLUSION

The main aim of this work was to investigate the viability of the palmae sp. and acacia sp. as a local source for the isolation of nanocellulose crystals. This aim was achieved with the successful isolation of CNCs from both plant biomasses.

Although harsh alkaline and acid hydrolysis conditions are needed for the extraction of CNCs, the processes are highly sensitive to temperature and duration. For instance, temperature beyond 80 ^{o}C for alkaline treatment and 45 ^{o}C for acid treatment tends to lead to the charring of CNCs into dark particles. Thus, careful attention is needed in ensuring the successful isolation of CNCs.

The width dimension of the CNCs was approximately 200 nm with few micrometers of length. Thus nanosized particles were produced in one dimension signifying the effectiveness of base hydrolysis and bleaching. However, acid treatment appeared not to have been effective resulting in longer sheets of cellulose.

The findings from the study suggest that, acacia sp. and palmae sp. may serve as good sources for the production of nanocellulose crystals for potential use in diverse applications.

5.2 RECOMMENDATION

Quite clearly, the conditions of extraction affect the nature and quality of nanocrystals formed. Thus, optimization of the isolation processes to produce high quality nanoparticles is highly encouraged. In this regard, the identification of important local sources of cellulose is encouraged.

Additionally, investigations into alternate approaches in the extraction and isolation process aimed at utilizing more eco-friendly and cheaper reagents are highly recommended.

Finally, it is recommended that the CNCs will be used as reinforcement material in the production of biodegradable plastics.

REFERENCES

Abe, K., & Yano, H. (2009). Comparison of the characteristics of cellulose microfibril aggregates of wood, rice straw and potato tuber. *Cellulose, 16*(6), 1017.

Abraham, E., Deepa, B., Pothan, L., Jacob, M., Thomas, S., Cvelbar, U., & Anandjiwala, R. (2011). Extraction of nanocellulose fibrils from lignocellulosic fibres: A novel approach. *Carbohydrate Polymers, 86*(4), 1468-1475.

Abraham, E., Deepa, B., Pothen, L., Cintil, J., Thomas, S., John, M. J., . . . Narine, S. (2013). Environmental friendly method for the extraction of coir fibre and isolation of nanofibre. *Carbohydrate Polymers, 92*(2), 1477-1483.

Ahmadi, M., Madadlou, A., & Sabouri, A. A. (2015). Isolation of micro- and nano-crystalline cellulose particles and fabrication of crystalline particles-loaded whey protein cold-set gel. *Food Chem, 174*, 97-103. doi:10.1016/j.foodchem.2014.11.038

Alemdar, A., & Sain, M. (2008a). Biocomposites from wheat straw nanofibers: morphology, thermal and mechanical properties. *Composites Science and Technology, 68*(2), 557-565.

Alemdar, A., & Sain, M. (2008b). Isolation and characterization of nanofibers from agricultural residues–Wheat straw and soy hulls. *Bioresource technology, 99*(6), 1664-1671.

Barud, H. O., Barud, H. d. S., Cavicchioli, M., do Amaral, T. S., de Oliveira Junior, O. B., Santos, D. M., . . . de Oliveira, C. I. (2015). Preparation and characterization of a bacterial cellulose/silk fibroin sponge scaffold for tissue regeneration. *Carbohydrate Polymers, 128*, 41-51.

Beck-Candanedo, S., Roman, M., & Gray, D. G. (2005). Effect of reaction conditions on the properties and behavior of wood cellulose nanocrystal suspensions. *Biomacromolecules, 6*(2), 1048-1054.

Beltramino, F., Roncero, M. B., Vidal, T., Torres, A. L., & Valls, C. (2015). Increasing yield of nanocrystalline cellulose preparation process by a cellulase pretreatment. *Bioresour Technol, 192*, 574-581. doi:10.1016/j.biortech.2015.06.007

Bendahou, A., Habibi, Y., Kaddami, H., & Dufresne, A. (2009). Physico-Chemical Characterization of Palm from <I>Phoenix Dactylifera</I>–L, Preparation of Cellulose Whiskers and Natural Rubber–Based Nanocomposites. *Journal of Biobased Materials and Bioenergy, 3*(1), 81-90. doi:10.1166/jbmb.2009.1011

Bercea, M., & Navard, P. (2000). Shear dynamics of aqueous suspensions of cellulose whiskers. *Macromolecules, 33*(16), 6011-6016.

Bilgi, E., Özdemir, H. H., Bingol, A., & Bulut, S. (2015). Evaluation of the effects of group psychotherapy on cognitive function in patients with multiple sclerosis with cognitive dysfunction and depression. *Arquivos de neuro-psiquiatria, 73*(2), 90-95.

Boerjan, W., Ralph, J., & Baucher, M. (2003). Lignin biosynthesis. *Annual review of plant biology, 54*(1), 519-546.

Bondeson, D., Mathew, A., & Oksman, K. (2006). Optimization of the isolation of nanocrystals from microcrystalline cellulose by acid hydrolysis. *Cellulose, 13*(2), 171-180. doi:10.1007/s10570-006-9061-4

Brinchi, L., Cotana, F., Fortunati, E., & Kenny, J. (2013). Production of nanocrystalline cellulose from lignocellulosic biomass: technology and applications. *Carbohydrate Polymers, 94*(1), 154-169.

Chartas, G., Bautz, M., Garmire, G., Jones, C., & Schneider, D. (2001). Chandra observations of the gravitationally lensed system 2016+ 112. *The Astrophysical Journal Letters, 550*(2), L163.

Chen, D., Lawton, D., Thompson, M., & Liu, Q. (2012). Biocomposites reinforced with cellulose nanocrystals derived from potato peel waste. *Carbohydrate Polymers, 90*(1), 709-716.

Chen, W., Yu, H., Liu, Y., Hai, Y., Zhang, M., & Chen, P. (2011). Isolation and characterization of cellulose nanofibers from four plant cellulose fibers using a chemical-ultrasonic process. *Cellulose, 18*(2), 433-442.

Chen, Y., Liu, C., Chang, P. R., Cao, X., & Anderson, D. P. (2009). Bionanocomposites based on pea starch and cellulose nanowhiskers hydrolyzed from pea hull fibre: Effect of hydrolysis time. *Carbohydrate Polymers*, *76*(4), 607-615. doi:10.1016/j.carbpol.2008.11.030

Chen, Y. W., Lee, H. V., Juan, J. C., & Phang, S.-M. (2016). Production of new cellulose nanomaterial from red algae marine biomass Gelidium elegans. *Carbohydrate Polymers, 151*, 1210-1219.

Cherian, B. M., Leão, A. L., de Souza, S. F., Costa, L. M. M., de Olyveira, G. M., Kottaisamy, M., . . . Thomas, S. (2011). Cellulose nanocomposites with nanofibres isolated from pineapple leaf fibers for medical applications. *Carbohydrate Polymers*, *86*(4), 1790-1798. doi:10.1016/j.carbpol.2011.07.009

Cherian, B. M., Leão, A. L., de Souza, S. F., Thomas, S., Pothan, L. A., & Kottaisamy, M. (2010). Isolation of nanocellulose from pineapple leaf fibres by steam explosion. *Carbohydrate Polymers, 81*(3), 720-725.

Cherian, B. M., Pothan, L. A., Nguyen-Chung, T., Mennig, G. n., Kottaisamy, M., & Thomas, S. (2008). A novel method for the synthesis of cellulose nanofibril whiskers from banana fibers and characterization. *Journal of agricultural and food chemistry*, *56*(14), 5617-5627.

Chi, K., & Catchmark, J. M. (2017). The influences of added polysaccharides on the properties of bacterial crystalline nanocellulose. *Nanoscale, 9*(39), 15144-15158. doi:10.1039/c7nr05615j

Chieng, B., Lee, S., Ibrahim, N., Then, Y., & Loo, Y. (2017). Isolation and Characterization of Cellulose Nanocrystals from Oil Palm Mesocarp Fiber. *Polymers, 9*(12), 355. doi:10.3390/polym9080355

Chirayil, C. J., Mathew, L., & Thomas, S. (2014). REVIEW OF RECENT RESEARCH IN NANO CELLULOSE PREPARATION FROM DIFFERENT LIGNOCELLULOSIC FIBERS. *Reviews on advanced materials science, 37*.

Costa, L., Fonseca, A. F., Pereira, F. V., & Druzian, J. I. (2015). Extraction and characterization of cellulose nanocrystals from corn stover. *Cell Chem Technol, 49*(2), 127-133.

Csiszar, A., Nagy, G., Gergely, P., Pozsonyi, T., & Pocsik, E. (2000). Increased interferon-gamma (IFN-γ), IL-10 and decreased IL-4 mRNA expression in peripheral blood mononuclear cells (PBMC) from patients with systemic lupus erythematosus (SLE). *Clinical & Experimental Immunology, 122*(3), 464-470.

Csiszar, E., & Nagy, S. (2017). A comparative study on cellulose nanocrystals extracted from bleached cotton and flax and used for casting films with glycerol and sorbitol plasticisers. *Carbohydr Polym, 174*, 740-749. doi:10.1016/j.carbpol.2017.06.103

de Candolle, A. P. (1813). *Théorie élémentaire de la botanique*: Deterviile.

de Morais Teixeira, E., Corrêa, A. C., Manzoli, A., de Lima Leite, F., de Oliveira, C. R., & Mattoso, L. H. C. (2010). Cellulose nanofibers from white and naturally colored cotton fibers. *Cellulose, 17*(3), 595-606. doi:10.1007/s10570-010-9403-0

de Oliveira, F. B., Bras, J., Pimenta, M. T. B., da Silva Curvelo, A. A., & Belgacem, M. N. (2016). Production of cellulose nanocrystals from sugarcane bagasse fibers and pith. *Industrial Crops and Products, 93*, 48-57.

de Souza Lima, M. M., & Borsali, R. (2004). Rodlike cellulose microcrystals: structure, properties, and applications. *Macromolecular rapid communications, 25*(7), 771-787.

Deepa, B., Abraham, E., Cherian, B. M., Bismarck, A., Blaker, J. J., Pothan, L. A., . . . Kottaisamy, M. (2011). Structure, morphology and thermal characteristics of banana nano fibers obtained by steam explosion. *Bioresour Technol, 102*(2), 1988-1997. doi:10.1016/j.biortech.2010.09.030

Dong, S., Bortner, M. J., & Roman, M. (2016). Analysis of the sulfuric acid hydrolysis of wood pulp for cellulose nanocrystal production: a central composite design study. *Industrial Crops and Products, 93*, 76-87.

Du, L., Wang, J., Zhang, Y., Qi, C., Wolcott, M. P., & Yu, Z. (2017). Preparation and Characterization of Cellulose Nanocrystals from the Bio-ethanol Residuals. *Nanomaterials (Basel), 7*(3). doi:10.3390/nano7030051

Eronen, P., Österberg, M., Heikkinen, S., Tenkanen, M., & Laine, J. (2011). Interactions of structurally different hemicelluloses with nanofibrillar cellulose. *Carbohydrate Polymers, 86*(3), 1281-1290. doi:10.1016/j.carbpol.2011.06.031

Favier, V., Canova, G., Cavaillé, J., Chanzy, H., Dufresne, A., & Gauthier, C. (1995). Nanocomposite materials from latex and cellulose whiskers. *Polymers for Advanced Technologies, 6*(5), 351-355.

Filson, P. B., & Dawson-Andoh, B. E. (2009). Sono-chemical preparation of cellulose nanocrystals from lignocellulose derived materials. *Bioresource technology, 100*(7), 2259-2264.

Fortunati, E., Rinaldi, S., Peltzer, M., Bloise, N., Visai, L., Armentano, I., . . . Kenny, J. M. (2014). Nano-biocomposite films with modified cellulose nanocrystals and synthesized silver nanoparticles. *Carbohydr Polym, 101*, 1122-1133. doi:10.1016/j.carbpol.2013.10.055

Frost, R. L., & Weier, M. L. (2003). Thermal treatment of weddellite—a Raman and infrared emission spectroscopic study. *Thermochimica Acta, 406*(1-2), 221-232.

George, J. (2012). High performance edible nanocomposite films containing bacterial cellulose nanocrystals. *Carbohydrate Polymers, 87*(3), 2031-2037.

George, J., Kumar, R., Sajeevkumar, V. A., Ramana, K. V., Rajamanickam, R., Abhishek, V., . . . Siddaramaiah. (2014). Hybrid HPMC nanocomposites containing bacterial cellulose nanocrystals and silver nanoparticles. *Carbohydr Polym, 105*, 285-292. doi:10.1016/j.carbpol.2014.01.057

George, J., Ramana, K., & Bawa, A. (2011). Bacterial cellulose nanocrystals exhibiting high thermal stability and their polymer nanocomposites. *International journal of biological macromolecules, 48*(1), 50-57.

George, J., Ramana, K. V., Bawa, A. S., & Siddaramaiah. (2011). Bacterial cellulose nanocrystals exhibiting high thermal stability and their polymer nanocomposites. *Int J Biol Macromol, 48*(1), 50-57. doi:10.1016/j.ijbiomac.2010.09.013

George, J., Sajeevkumar, V. A., Ramana, K. V., Sabapathy, S. N., & Siddaramaiah. (2012). Augmented properties of PVA hybrid nanocomposites containing cellulose nanocrystals

and silver nanoparticles. *Journal of Materials Chemistry, 22*(42). doi:10.1039/c2jm35235d

George, M., Shen, W.-Z., Qi, Z., Bhatnagar, A., & Montemagno, C. (2017). Characterization of Cellulose Nanocrystals and PLA Based Thin Films with either Silver or Antimicrobial Peptide. *IOSR Journal of Polymer and Textile Engineering, 04*(03), 08-24. doi:10.9790/019x-04030824

Grishkewich, N., Mohammed, N., Tang, J., & Tam, K. C. (2017). Recent advances in the application of cellulose nanocrystals. *Current Opinion in Colloid & Interface Science, 29*, 32-45.

Hajlane, A., Kaddami, H., & Joffe, R. (2017). Chemical modification of regenerated cellulose fibres by cellulose nano-crystals: Towards hierarchical structure for structural composites reinforcement. *Industrial Crops and Products, 100*, 41-50. doi:10.1016/j.indcrop.2017.02.006

Han, J. S., & Rowell, J. S. (1997). Chemical composition of fibers. *Paper and composites from agro-based resources*, 83-134.

Hasani, M., Cranston, E. D., Westman, G., & Gray, D. G. (2008). Cationic surface functionalization of cellulose nanocrystals. *Soft Matter, 4*(11), 2238-2244.

Huang, F., Wu, X., Yu, Y., Lu, Y., & Chen, Q. (2017). Acylation of cellulose nanocrystals with acids/trifluoroacetic anhydride and properties of films from esters of CNCs. *Carbohydr Polym, 155*, 525-534. doi:10.1016/j.carbpol.2016.09.010

Huang, S., Zhou, L., Li, M.-C., Wu, Q., & Zhou, D. (2017). Cellulose nanocrystals (CNCs) from corn stalk: Activation energy analysis. *Materials, 10*(1), 80.

Jiang, F., & Hsieh, Y.-L. (2015). Cellulose nanocrystal isolation from tomato peels and assembled nanofibers. *Carbohydrate Polymers, 122*, 60-68.

Jung, M., Kim, K., Kim, B., Lee, K. J., Kang, J. W., & Jeon, S. (2017). Vertically stacked nanocellulose tactile sensor. *Nanoscale, 9*(44), 17212-17219. doi:10.1039/c7nr03685j

Kallel, F., Bettaieb, F., Khiari, R., García, A., Bras, J., & Chaabouni, S. E. (2016). Isolation and structural characterization of cellulose nanocrystals extracted from garlic straw residues. *Industrial Crops and Products, 87*, 287-296.

Kargarzadeh, H., Ahmad, I., Abdullah, I., Dufresne, A., Zainudin, S. Y., & Sheltami, R. M. (2012). Effects of hydrolysis conditions on the morphology, crystallinity, and thermal stability of cellulose nanocrystals extracted from kenaf bast fibers. *Cellulose, 19*(3), 855-866. doi:10.1007/s10570-012-9684-6

Khoshkava, V., & Kamal, M. R. (2014). Effect of cellulose nanocrystals (CNC) particle morphology on dispersion and rheological and mechanical properties of polypropylene/CNC nanocomposites. *ACS applied materials & interfaces, 6*(11), 8146-8157.

Kiziltas, E. E., Kiziltas, A., Bollin, S. C., & Gardner, D. J. (2015). Preparation and characterization of transparent PMMA–cellulose-based nanocomposites. *Carbohydrate Polymers, 127*, 381-389.

Lavoine, N., & Bergström, L. (2017). Nanocellulose-based foams and aerogels: processing, properties, and applications. *Journal of Materials Chemistry A, 5*(31), 16105-16117. doi:10.1039/c7ta02807e

Li, B., Xu, W., Kronlund, D., Maattanen, A., Liu, J., Smatt, J. H., . . . Xu, C. (2015). Cellulose nanocrystals prepared via formic acid hydrolysis followed by TEMPO-mediated oxidation. *Carbohydr Polym, 133*, 605-612. doi:10.1016/j.carbpol.2015.07.033

Li, J., Xu, M., Huang, H., Zhou, J., Abdel-Halimb, E., Zhang, J.-R., & Zhu, J.-J. (2011). Aptamer-quantum dots conjugates-based ultrasensitive competitive electrochemical cytosensor for the detection of tumor cell. *Talanta, 85*(4), 2113-2120.

Li, Z., Zhang, M., Cheng, D., & Yang, R. (2016). Preparation of silver nano-particles immobilized onto chitin nano-crystals and their application to cellulose paper for imparting antimicrobial activity. *Carbohydr Polym, 151*, 834-840. doi:10.1016/j.carbpol.2016.06.012

Lu, P., & Hsieh, Y.-L. (2010). Preparation and properties of cellulose nanocrystals: Rods, spheres, and network. *Carbohydrate Polymers, 82*(2), 329-336. doi:10.1016/j.carbpol.2010.04.073

Lu, P., & Hsieh, Y.-L. (2012). Preparation and characterization of cellulose nanocrystals from rice straw. *Carbohydrate Polymers, 87*(1), 564-573. doi:10.1016/j.carbpol.2011.08.022

Lustri, W. R., de Oliveira Barud, H. G., da Silva Barud, H., Peres, M. F., Gutierrez, J., Tercjak, A., . . . Ribeiro, S. J. L. (2015). Microbial Cellulose—Biosynthesis Mechanisms and Medical Applications. In *Cellulose-Fundamental Aspects and Current Trends*: InTech.

Maiti, S., Jayaramudu, J., Das, K., Reddy, S. M., Sadiku, R., Ray, S. S., & Liu, D. (2013). Preparation and characterization of nano-cellulose with new shape from different precursor. *Carbohydr Polym, 98*(1), 562-567. doi:10.1016/j.carbpol.2013.06.029

Majoinen, J., Kontturi, E., Ikkala, O., & Gray, D. G. (2012). SEM imaging of chiral nematic films cast from cellulose nanocrystal suspensions. *Cellulose, 19*(5), 1599-1605.

Mandal, A., & Chakrabarty, D. (2011). Isolation of nanocellulose from waste sugarcane bagasse (SCB) and its characterization. *Carbohydrate Polymers, 86*(3), 1291-1299.

Meyabadi, T. F., Dadashian, F., Sadeghi, G. M. M., & Asl, H. E. Z. (2014). Spherical cellulose nanoparticles preparation from waste cotton using a green method. *Powder Technology, 261*, 232-240.

Mihranyan, A. (2011). Cellulose from cladophorales green algae: From environmental problem to high-tech composite materials. *Journal of Applied Polymer Science, 119*(4), 2449-2460. doi:10.1002/app.32959

Mohammadkazemi, F., Doosthoseini, K., Ganjian, E., & Azin, M. (2015). Manufacturing of bacterial nano-cellulose reinforced fiber–cement composites. *Construction and Building Materials, 101*, 958-964. doi:10.1016/j.conbuildmat.2015.10.093

Morais, J. P., Rosa Mde, F., de Souza Filho Mde, S., Nascimento, L. D., do Nascimento, D. M., & Cassales, A. R. (2013). Extraction and characterization of nanocellulose structures from raw cotton linter. *Carbohydr Polym, 91*(1), 229-235. doi:10.1016/j.carbpol.2012.08.010

Morán, J. I., Alvarez, V. A., Cyras, V. P., & Vázquez, A. (2008). Extraction of cellulose and preparation of nanocellulose from sisal fibers. *Cellulose, 15*(1), 149-159.

Moreno, M., Armentano, I., Fortunati, E., Mattioli, S., Torre, L., Lligadas, G., . . . Cádiz, V. (2016). Cellulose nano-biocomposites from high oleic sunflower oil-derived thermosets. *European Polymer Journal, 79*, 109-120. doi:10.1016/j.eurpolymj.2016.04.018

Moriana, R., Vilaplana, F., & Ek, M. (2016). Cellulose Nanocrystals from Forest Residues as Reinforcing Agents for Composites: A Study from Macro- to Nano-Dimensions. *Carbohydr Polym, 139*, 139-149. doi:10.1016/j.carbpol.2015.12.020

Muthulakshmi, L., Rajini, N., Nellaiah, H., Kathiresan, T., Jawaid, M., & Rajulu, A. V. (2017). Preparation and properties of cellulose nanocomposite films with in situ generated copper nanoparticles using Terminalia catappa leaf extract. *International journal of biological macromolecules, 95*, 1064-1071.

Neto, W. P. F., Mariano, M., da Silva, I. S. V., Silvério, H. A., Putaux, J.-L., Otaguro, H., . . . Dufresne, A. (2016). Mechanical properties of natural rubber nanocomposites reinforced with high aspect ratio cellulose nanocrystals isolated from soy hulls. *Carbohydrate Polymers, 153*, 143-152.

Neto, W. P. F., Silvério, H. A., Dantas, N. O., & Pasquini, D. (2013). Extraction and characterization of cellulose nanocrystals from agro-industrial residue–Soy hulls. *Industrial Crops and Products, 42*, 480-488.

Ng, H.-M., Sin, L. T., Tee, T.-T., Bee, S.-T., Hui, D., Low, C.-Y., & Rahmat, A. (2015). Extraction of cellulose nanocrystals from plant sources for application as reinforcing agent in polymers. *Composites Part B: Engineering, 75*, 176-200.

Nogi, M., & Yano, H. (2008). Transparent Nanocomposites Based on Cellulose Produced by Bacteria Offer Potential Innovation in the Electronics Device Industry. *Advanced Materials, 20*(10), 1849-1852. doi:10.1002/adma.200702559

Postek, M. T., Howard, K. S., Johnson, A. H., & McMichael, K. L. (1997). The scanning electron microscope. *Handbook of charged particle optics*, 363-399.

Razalli, R. L., Abdi, Mahnaz M., Tahir, P. M., Moradbak, A., Sulaiman, Y., & Heng, L. Y. (2017). Polyaniline-modified nanocellulose prepared from Semantan bamboo by chemical polymerization: preparation and characterization. *RSC Advances, 7*(41), 25191-25198. doi:10.1039/c7ra03379f

Reddy, N., & Yang, Y. (2005a). Biofibers from agricultural byproducts for industrial applications. *TRENDS in Biotechnology, 23*(1), 22-27.

Reddy, N., & Yang, Y. (2005b). Structure and properties of high quality natural cellulose fibers from cornstalks. *Polymer, 46*(15), 5494-5500.

Ritter, G. J. (1929). Determination of alpha-cellulose. *Industrial & Engineering Chemistry Analytical Edition, 1*(1), 52-54.

Rosa, M., Medeiros, E., Malmonge, J., Gregorski, K., Wood, D., Mattoso, L., . . . Imam, S. (2010). Cellulose nanowhiskers from coconut husk fibers: Effect of preparation conditions on their thermal and morphological behavior. *Carbohydrate Polymers, 81*(1), 83-92.

Rosa, M. F., Medeiros, E. S., Malmonge, J. A., Gregorski, K. S., Wood, D. F., Mattoso, L. H. C., . . . Imam, S. H. (2010). Cellulose nanowhiskers from coconut husk fibers: Effect of preparation conditions on their thermal and morphological behavior. *Carbohydrate Polymers, 81*(1), 83-92. doi:10.1016/j.carbpol.2010.01.059

Santos, R. B., Hart, P., Jameel, H., & Chang, H.-m. (2013). Wood based lignin reactions important to the biorefinery and pulp and paper industries. *BioResources, 8*(1), 1456-1477.

Santos, R. M. d., Flauzino Neto, W. P., Silvério, H. A., Martins, D. F., Dantas, N. O., & Pasquini, D. (2013). Cellulose nanocrystals from pineapple leaf, a new approach for the reuse of this agro-waste. *Industrial Crops and Products, 50*, 707-714. doi:10.1016/j.indcrop.2013.08.049

Segal, L., Creely, J., Martin Jr, A., & Conrad, C. (1959). An empirical method for estimating the degree of crystallinity of native cellulose using the X-ray diffractometer. *Textile Research Journal, 29*(10), 786-794.

Shankar, S., Oun, A. A., & Rhim, J. W. (2018). Preparation of antimicrobial hybrid nano-materials using regenerated cellulose and metallic nanoparticles. *Int J Biol Macromol, 107*(Pt A), 17-27. doi:10.1016/j.ijbiomac.2017.08.129

Sheltami, R. M., Abdullah, I., Ahmad, I., Dufresne, A., & Kargarzadeh, H. (2012). Extraction of cellulose nanocrystals from mengkuang leaves (Pandanus tectorius). *Carbohydrate Polymers, 88*(2), 772-779. doi:10.1016/j.carbpol.2012.01.062

Singh, S., Gaikwad, K. K., Park, S.-I., & Lee, Y. S. (2017). Microwave-assisted step reduced extraction of seaweed (Gelidiella aceroso) cellulose nanocrystals. *International journal of biological macromolecules, 99*, 506-510.

Song, H. Z., Luo, Z. Q., Wang, C. Z., Hao, X. F., & Gao, J. G. (2013). Preparation and characterization of bionanocomposite fiber based on cellulose and nano-SiO2 using ionic liquid. *Carbohydr Polym, 98*(1), 161-167. doi:10.1016/j.carbpol.2013.05.079

Soni, B., & Mahmoud, B. (2015). Chemical isolation and characterization of different cellulose nanofibers from cotton stalks. *Carbohydrate Polymers, 134*, 581-589.

Suopajärvi, T., Liimatainen, H., Hormi, O., & Niinimäki, J. (2013). Coagulation–flocculation treatment of municipal wastewater based on anionized nanocelluloses. *Chemical Engineering Journal, 231*, 59-67.

Taflick, T., Schwendler, L. A., Rosa, S. M., Bica, C. I., & Nachtigall, S. M. (2017). Cellulose nanocrystals from acacia bark–Influence of solvent extraction. *International journal of biological macromolecules, 101*, 553-561.

Tan, X. Y., Abd Hamid, S. B., & Lai, C. W. (2015). Preparation of high crystallinity cellulose nanocrystals (CNCs) by ionic liquid solvolysis. *Biomass and Bioenergy, 81*, 584-591. doi:10.1016/j.biombioe.2015.08.016

Tang, Y., Shen, X., Zhang, J., Guo, D., Kong, F., & Zhang, N. (2015). Extraction of cellulose nano-crystals from old corrugated container fiber using phosphoric acid and enzymatic hydrolysis followed by sonication. *Carbohydr Polym, 125*, 360-366. doi:10.1016/j.carbpol.2015.02.063

Tummala, G. K., Joffre, T., Rojas, R., Persson, C., & Mihranyan, A. (2017). Strain-induced stiffening of nanocellulose-reinforced poly(vinyl alcohol) hydrogels mimicking collagenous soft tissues. *Soft Matter, 13*(21), 3936-3945. doi:10.1039/c7sm00677b

Usha, M., Chandra, T. S., Sarada, R., & Chauhan, V. (2016). Removal of nutrients and organic pollution load from pulp and paper mill effluent by microalgae in outdoor open pond. *Bioresource technology, 214*, 856-860.

Wang, Q. Q., Zhu, J. Y., Reiner, R. S., Verrill, S. P., Baxa, U., & McNeil, S. E. (2012). Approaching zero cellulose loss in cellulose nanocrystal (CNC) production: recovery and characterization of cellulosic solid residues (CSR) and CNC. *Cellulose, 19*(6), 2033-2047. doi:10.1007/s10570-012-9765-6

Wang, X., Li, X., Sun, X., Li, F., Liu, Q., Wang, Q., & He, D. (2011). Nanostructured NiO electrode for high rate Li-ion batteries. *Journal of Materials Chemistry, 21*(11), 3571-3573.

Wang, Y., Cao, X., & Zhang, L. (2006). Effects of cellulose whiskers on properties of soy protein thermoplastics. *Macromol Biosci, 6*(7), 524-531. doi:10.1002/mabi.200600034

Wu, X., Wagner, R., Raman, A., Moon, R., Martini, A., & Center, B. N. (2010). Elastic deformation mechanics of cellulose nanocrystals. *Review Process: Non-Refereed (Other)*.

Yang, X., Zhao, Y., Mussana, H., Tessema, M., & Liu, L. (2018). Characteristics of cotton fabric modified with chitosan (CS)/cellulose nanocrystal (CNC) nanocomposites. *Materials Letters, 211,* 300-303. doi:10.1016/j.matlet.2017.09.075

Yoshida, M., Liu, Y., Uchida, S., Kawarada, K., Ukagami, Y., Ichinose, H., . . . Fukuda, K. (2008). Effects of cellulose crystallinity, hemicellulose, and lignin on the enzymatic hydrolysis of Miscanthus sinensis to monosaccharides. *Biosci Biotechnol Biochem, 72*(3), 805-810. doi:10.1271/bbb.70689

Yu, H.-Y., Qin, Z.-Y., Liu, L., Yang, X.-G., Zhou, Y., & Yao, J.-M. (2013). Comparison of the reinforcing effects for cellulose nanocrystals obtained by sulfuric and hydrochloric acid hydrolysis on the mechanical and thermal properties of bacterial polyester. *Composites Science and Technology, 87,* 22-28. doi:10.1016/j.compscitech.2013.07.024

Yu, H.-Y., Qin, Z.-Y., Sun, B., Yan, C. F., & Yao, J.-M. (2014). One-pot green fabrication and antibacterial activity of thermally stable corn-like CNC/Ag nanocomposites. *Journal of nanoparticle research, 16*(1), 2202.

Yu, H., Qin, Z., Liang, B., Liu, N., Zhou, Z., & Chen, L. (2013). Facile extraction of thermally stable cellulose nanocrystals with a high yield of 93% through hydrochloric acid hydrolysis under hydrothermal conditions. *Journal of Materials Chemistry A, 1*(12). doi:10.1039/c3ta01150j

APPENDICES

APPENDIX A

FTIR spectra of acacia sp.

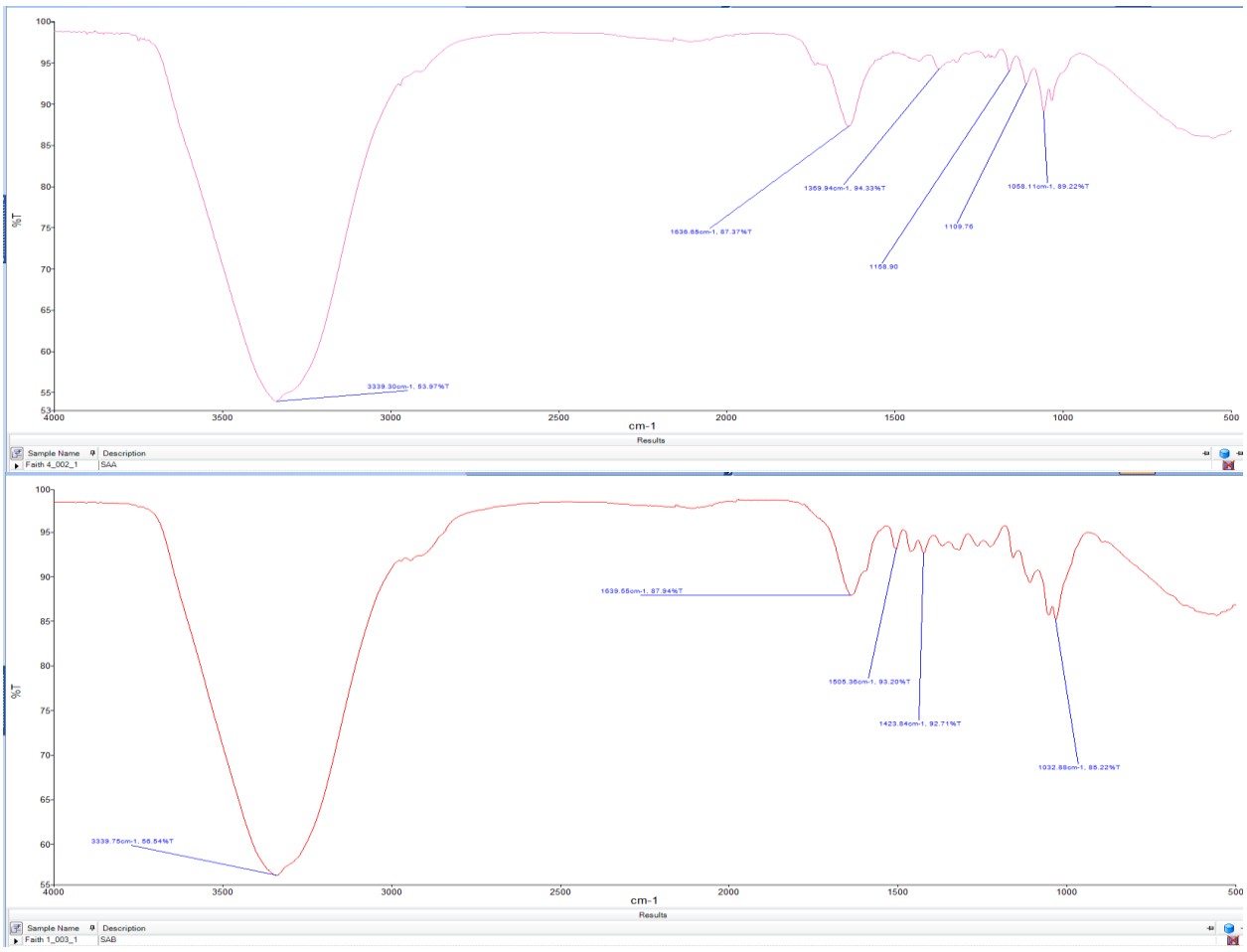

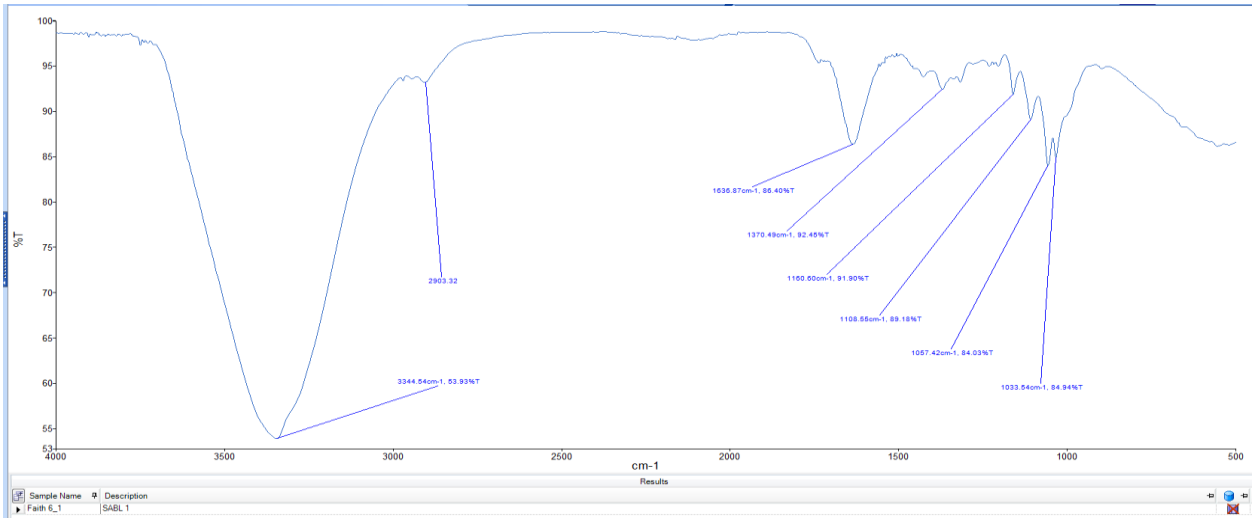

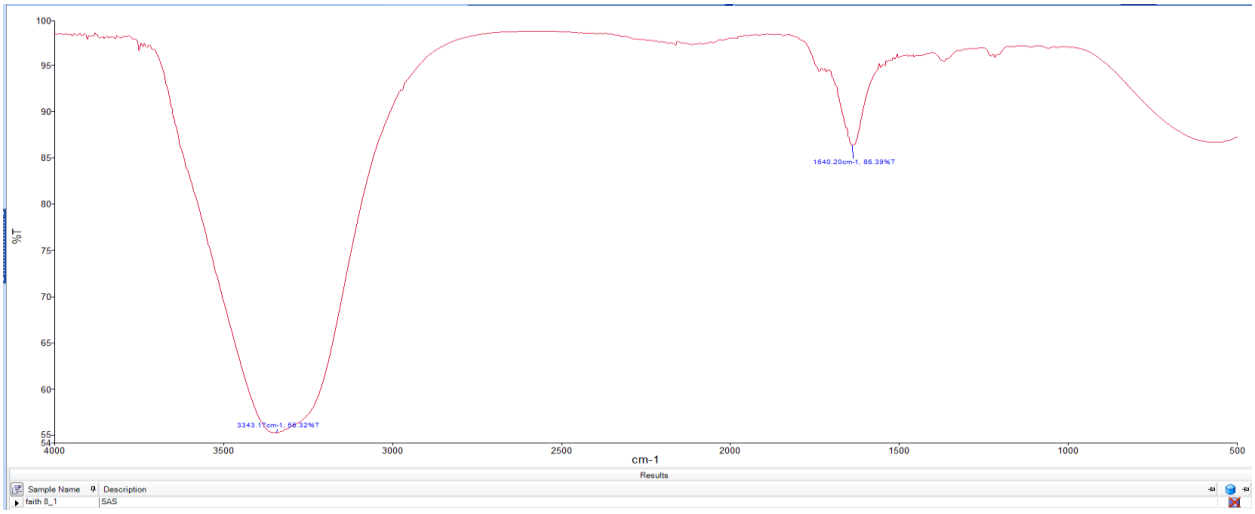

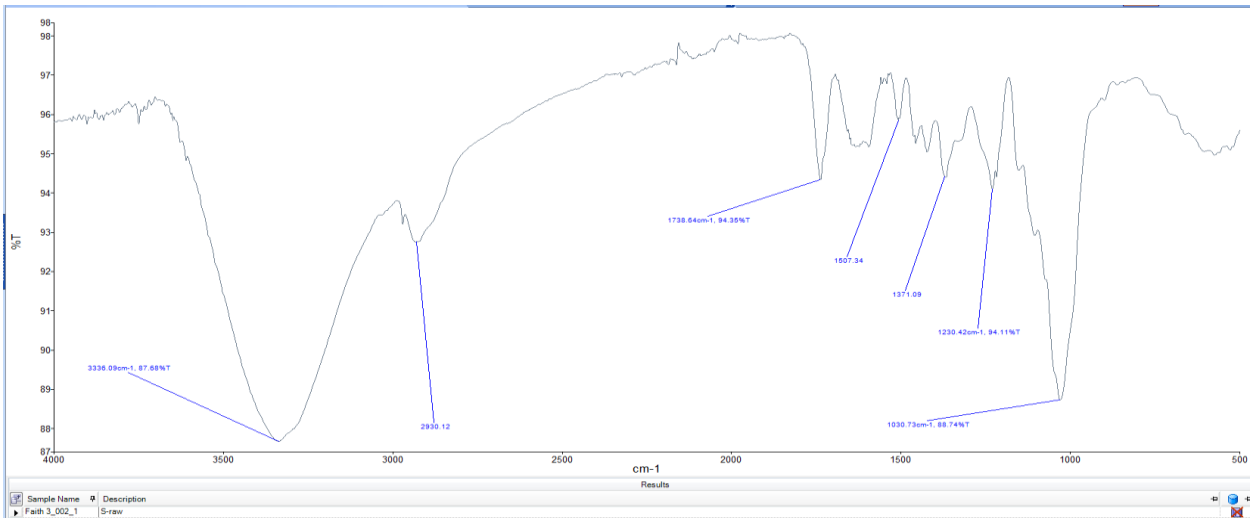

FTIR spectra of palmae sp.

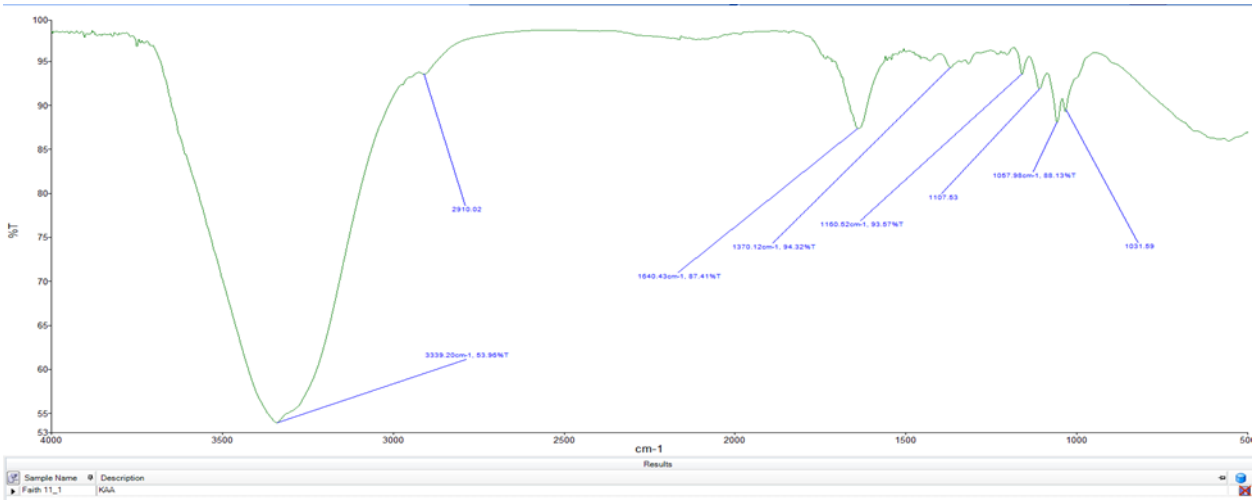

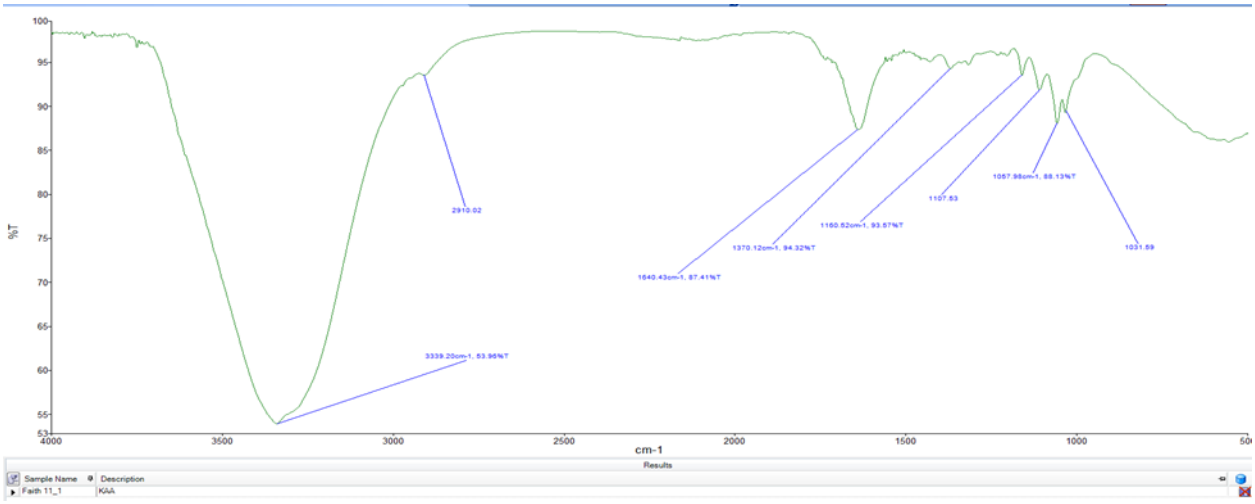

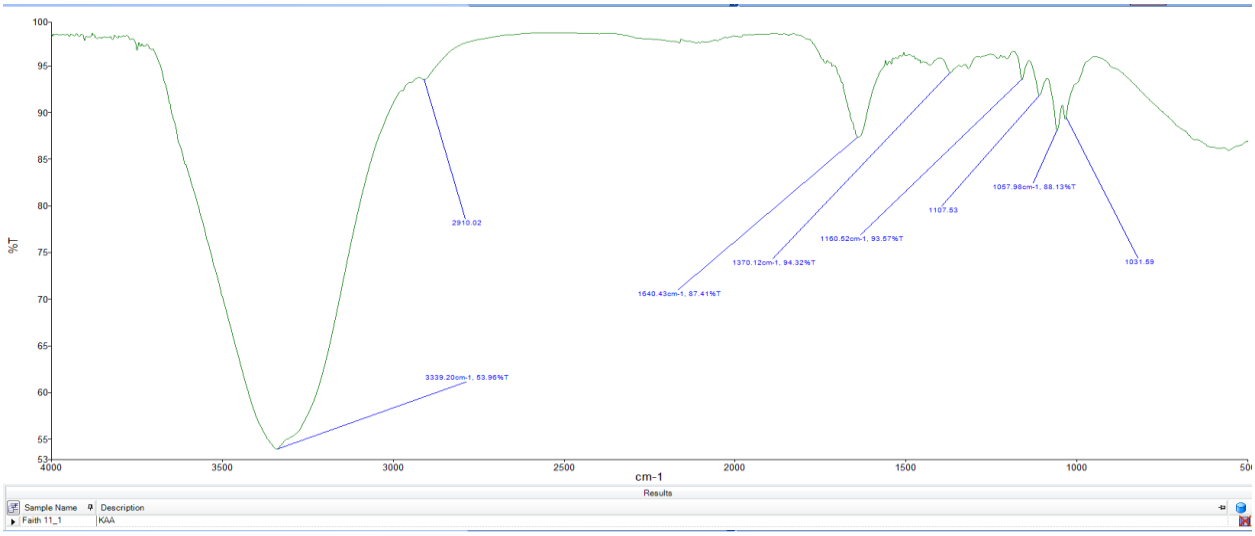

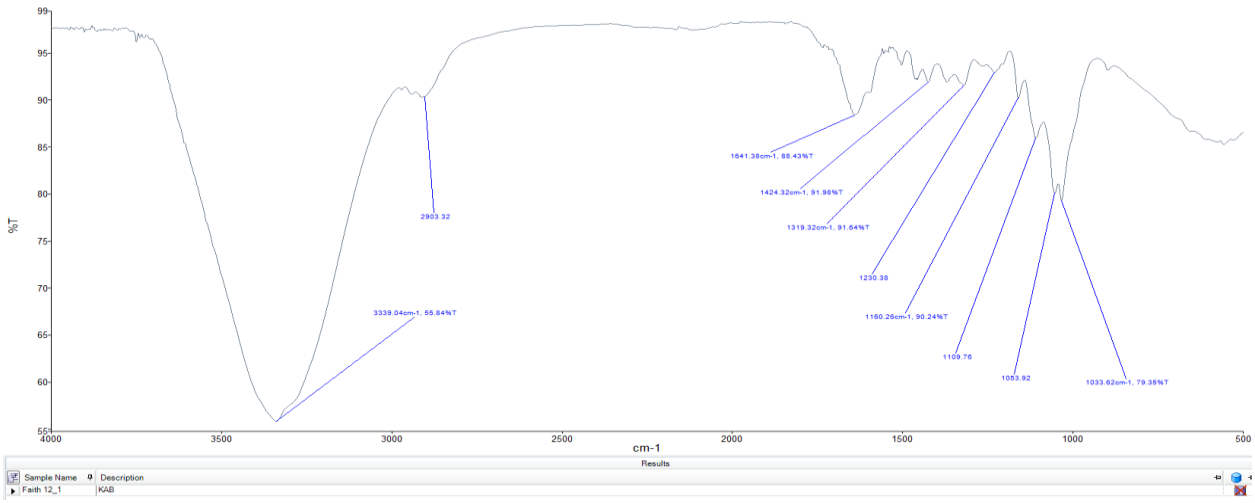

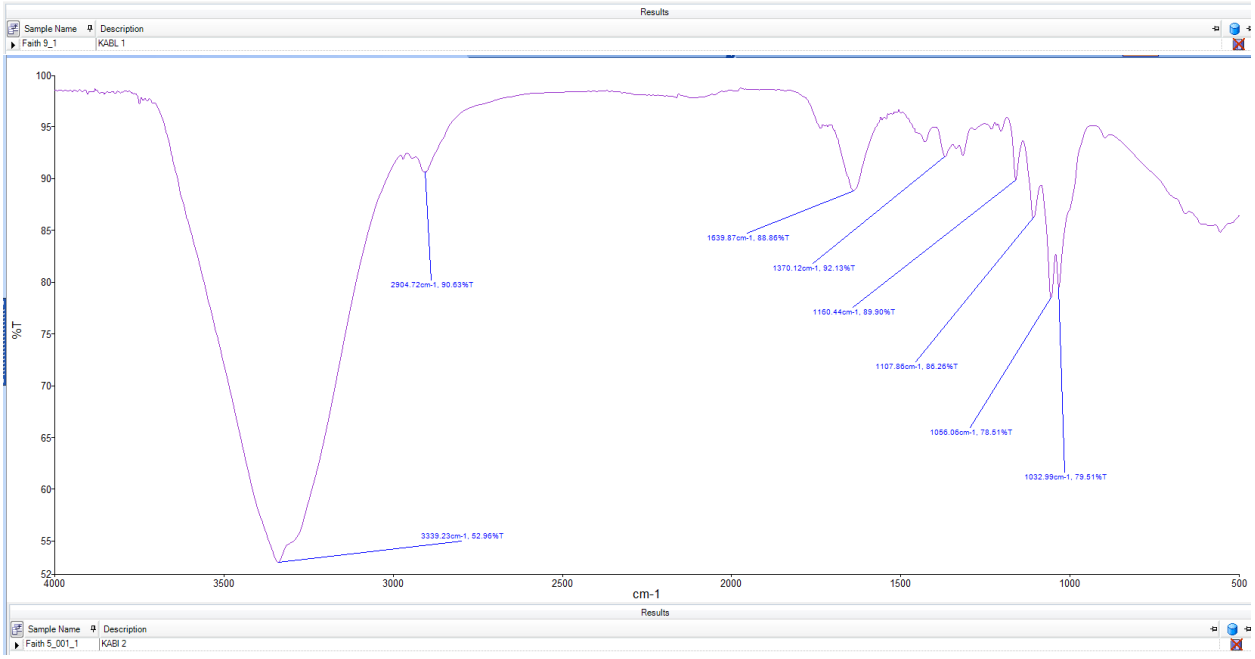

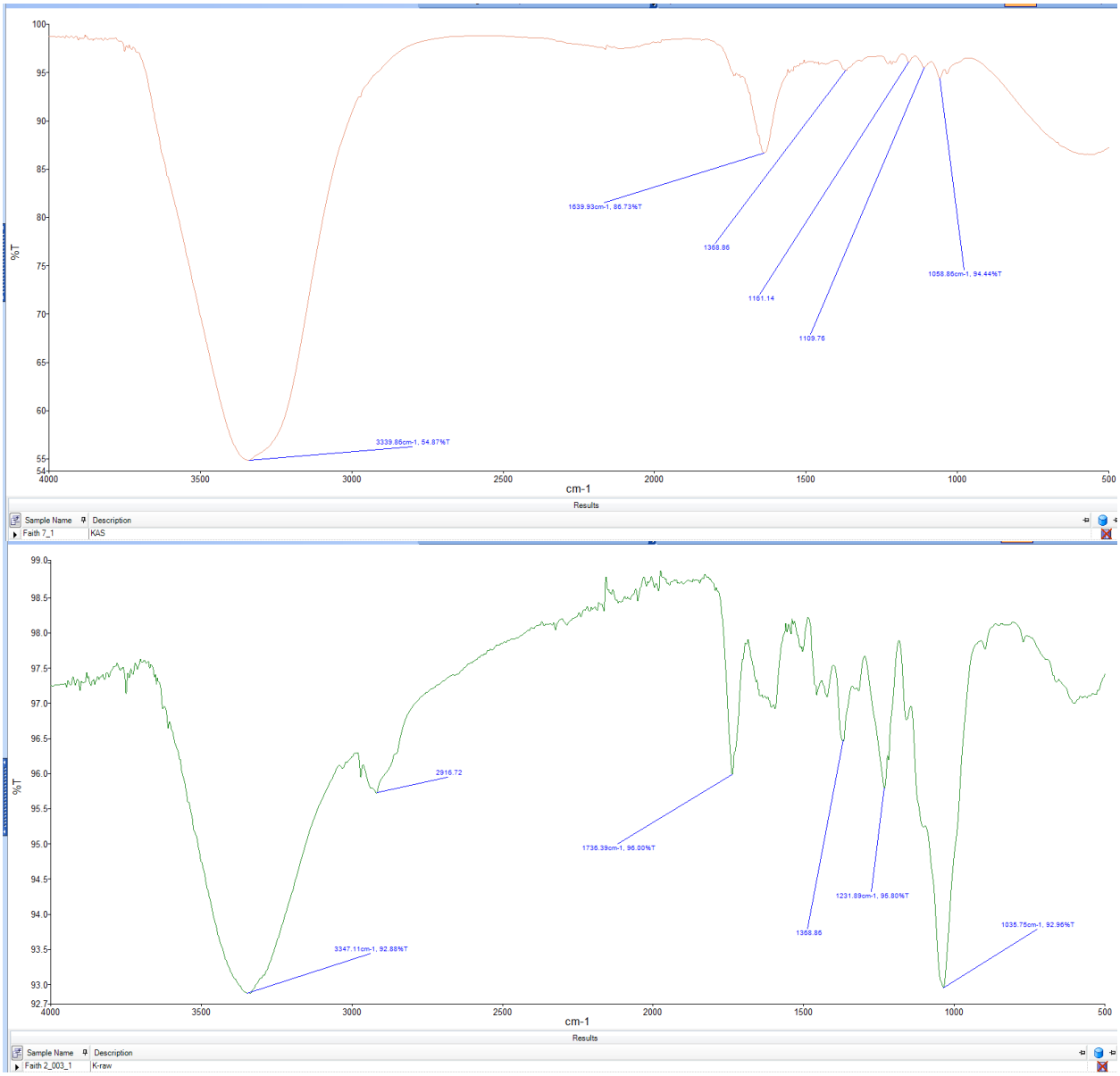

APPENDIX B

TGA THERMOGRAPHS

TGA of Acacia sp.

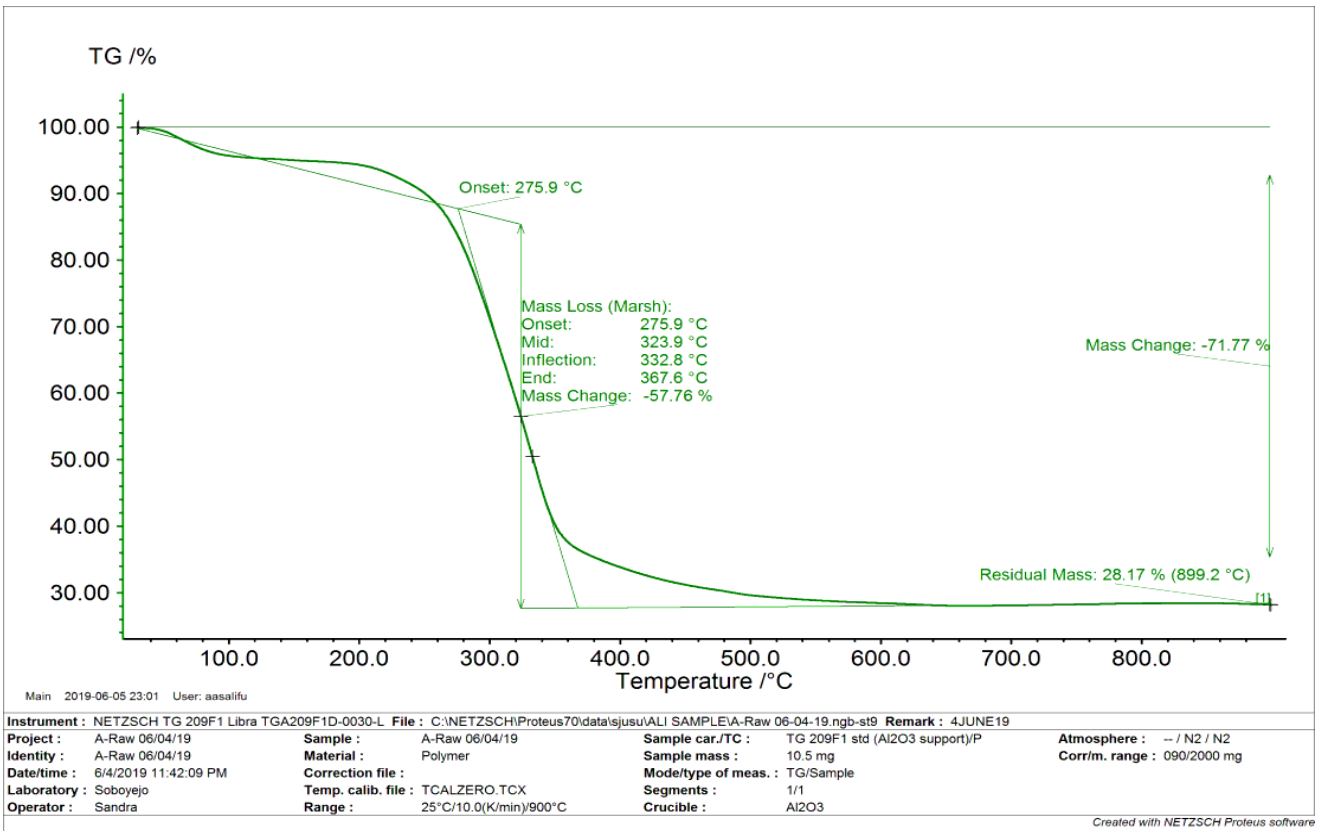

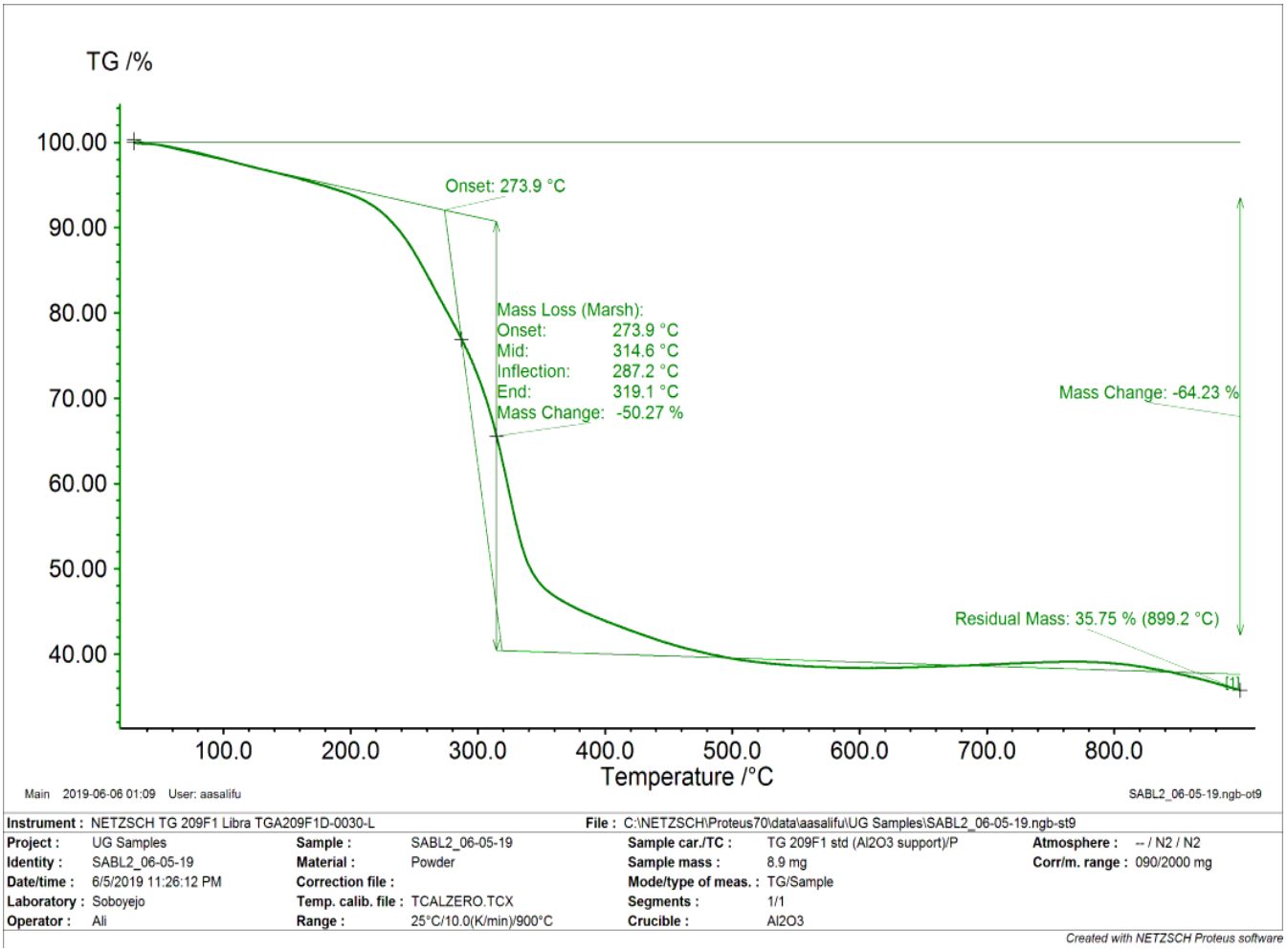

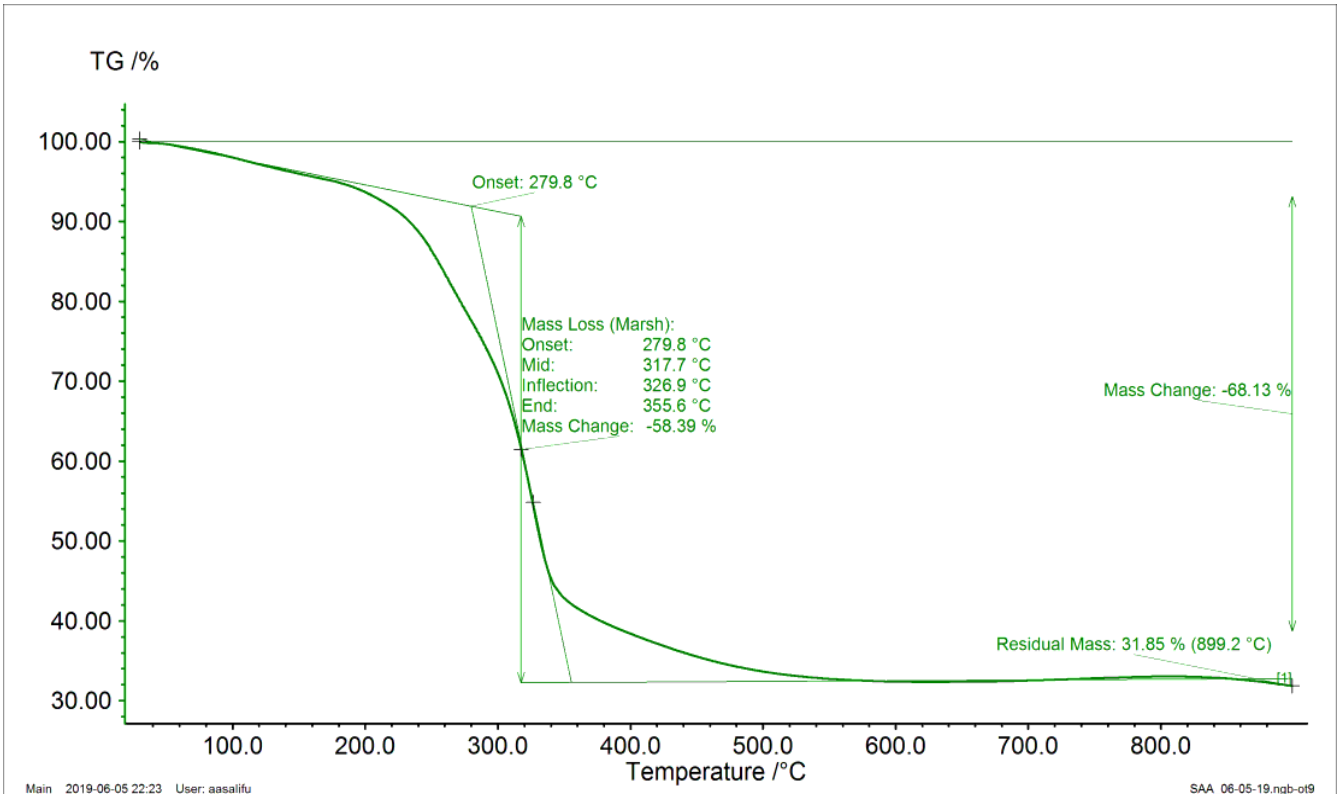

Instrument :	NETZSCH TG 209F1 Libra TGA209F1D-0030-L			**File :**	C:\NETZSCH\Proteus70\data\aasalifu\UG Samples\SAA_06-05-19.ngb-st9		
Project :	UG Samples	**Sample :**	SAA_06-05-19	**Sample car./TC :**	TG 209F1 std (Al2O3 support)/P	**Atmosphere :**	-- / N2 / N2
Identity :	SAA_06-05-19	**Material :**	Powder	**Sample mass :**	10.2 mg	**Corr/m. range :**	090/2000 mg
Date/time :	6/5/2019 8:35:19 PM	**Correction file :**		**Mode/type of meas. :**	TG/Sample		
Laboratory :	Soboyejo	**Temp. calib. file :**	TCALZERO.TCX	**Segments :**	1/1		
Operator :	Ali	**Range :**	25°C/10.0(K/min)/900°C	**Crucible :**	Al2O3		

Created with NETZSCH Proteus software

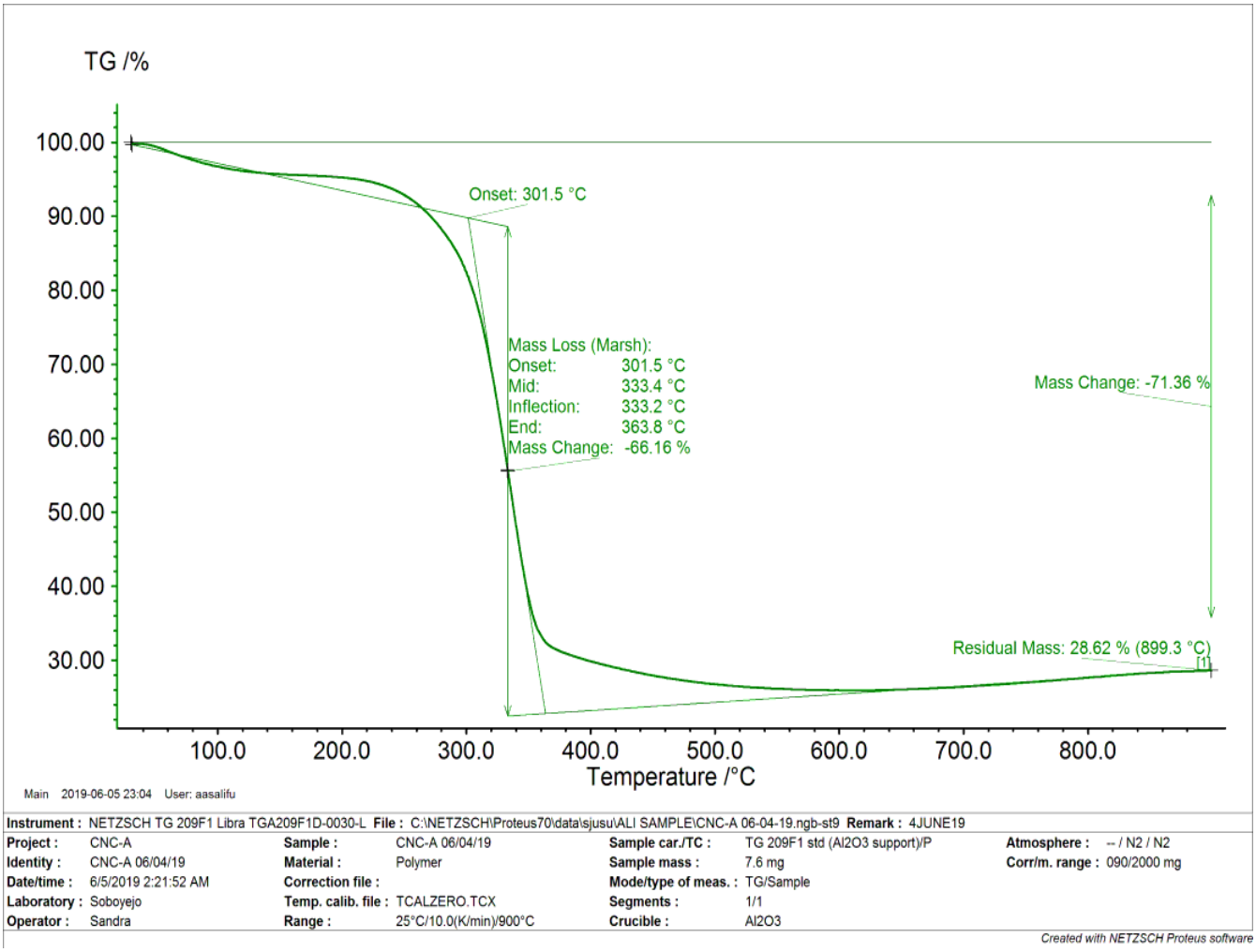

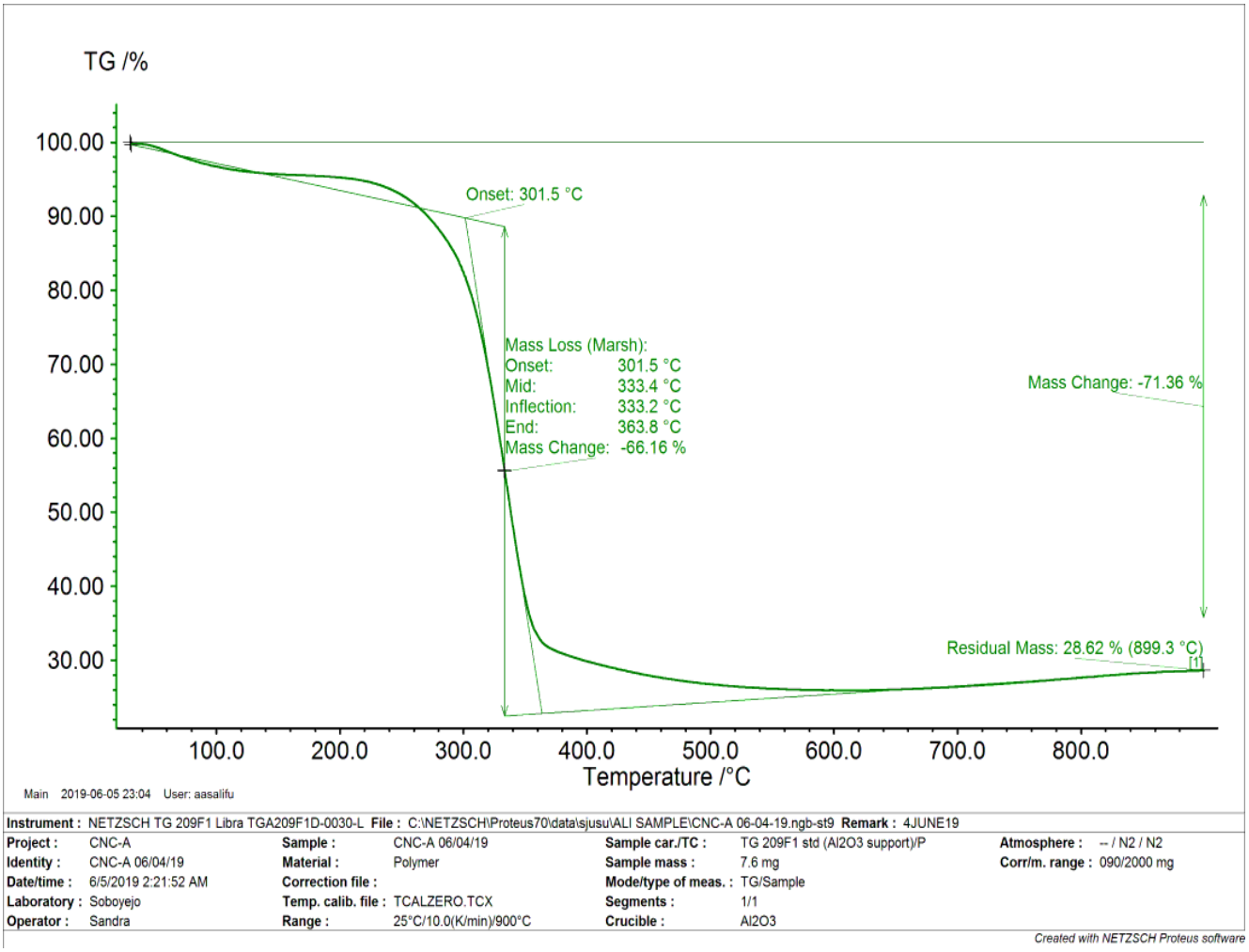

TGA of Palmae sp.

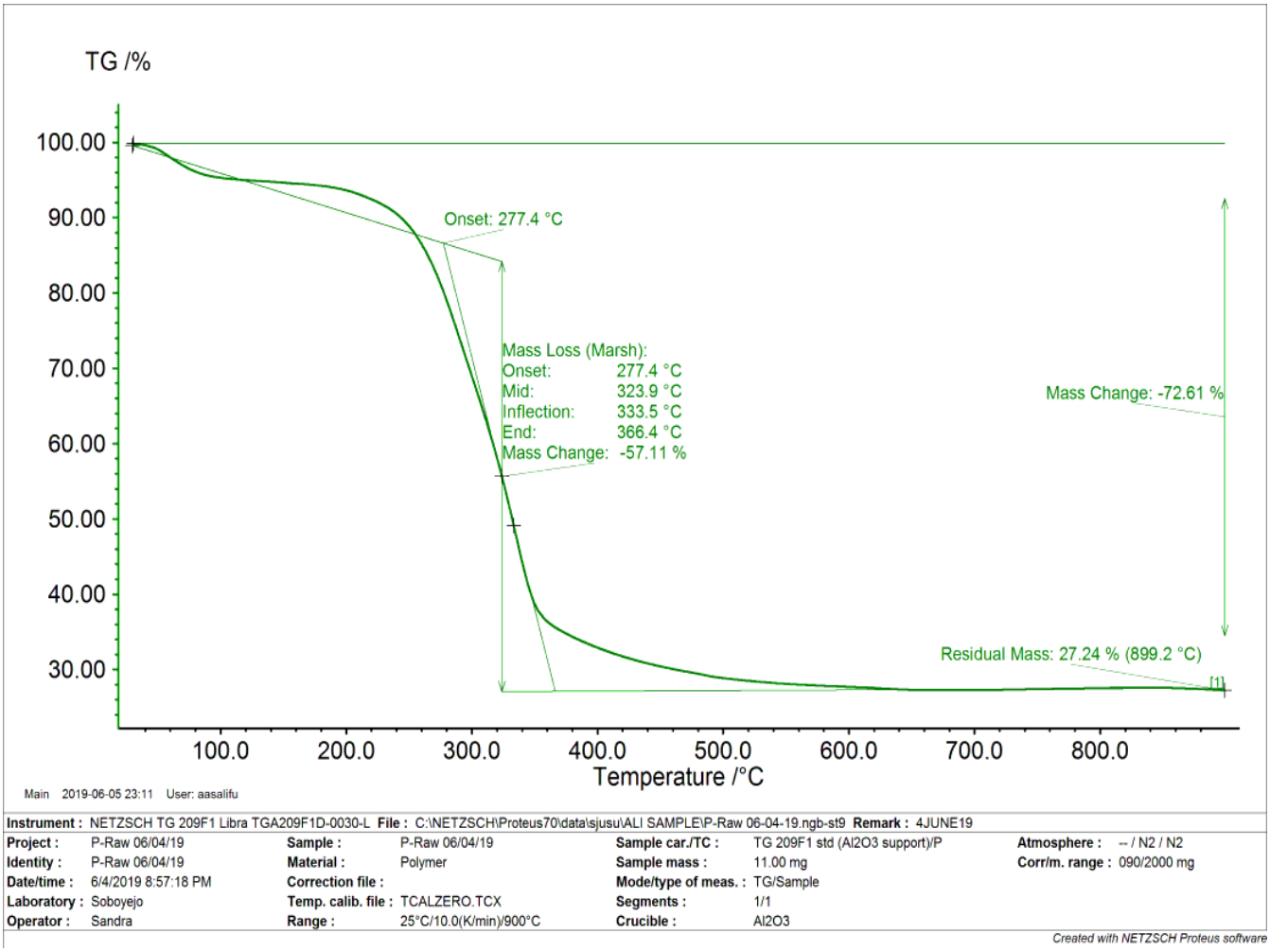

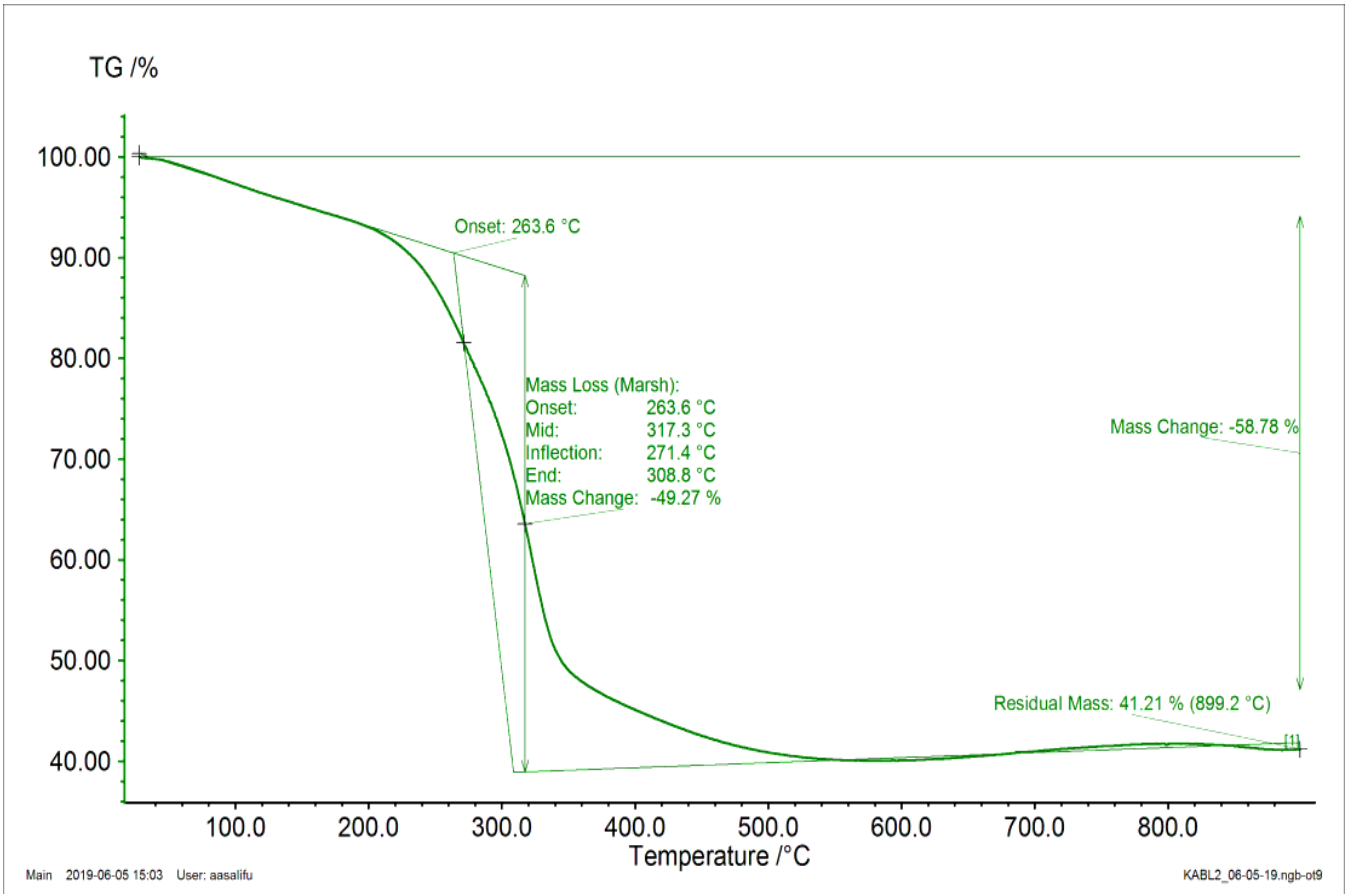

Instrument :	NETZSCH TG 209F1 Libra TGA209F1D-0030-L			**File :**	C:\NETZSCH\Proteus70\data\aasalifu\UG Samples\KABL2_06-05-19.ngb-st9		
Project :	UG Samples	**Sample :**	KABL2_06-05-19	**Sample car./TC :**	TG 209F1 std (Al2O3 support)/P	**Atmosphere :**	-- / N2 / N2
Identity :	KABL2_06-05-19	**Material :**	Powder	**Sample mass :**	9.1 mg	**Corr/m. range :**	090/2000 mg
Date/time :	6/5/2019 1:06:07 PM	**Correction file :**		**Mode/type of meas. :**	TG/Sample		
Laboratory :	Soboyejo	**Temp. calib. file :**	TCALZERO.TCX	**Segments :**	1/1		
Operator :	Ali	**Range :**	25°C/10.0(K/min)/900°C	**Crucible :**	Al2O3		

Created with NETZSCH Proteus software

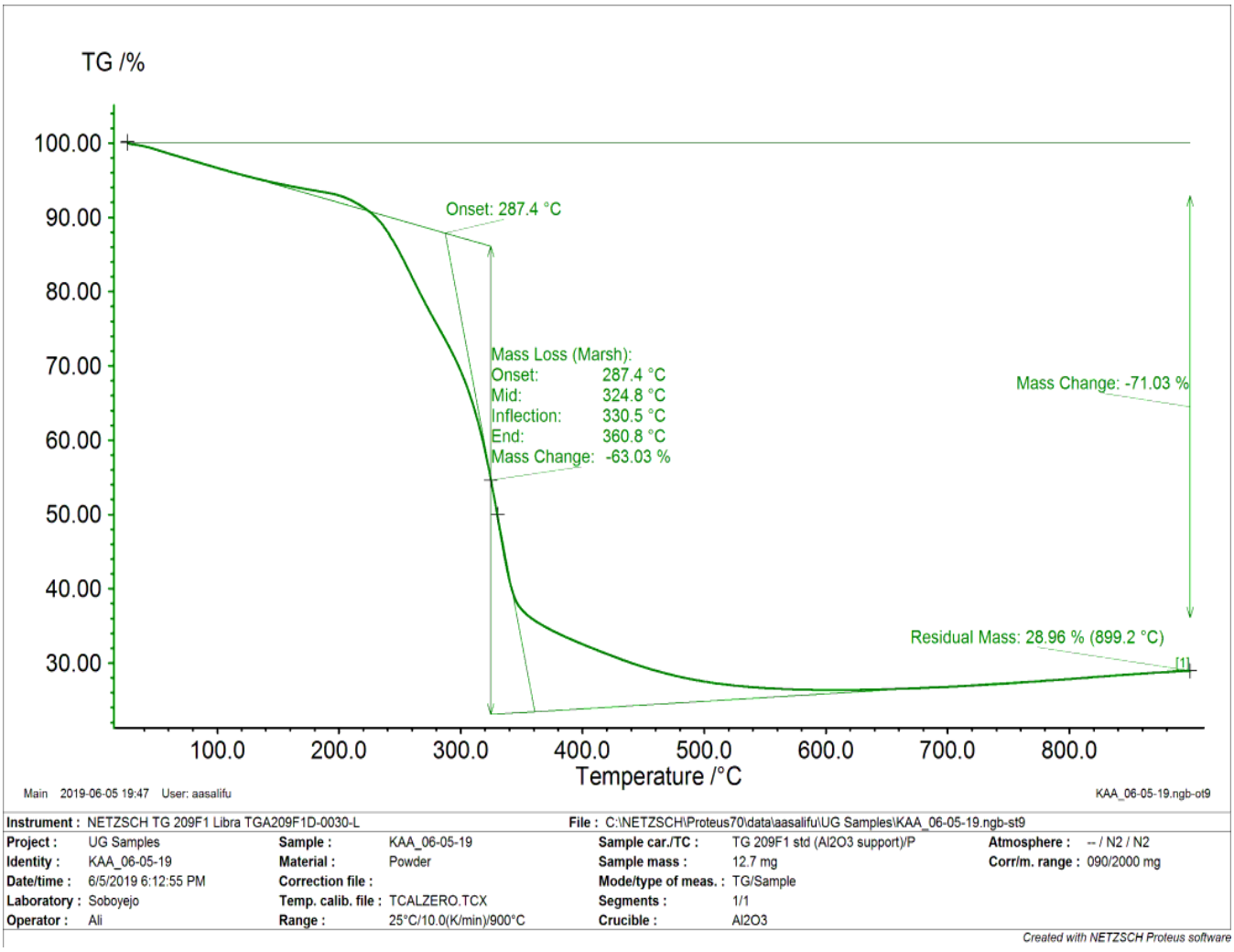

Instrument :	NETZSCH TG 209F1 Libra TGA209F1D-0030-L			**File :**	C:\NETZSCH\Proteus70\data\aasalifu\UG Samples\KAA_06-05-19.ngb-st9		
Project :	UG Samples	**Sample :**	KAA_06-05-19	**Sample car./TC :**	TG 209F1 std (Al2O3 support)/P	**Atmosphere :**	-- / N2 / N2
Identity :	KAA_06-05-19	**Material :**	Powder	**Sample mass :**	12.7 mg	**Corr/m. range :**	090/2000 mg
Date/time :	6/5/2019 6:12:55 PM	**Correction file :**		**Mode/type of meas. :**	TG/Sample		
Laboratory :	Soboyejo	**Temp. calib. file :**	TCALZERO.TCX	**Segments :**	1/1		
Operator :	Ali	**Range :**	25°C/10.0(K/min)/900°C	**Crucible :**	Al2O3		

Created with NETZSCH Proteus software